EXPLORING THE ROLE OF FGFS ON RADIAL PATTERNING OF THE EMBRYONIC CHICKEN COCHLEA

by

Elizabeth Wehren

A Thesis

Submitted to the Faculty of Purdue University

In Partial Fulfillment of the Requirements for the degree of

Master of Science

Department of Biological Sciences

West Lafayette, Indiana

May 2021

THE PURDUE UNIVERSITY GRADUATE SCHOOL
STATEMENT OF COMMITTEE APPROVAL

Dr. Donna M. Fekete, Chair

Department of Biological Sciences

Dr. Donald F. Ready

Department of Biological Sciences

Dr. David M. Umulis

Department of Agricultural & Biological Engineering

Approved by:

Dr. Janice P. Evans

To my family and friends for always supporting me

ACKNOWLEDGMENTS

I would like to thank Dr. Donna Fekete for her continued support as my advisor and the other members of the Fekete lab who have assisted me in this project: Deborah Biesemeier, Dr. Katie Scott, Vashi Negi, Rachel Maibach, Nabilah Hamdiah Binti Che Sammudin, and Adam Lorch. Additionally, I want to thank Jennifer Lee and Sneha Subramanian of Dr. Ruben Aguilar's lab and Dr. Aguilar himself for assistance in running Westerns Blots and the labs of Dr. Matías Hidalgo-Sánchez (University of Extremadura) and Dr. Ohuchi (Okayama University) for generously donating reagents for this project. Finally, I would like to thank my committee and Purdue's Department of Biological Sciences for their support throughout my degree and the National Institute on Deafness and Other Communication Disorders for the grant supporting this work.

TABLE OF CONTENTS

LIST OF TABLES 8
LIST OF FIGURES 9
LIST OF ABBRIEVATIONS 12
ABSTRACT 16
CHAPTER 1. INTRODUCTION 18
1.1 Inner Ear Overview 18
1.2 Wnt Overview 18
1.3 Fgf Overview 18
1.4 Vertebrate Inner Ear Development 19
1.5 Cochlear Cell Specification by Fgfs 21
1.6 Innervation of the Cochlea 24
1.7 The Auditory Organ of the Bird 24
1.8 Wnt9a Involvement in Radial Patterning of the Basilar Papilla 26
1.9 Fgf19 Overview 27
1.10 Fgf19 Secretion and Signaling 27
1.11 The Roles of Fgf19 in Human Adult Tissue and Disease 29
1.12 Fgf19's Effect on Cell Proliferation 30
1.13 Fgf19's Role in Chick Eye Development 31
CHAPTER 2. METHODS 34
2.1 Virus Injection and Tissue Sectioning 34
2.2 DAB (immunostaining) 34
2.3 Transformation of DH5-α cells with cFgf3 or cFgf19 Plasmid 35
2.4 MaxiPrep of Transformed DH5-α cells with cFgf3, cFgf19 or cFzd4 Plasmid 36
2.5 Linearization and Purification of cFgf3, cFgf19, and cFzd4 Plasmids 37
2.6 Creation of cFgf3, cFgf19, and cFzd4 In Situ Hybridization mRNA DIG Probes 37
2.7 DIG Probe In situ Hybridization 38
2.8 Viral Design 39
2.9 Virus creation 46
2.10 Virus Concentration 48

2.11 Immunocytochemistry (ICC) 51
2.12 Western Blot Analysis 51
2.13 Immunohistochemistry (IHC) 53
2.14 Alcian Blue Staining 53
2.15 RNAscope In Situ Hybridization 54
2.16 Imaging 56
CHAPTER 3. RESULTS 57
3.1 cWnt9a Overexpression Results in Increased and/or Ectopic cFgf3, cFgf19, and cFzd4 mRNA Expression 57
3.2 RCAS(A)/EGFP-P2A-Fgf19 and RCAS(B)/Fgf19-P2A-EGFP Virus Proof of Concept 62
3.3 Comparison of 3C2 and GFP within DF-1 Cells Transfected with RCAS(B), RCAS(A)/EGFP-P2A-FGF19 or RCAS(B)/Fgf19-P2A-EGFP 62
3.4 Western Blot Analysis of cFgf19 and GFP Secretion 65
3.5 Comparison of 3C2 and GFP within RCAS(A)/EGFP-P2A-FGF19 Infected Chick Embryos 68
3.6 Effect of cFgf19 Overexpression on Innervation and Hair Cells 70
3.7 Effect of cFgf19 Overexpression on Cartilage Development around the Cochlear Duct 73
3.8 Effect of cFgf19 Overexpression on Proliferation within the Cochlear Duct 74
3.9 Test of cFgf19 Downstream Signaling 74
3.10 Effect of Fgf19 Overexpression on Fgf3 mRNA production 77
3.11 cFgfr4 Expression within and around the Developing Inner Ear 78
CHAPTER 4. DISCUSSION 80
4.1 Differences in cFg3 and cFgf19 Expression Within the Chick Basilar Papilla Compared to Published Data 80
4.2 Mechanisms of Action of cWnt9a, cFgf3, and cFgf19 to Induce Neural Side Fate in the Basilar Papilla 80
4.3 Reduction in GFP Production from RCAS(B)/Fgf19-P2A-EGFP DF-1 Transfected Cells 82
4.4 Fgf19 and EGFP Secretion by RCAS(A)/EGFP-P2A-FGF19 or RCAS(B)/Fgf19-P2A-EGFP Transfected DF-1 Cells 82

4.5 3C2 and GFP Expression Differences in RCAS(A)/EGFP-P2A-FGF19 Infected Chick Embryos 84
4.6 cFgf19 Overexpression Effect on Cartilage Formation 84
4.7 Fgf19 Overexpression Effect on p-ERK 85
4.8 Fgf19 Overexpression Effect on Fgf3 Expression 85
4.9 Fgfr4 Expression Around the Cochlear Duct 85
4.10 Fgf19 Overexpression Failure to Induce Phenotypic Changes in the Basilar Papilla or the Region Surrounding the Cochlear Duct 85
CHAPTER 5. FUTURE EXPERIMENTS 87
5.1 Examine Downstream Proliferation Genes in Response to cFgf19 87
5.2 Block Fgf Signaling to Determine the Role of cFgf19 with cWnt9a Overexpression 87
5.3 Determine the Role of cFgfr3 in the Chick Basilar Papilla Regarding Radial Asymmetry 89
REFERENCES 92

LIST OF TABLES

Table 1.1: Average normalized counts of transcripts for proteins linked to cWnt9a or the Fgf pathway following cWnt9a-overexpression (cWnt9a OE) RNA-seq data. n/s: no significant difference found between control and cWnt9a overexpression embryos. *: p-value < 0.05. Note the very low number of transcripts for a potential co-receptor for Fgfrs, β-Klotho, in both control and experimental samples. There is a high level of transcription for the four Fgfr genes. Data from (Munnamalai et al., 2017). 27

Table 2.1: List of virus concentrations for RCAS(A)/EGFP-P2A-Fgf19 and RCAS(B)/Fgf19-P2A-EGFP for day 1 and day 2 unconcentrated and concentrated vials.....50

LIST OF FIGURES

Figure 1.1: Bird and mammalian inner ears are homologous. A: Bird basilar papilla with hair cells labeled. The red neurons are the afferents and the blue neurons are the efferents. B: Mammalian cochlea with hair cells and innervation labeled. Adapted from (Fettiplace and Kim, 2014). 25

Figure 2.1: Maps of plasmids for cFgf19 overexpression. A) Map of RCAS(A)/EGFP-P2A-Fgf19 plasmid. Designed by Dr. M. Katie Scott with cloning done by GenScript using ClaI to insert EGFP-P2A-Fgf19 into the RCAS(A) virus as the backbone. B) Map of RCAS(B)/Fgf19-P2A-EGFP plasmid. Designed by Vashi Negi using Dr. M. Katie Scott's design as basis. Cloning done by GenScript using ClaI to insert Fgf19-P2A-EGFP into the RCAS(B) virus as the backbone. Notes: ClaI* site is blocked by Dam methylation. Slax12 was part of the shuttle vector used that provided ClaI sites. The unlabeled orange and green arrows represent the directions of the open reading frames. Abbreviations: gag: group-specific antigen; pol: DNA polymerase; env: envelope protein; Slax12 5'UTR/Slax12 Fragment: part of shuttle vector; RSV promoter: Rous sarcoma virus enhancer/promoter; lac operator: operator that lac repressor binds to; lac UV5 promoter: promoter for lac operator; AmpR promoter: promoter for β-lactamase production; AmpR: β-lactamase: confers resistance to ampicillin, carbenicillin, and other related antibiotics; ori: origin of bacterial replication; bom: basis of mobility region; rop: repressor of primer, keep plasmids at low-copy number 41

Figure 3.1: Wnt9a overexpression induced cFgf3 and cFgf19 expression. A & B: 3C2 (brown) expression indicated viral infection and the comparison shows cWnt9a expression only in the right ear. C & D: cFgf3 expression was robust throughout the basilar papilla with cWnt9a overexpression compared to a weak signal on the abneural side in the control left ear. E & F: Strong cFgf19 expression was found throughout the basilar papilla with cWnt9a overexpression, while it was confined to an abneural domain in the control left ear. In the SAG, the intensity of cFgf19 expression increased with cWnt9a overexpression. CD: cochlear duct; Ab: abneural side of basilar papilla; N: neural side of basilar papilla; SAG: statoacoustic ganglion 59

Figure 3.2: Wnt9a overexpression induced cFzd4 expression. A & B: 3C2 (brown) expression indicated viral infection and cWnt9a expression in the right ear. C & D: cFzd4 expression was found in the future homogene cell region and neural side of the basilar papilla in the wild-type embryos, but expression was extended in the basilar papilla of the right ears. CD: cochlear duct; Ab: abneural side of basilar papilla; N: neural side of basilar papilla 61

Figure 3.3: RCAS(A)/EGFP-P2A-Fgf19 and RCAS(B)/Fgf19-P2A-EGFP both produce GFP, but in different quantities. DF-1 cells were transfected with RCAS(B) (A & B), RCAS(A)/EGFP-P2A-Fgf19 (C & D), or RCAS(B)/Fgf19-P2A-EGFP (E & F). The cells were imaged with the same settings. All of three transfections showed similar expression of RCAS core protein (3C2+), but RCAS(B), without an insert, produced no GFP and RCAS(A)/EGFP-P2A-Fgf19 produced more GFP than RCAS(B)/Fgf19-P2A-EGFP. .....**Error! Bookmark not defined.**

Figure 3.4: RCAS(A)/EGFP-P2A-Fgf19 and RCAS(B)/Fgf19-P2A-EGFP both produce Fgf19 and GFP, but the protein sizes differ. DF-1 cells were transfected with RCAS(B), RCAS(A)/EGFP-P2A-Fgf19, or RCAS(B)/Fgf19-P2A-EGFP. Western blot analysis was done on membranes incubated with α-cFgf19 antibody and exposed to 1 or 20 minutes of chemiluminescence (A & B)

or GFP but the GFP membrane was incubated with α-GFP antibody and exposed to 1 minute of chemiluminescence (C). RCAS(A)/EGFP-P2A-Fgf19 transfected cells secreted cFgf19 at ~30 and ~35 kDa and GFP at ~25 and ~30 kDa. RCAS(B)/Fgf19-P2A-EGFP transfected cells secreted cFgf19 at ~25 kDa and GFP at ~25 kDa. The positive control for cFgf19 antibody was rhFgf19 and for GFP was free GFP.....67

Figure 3.5: RCAS(A)/EGFP-P2A-FGF19 injected tissue showed no changes in mesenchyme, number of proliferating cells in the basilar papilla, or innervation at E6. A & B: 3C2 and GFP expression from one section which is adjacent to the section in D. C & D: No change in mesenchyme labeled by Alcian blue around the cochlear duct or in innervation, neurofilaments labeled by 3A10 (linear axonal profiles), or in proliferation, labeled with PH3 (isolated brown punctae), within the abneural side of the basilar papilla. CD: cochlear duct; Ab: abneural side of basilar papilla; N: neural side of basilar papilla; SAG: statoacoustic ganglion; PH3: antibody against proliferating cells; 3A10: antibody against afferent innervation; NFs: neurofilaments labeled with 3A10; Alcian blue: stain for developing cartilage 70

Figure 3.6: RCAS(A)/EGFP-P2A-FGF19 injected tissue showed no changes in cartilage or innervation at E10. A & B: No alterations in hair cells and innervation, neurofilaments labeled by 3A10, were found in the right side compared to the left. C: GFP expression in same tissue section as B. D & E: No alterations in cartilage labeled with Alcian blue. F: GFP expression in same tissue section as E. CD: cochlear duct; Ab: abneural side of basilar papilla; N: neural side of basilar papilla; SAG: statoacoustic ganglion; 3A10: antibody against afferent innervation; NFs: neurofilaments labeled with 3A10; HCs: hair cells labeled with HCS-1; HCS-1: antibody against hair cells 72

Figure 3.7: RCAS(A)/EGFP-P2A-FGF19 injected tissue showed no changes in hair cell differentiation or innervation at E14. A: Cochlear duct with GFP expression on the abneural side (B inset). B: Abneural side of the basilar papilla with GFP expression and smaller number of pre-synaptic ribbons of afferent innervation labeled in red (white arrow indicates one example). C: Neural side of the basilar papilla with less GFP expression and larger number of pre-synaptic ribbons of afferent innervation labeled in red (white arrow indicates one example). CD: cochlear duct; AG: auditory ganglion; HCS-1: antibody against hair cells (blue); Ctbp2: antibody against pre-synaptic ribbons (red).....73

Figure 3.8: RCAS(B), RCAS(A)/EGFP-P2A-Fgf19, and RCAS(B)/Fgf19-P2A-EGFP all produce similar amounts of p-ERK1/2. DF-1 cells were transfected with RCAS(B) and showed no GFP (A & B), RCAS(A)/EGFP-P2A-Fgf19 (C & D), or RCAS(B)/Fgf19-P2A-EGFP (E & F), both of which had similar GFP expression. Each fluorescent color was imaged with the same settings. GFP was not enhanced with an antibody. 76

Figure 3.9: Virus encoding Fgf19 does not alter Fgf3 expression. RCAS(A)/Wnt9a injected embryos were compared to RCAS(A)/EGFP-P2A-Fgf19 injected embryos to see the difference in cFgf3 expression. cWnt9a overexpression increased cFgf3 expression (A & B) but cFgf19 overexpression did not alter cFgf3 expression (C & D). These embryos underwent in situ hybridization at the same time. CD: cochlear duct; Ab: abneural side of basilar papilla; N: neural side of basilar papilla 78

Figure 3.10: cFgfr4 is found within the basilar papilla and around the cochlear duct. RNAscope in situ hybridization for Fgfr4 was done on wild-type E6 (A) and E8 embryos (B) and showed the

greatest expression in the epithelium of the cochlear duct, but in the surrounding precartilage and cartilage of the developing otic capsule. CD: cochlear duct; Ab: abneural side of basilar papilla; N: neural side of basilar papilla 79

LIST OF ABBRIEVATIONS

Wnts	wingless-related integration site
Fgfs	fibroblast growth factors
Fzds	frizzled
Lrp	LDL receptor related protein
ROR	receptor tyrosine kinase like orphan receptor
Fgfrs	fibroblast growth factor receptors
PPD	pre-placodal domain
Bmps	bone morphogenic proteins
OEPD	otic-epibranchial placode domain
Pax	paired-box containing genes
siRNA	small interfering RNA
HH	Hamburger-Hamilton stage
Dlx	distal-less homeobox
Nkx-5.1	H6 family homeobox 3
SOHo-1	sensory organ homeobox 1
E	embryonic day
Gbx	gastrulation brain homeobox
ETS	erythroblast transformation specific
Etv	ETS Variant
SRY	sex determining region Y
Sox	(SRY)-box
Foxg1	forkhead box G1
Neurog1	neurogenin 1
Neurod1	neurogenic differentiation 1
P	post-natal day
TUNEL	terminal deoxynucleotidyl transferase dUTP nick end labeling
Msx1	muscle segment homeobox 1
ALV	avian leukosis virus
RCAS	replication-competent ALV LTR with splice acceptor

OE	overexpression
kDa	kilodaltons
ERK	extracellular signal-regulated kinase
p-(gene)	phosphorylated (gene)
HEK293	human embryonic kidney 293 cells
EMT	epithelial-mesenchymal transition
CYP7A1	cholesterol 7 alpha-hydroxylase
Lp(a)	lipoprotein (a)
Elk-1	ETS like 1
Snail	snail family transcriptional repressor 1
Twist	twist family BHLH Transcription Factor
GSK-3β	glycogen synthase kinase 3β
TCF4	transcription factor 4
FRS2	fibroblast growth factor receptor substrate 2
PBS	phosphate buffered saline
Tgfb1	Transforming Growth Factor Beta 1
Lim1	lim homobox 1
Tbx5	T-box transcription factor
Vax	ventral anterior homeobox
Prox1	prospero homeobox protein 1
PFA	paraformaldehyde
TFM	tissue freezing media
3C2	antibody against RCAS core protein
PH3	phospho-histone H3
3A10	neurofilament associated antigen
DAB	3'-Diaminobenzidine
EDTA	Ethylenediamine Tetraccetic Acid, Disodium Salt Dihydrate
TE buffer	Tris-EDTA
LB media	Lysogeny broth
DTT	dithiothreitol
DIG	digoxigenin
DEPC	diethyl pyrocarbonate

SSC	saline sodium citrate
HemoDe	d-Limonene
gag	group-specific antigen
pol	DNA polymerase
env	envelope protein
UTR	untranslated region
Slax12 5'UTR/Slax12 Fragment	part of shuttle vector
RSV promoter	Rous sarcoma virus enhancer/promoter
lac operator	operator that lac repressor binds to
lac UV5 promoter	promoter for lac operator
AmpR promoter	promoter for β-lactamase production
AmpR	β-lactamase
ori	origin of bacterial replication
bom	basis of mobility region
rop	repressor of primer
FSB	fetal bovine serum
DMEM	Dulbecco's Modified Eagle's Medium
BSA	bovine serum albumin
ICC	immunocytochemistry
NMWCO	molecular weight cut-off
rhFgf19	recombinant Fgf19
IHC	immunohistochemistry
HCS-1	antibody against hair cells
Ctbp2	antibody against pre-synaptic ribbons
SAG	statoacoustic ganglion
CD	cochlear duct
Ab	abneural side of the basilar papilla
N	neural side of the basilar papilla
NFs	neurofilaments labeled with 3A10
Alcian blue	stain for developing cartilage
HCs	hair cells labeled with HCS-1
AG	auditory ganglion

Vcam1	vascular cell adhesion molecule 1
Vcl	Vinculin
STAT1	signal transducer and activator of transcription 1
Fm	fibromelanosis
FLT3	Fm related receptor tyrosine kinase 3
$p75^{NTR}$	pillar cell marker

ABSTRACT

Proper development of the inner ear, including the cochlea, is necessary for normal hearing. Development of the inner ear requires many signaling molecules under both spatial and temporal control. These signaling molecules include the wingless-related integration site (Wnts) and the fibroblast growth factors (Fgfs) gene families. The embryonic chick inner ear was chosen as the model to study cochlear development due to its homology with the mammalian cochlea and the ease of access to the inner ear *in ovo*. Both the mammalian cochlea and the homologous chick basilar papilla contain two domains with their own type of hair cells and innervation. The neural side of the basilar papilla contains the tall hair cells innervated by the afferent axons which takes the noise signal to the brain. The abneural side of the basilar papilla contains the short hair cells innervated by the efferent axons which receive signals from the brain to turn down added gain.

Previous research showed that virally induced cWnt9a overexpression within the basilar papilla generated a neural side phenotype across the basilar papilla (Munnamalai et al., 2017). These basilar papillas contained more tall hair cells and increased innervation at embryonic day 18 (E18) than their wild-type counterparts. Additionally, there were many differentially expressed genes found to be downstream of cWnt9a including cFgf3 and cFgf19. This project focused on determining the role of cFgf19 in inducing a neural side phenotype in the basilar papilla. First, in situ hybridization was used to determine the cFgf3 and cFgf19 mRNA transcript location with cWnt9a overexpression. Both Fgfs were found across the basilar papilla. Next, a possible cWnt9a receptor, cFzd4, which was upregulated with cWnt9a overexpression, was found in the neural side of the basilar papilla. cFgf19 was then overexpressed using one of two different vectors: RCAS(A)/EGFP-P2A-Fgf19 or RCAS(B)/Fgf19-P2A-EGFP in which the order of cFgf19 transcription was altered. RCAS(B)/Fgf19-P2A-EGFP was found to produce less GFP when transfected into DF-1 cells than RCAS(A)/EGFP-P2A-Fgf19. Additionally, RCAS(B)/Fgf19-P2A-EGFP transfected cells produced secreted fusion proteins of GFP and Fgf19, compared to RCAS(A)/EGFP-P2A-Fgf19 transfected cells which produced secreted individual proteins. The viruses were injected into the otocyst at E3 and the embryos harvested several days later including at E6, E10, and E14. Inner ears injected with either virus showed no changes in innervation, hair cells, proliferation, cartilage formation around the cochlear duct, cFgf3 expression, or phosphorylation of ERK. To determine understand where Fgf19 could be producing an effect, the

location of a possible receptor, Fgfr4, was determined in wild-type embryos. At E6 and E8, cFgfr4 was found within the basilar papilla, but many more transcripts were found surrounding the cochlear duct. Overall, the role of Fgf19 in neural side fate of the basilar papilla was not determined. Possible reasons for the lack of phenotypic changes include nonfunctional Fgf19 being secreted which could not bind and induce downstream signaling, Fgf19 being responsible for an untested aspect of the cWnt9a overexpression model, or other misregulated genes would be needed for the phenotypic change to occur.

CHAPTER 1. INTRODUCTION

1.1 Inner Ear Overview

Within the vertebrate inner ear are sensory organs for both balance and hearing. Mammalian balance is controlled by the vestibular organs: the cristae ampullares (anterior, posterior, and lateral), utricular macula, and saccular macula. Hearing is controlled by the organ of Corti within the cochlea, named for its coils in the mammalian inner ear. During development of these organs, many signaling molecules are required, including those of the wingless-related integration site (Wnts) and the fibroblast growth factors (Fgfs) gene families.

1.2 Wnt Overview

Members of the Wnt gene family are known for their roles in development and disease (Niehrs, 2012). These secreted proteins have many known receptors, including the ten frizzled proteins (Fzds). There are 19 human and mouse Wnts and 18 chick Wnts (Fokina and Frolova, 2006) (Niehrs, 2012). The three main signaling pathways used by Wnts are β-catenin dependent signaling and two β-catenin independent pathways: PCP signaling and Wnt-Ca^{2+} signaling (Niehrs, 2012). If a Wnt binds to a Fzd receptor, the signaling pathway followed depends on the presence or absence of other co-receptors, including LDL receptor related protein 5 (Lrp5), Lrp6, receptor tyrosine kinase like orphan receptor 1 (ROR 1), and ROR2 (Niehrs, 2012).

1.3 Fgf Overview

Fgfs are named for their function as growth factors for fibroblasts. They were discovered in the 1970's and were shown to be mitogens for a mouse embryonic fibroblast line, 3T3 cells (Gospodarowicz, 1974). In addition to roles in development, Fgfs also are involved in disease and metabolism (Itoh and Ornitz, 2011) (Ornitz and Itoh, 2015). There are three general groups of Fgfs, the canonical, intracellular, and hormone-like Fgfs. The canonical and hormone-like Fgfs are secreted and bind to fibroblast growth factor receptors (Fgfrs) for which they have different affinities. The canonical Fgfs include five different subfamilies, which are Fgf1/2/5, Fgf3/4/6, Fgf7/10/22, Fgf8/17/18, and Fgf9/16/20. These Fgfs act as paracrine factors, using heparin or heparin sulfate as co-factors. The intracellular Fgfs, Fgf11, Fgf12, Fgf13, and Fgf14, are not

secreted and act without binding to an Fgfr. The final group are hormone-like or endocrine Fgfs, which include Fgf15/19 (orthologs, 15: mice, 19: humans, chickens, etc.), Fgf21, and Fgf23 (Wright et al., 2004) (Itoh and Ornitz, 2011) (Ornitz and Itoh, 2015). Fgf15/19 and Fgf21 use β-Klotho as a co-factor, and Fgf23 uses α-Klotho; however, they can still bind to heparin or heparin sulfate but with reduced affinity (Ornitz and Itoh, 2015).

1.4 Vertebrate Inner Ear Development

Early development of the inner ear can be traced to the pre-placodal domain (PPD), which is formed after exposure to Fgfs from the neural plate and cranial mesoderm and the inhibition of Wnts and bone morphogenic proteins (Bmps) reviewed by (Groves and Fekete, 2012). Fgf signaling induces specification of the PPD into the otic-epibranchial placode domain (OEPD) and the ectoderm. Then the OEPD is segregated into the otic placode, epibranchial placode, and epidermis using Wnt and Fgf signaling. The otic placode is marked by paired-box containing genes 2 & 5 (Pax-2/5). Which Fgfs are required for development from the PPD to the otic placode varies by species.

In the chick embryo, otic placode development requires endoderm-derived cFgf8 inducing cFgf19 expression in the mesoderm (Ladher et al., 2005). cFgf8 involvement in otic placode development was discovered by electroporating small interfering RNA (siRNA) against cFgf8 into one side of the chick embryo at Hamburger-Hamilton stage (HH) 4. At stage 7, the siRNA side had reduced Fgf19 mRNA expression and at stage 12, there was less Pax-2 mRNA with either no or a smaller otic placode.

cFgf19 turns on cWnt8a (originally called cWnt8c), observed when Fgf19-soaked beads were added to pre-neurula stage 5 ectoderm and cWnt8a expression was stimulated, although cWnt8a was not found in the presumptive otic region (Ladher et al., 2000). cWnt8a then turned on cFgf3. cWnt8a was transfected into COS cells, a fibroblast-like cell line from African green monkey kidneys, and the cells were added to a stage 7 mesendoderm (presumptive otic region), resulting in cFgf3 expression. When both Fgf19 beads and Wnt8a-transfected COS cells were added to the stage 7 mesendoderm (presumptive otic region), then otic placode markers were expressed, including distal-less homeobox 5 (Dlx-5), Pax-2, Nkx-5.1, also known as H6 family homeobox 3, and sensory organ homeobox 1 (SOHo-1). In summary, the pathway appears to be

Fgf8 → Fgf19 → Wnt8a → Fgf3 → otic placode. Altogether these data suggest that cFgf8, cFgf19, and cWnt8a are all involved in creating the otic placode in the chick embryo.

In contrast, otic induction within the mouse uses different members of the same families of signaling molecules. In mice where Fgf15 (the mouse ortholog of Fgf19) was eliminated, there were no changes to the otic vesicle at embryonic day 9.5 or 10 (E9.5 or E10.5) (Wright et al., 2004). However, Fgf15-expressing cells were able to induce expression of Pax-2 and Nkx-5.1 expression in 81% and 100%, respectively, of stage 4 ectodermal explants compared to 66% and 100%, respectively, with Fgf19-coated beads (Wright et al., 2004). This shows that Fgf15 and Fgf19 similarly induce otic placode markers. Fgf15 has a role in otic development but there is likely one or more redundant signaling molecules for Fgf15 in the mouse developing ear.

Two other Fgfs with roles in mouse otic development are Fgf3 and Fgf10. In mouse embryos in which Fgf3 and Fgf10 were both absent, the expression patterns of otic placode markers Pax-2, Pax-8, Dlx-5, and gastrulation brain homeobox 2 (Gbx2) are all altered (Wright and Mansour, 2003). Both Pax-2 and Pax-8 were present in the otic placode when the embryos were heterozygous mutants for both Fgf3 and Fgf10; however, when both Fgfs were completely knocked out, neither Pax-2 nor Pax-8 were present in the region where the otic placode was expected. Dlx-5 was found in the heterozygous mutants within the otic cup, but the Fgf3/10 double-knockout showed Dlx-5 expression in a region of thickened ectoderm more ventral and not in the region that should have been the otic cup.

However, Fgf3 and Fgf10 are not completely redundant molecules within the mouse embryo during otic development. Fgf3-knockout mice (with intact Fgf10) had increased levels of Dlx-5 in the otic vesicle compared to when Fgf10 was knocked out and Fgf3 was present (Wright and Mansour, 2003). As such, Fgf10 is needed to induce Dlx-5 expression. Pax-2 was different, though: the levels and location of Pax-2 within the otic vesicle were not altered when only one of the Fgfs was removed compared to when both were present. Fgf3 and Fgf10 are both needed for normal otic placode development in the mouse with some redundant and some differing roles. Later, the otic placode invaginates to form the otic pit reviewed by (Groves and Fekete, 2012). This otic pit or cup later closes to form the otic vesicle, also called the otocyst. Fgf3 and Fgf10 are not involved in otic vesicle formation as when they were conditionally deleted with a Pax-2-Cre driver starting at E8.5, the otic vesicle still formed (Urness et al., 2018).

The combination of Fgf3 and Fgf10 are needed for proper morphogenesis of the mouse inner ear into the semicircular canals and cochlear duct (Urness et al., 2018). When Fgf10 was conditionally knocked out using a Pax-2-Cre driver, the posterior semicircular canals did not form, and the cochlear duct was shorter and narrower than the no-Cre control; however, if Fgf3 was conditionally knocked out, no morphological changes are observed. When Fgf10 was knocked out and only one copy of Fgf3 remained, the semicircular canals were missing, and the cochlear duct was much smaller. Finally, if both copies of both genes were knocked out, the resulting ear had no visible organs.

The specific role of Fgf3 and Fgf10 is to turn on various lateral otic vesicle genes, including erythroblast transformation pecific (ETS) Variant 5 (Etv5), sex determining region Y (SRY)-box 2 (Sox2), forkhead box G1 (Foxg1), and Bmp4, and for otic ganglion development (Urness et al., 2018). All of these downstream genes were downregulated when both Fgf3 and Fgf10 were conditionally knocked out. Interestingly, expression of Pax-2, which marks the more medial and ventral parts of the developing otocyst, was upregulated when both Fgfs were knocked out. Additionally, by E10.5 both neurogenin 1 (Neurog1) and neurogenic differentiation 1 (Neurod1), genes found in the otic ganglion, were also downregulated. As such Fgf3 and Fgf10 help specific the lateral side of the inner ear and the otic ganglion and so these double knock-out experiments gave the inner ear a medial fate instead.

The likely receptor for mediating this otic patterning function of Fgf3 and Fgf10 is Fgfr2b. When a dominant-negative form of Fgfr2b was introduced and sustained starting at E8.5 to E13.5 and ending at E15.5, the inner ears are deformed with various organs smaller or non-existent; the most deformed phenotypes were observed when the dominant-negative was introduced earlier, phenocopying the Fgf3 and Fgf10 double knock-out experiments (Urness et al., 2018). One specific role for the Fgfr2b ligands is proliferation: when the Fgfr2b dominant-negative was present from E9.25 to E10.25, there was a significant decrease in otic epithelial proliferation at E10.25. Overall, these data show that Fgf3 and Fgf10, and possibly other ligands that interact with Fgfr2b, are needed for normal morphogenesis of the inner ear in the mouse.

1.5 Cochlear Cell Specification by Fgfs

Within the mammalian organ of Corti are the lateral and medial compartments that contain distinct types of hair cells and supporting cells (Wan et al., 2013). On the lateral side there are

three rows of outer hair cells,distinct supporting cells: the Deiters' cells and the outer pillar cells, and Hensen's cells. These hair cells are primarily innervated by efferent nerves. On the medial side there is one row of inner hair cells, supporting cells: inner phalangeal cells, and other cells: the inner pillar cells, inner border cells, and border cells. These hair cells are innervated by the afferent neurons. This section describes how the genetic manipulation of the Fgf signaling pathway in mice, often targeted to the inner ear or its surrounding tissues, has provide experimental evidence about the role of Fgfs in cochlear cell fate specification and patterning.

Prior to cell differentiation, there is a prosensory domain comprised of sensory progenitors. Fgfs are involved in determining the number of progenitors found within the ear. More progenitors generates a longer and/or wider cochlea due to more cells being present. Two possible Fgfs involved are Fgf20 and Fgf9. In E11.5 mice embryos, Fgf9 was found within the nonsensory part of the cochlear duct, whereas Fgf20 was found in part of the Sox2-positive prosensory region (Huh et al., 2015). In mice with loss of Fgf20 and Fgf9, the length of the cochlea was significantly shorter than normal or when the mice had loss of only one of the genes. Mechanistically, Fgf9 was needed at both E11.5 and 12.5 for sensory progenitor proliferation. When Fgf20 was inactivated, there was no difference in the amount of Sox2-positive proliferating cells at these same ages. This could indicate an alternative role for Fgf20 in determining the length of the cochlea; it plays a later role in the timing of sensory cell differentiation, as discussed below.

Surprisingly, both Fgfr1 and Fgfr2, found in the mesenchyme surrounding the inner ear, are needed to ensure correct numbers of sensory progenitors in the inner ear epithelium (Huh et al., 2015). When Fgfr1 and Fgfr2 were both conditionally knocked out in the mesenchyme there was a significant decrease in cochlear length even more so than if just one of the Fgfrs was knocked out. Moreover, there are fewer Sox2-positive proliferating cells found when both Fgfrs were knocked out. However, Fgf20 may not serve as the only ligand for Fgfr1 for the specification of the prosensory epithelium because when Fgfr1 was conditionally knocked out, there was a decrease in Sox2 mRNA and protein which was greater than when Fgf20 was knocked out (Yang et al., 2019a). When Sox2 expression was decreased in mice with one hypomorphic allele of Sox2 and the loss of the other allele, the cells exit the cell cycle slower indicating a delay in prosensory specification, as cells must exit the cell cycle for specification to finish. Moreover, Sox2 was found to be upstream of Fgf20 as the hypomorphic Sox2 mouse lost Fgf20 expression but not Fgfr1 expression. These data suggest a model whereby Fgf9, Fgf20, and one or more Fgfs are

produced in the epithelium of the otic vesicle and are secreted into the surrounding mesenchyme where they bind to Fgfr1 and Fgfr2. The cells then send signals back to the otic vesicle to determine the number of sensory progenitors found within the cochlea by ensuring the proper amount of proliferation and possibly another function (as Fgf20 does not reduce proliferation), and therefore the cochlear length.

Differentiation of these sensory progenitors also involves Fgfs, including Fgf20. Fgf20 null mice, in which one exon of both copies of Fgf20 was changed to b-galactosidase, are hearing impaired (Huh et al., 2012). At post-natal day 4 (P4), these mice have normal amounts of inner hair cells and significantly fewer outer hair cells compared to heterozygous (control) mice in which only one copy of Fgf20 was modified. However, by P7, the control and experimental mice had similar amounts of hair cell markers, indicating that hair cell differentiation was only delayed with loss of Fgf20. The supporting cells were not delayed but some were missing as there were fewer lateral compartment cells (Deiters' cells and outer pillar cells) per unit area. Fgf20 likely is involved in hair cell differentiation prior to E15.5 due to the ability of Fgf9 to partially rescue outer hair cells if delivered to the experimental mice cochlea explants at E14.5 but not E15.5. However, in mouse embryos where Fgf9 was knocked out, there was no change in outer hair cells per unit area, but there was a decrease when Fgf20 was nonfunctional (Huh et al., 2015). This suggests that Fgf20 is the usual signaling molecule to specify outer hair cells but that Fgf9 can be used if needed to partially supplement it. Supporting cells were also increased with the addition of Fgf9 at E14 in the cochlear explants from experimental mice (Huh et al., 2012) . Fgf20 and/or Fgf9 are therefore needed for normal lateral compartment development.

Fgf20 likely binds to Fgfr1 to specify outer hair cells. Both of these genes are found in the otic epithelium and when a Fgf20-Cre driver was used to knock out Fgfr1, the outer hair cell number greatly decreased, but not if Fgfr2 was knocked out (Huh et al., 2015). However, Fgf20 is not likely the only signal necessary for the development of outer hair cells. When Fgf20 knockout mice were compared to conditional knockout Fgfr1 knockout mice, there is a difference in the number of outer hair cells present (Yang et al., 2019a). There was a 76% reduction in the number of outer hair cells with the Fgf20 knockout mouse, but a 97% loss with the Fgfr1 conditional knockout. This suggests that multiple ligands, in addition to Fgf20, may bind to Fgfr1 to specify outer hair cells in mice.

1.6 Innervation of the Cochlea

The hair cells of the inner ear must be innervated to send signals to the brain. Afferent neurons innervate the inner hair cells and are responsible for sending the sound information into the brain for it to be processed by the brain. Efferent neurons innervate the outer hair cells and are responsible for turning down the added gain through the axons receiving signals from the brain. Fgfs also appear to play a role in the afferent innervation of the inner ear. When Fgf8, 10, or 19 were added to chicken statoacoustic ganglion neurite explants staged as stages 20-25, all three Fgfs resulted in increases in neurite outgrowth and significant decreases in cell death measured through a terminal deoxynucleotidyl transferase dUTP nick end labeling (TUNEL) assay (Fantetti and Fekete, 2012). These three Fgfs then may play a role in inner ear innervation at earlier ages based on these data, possibly by influencing neuronal survival.

Later ages may require other Fgfs for cochlear innervation such as Fgf2. When Fgf2 was added to chicken statoacoustic ganglia cultured at stages 20-25 (E4-E5), there was no change in neurite outgrowth (Fantetti and Fekete, 2012). It should be noted these neurites could be vestibular or cochlear. However, when Fgf2 was added to chick cochlear ganglion cell explants at later ages, the survival of the neurons was increased when added at stage 29 (E6) to stage 36 (E10) (Carnicero et al., 2001). At stage 34, Fgf2 addition increased neurite extension of the cochlear neurons and Fgfr1, a possible receptor, was expressed and colabeled with TuJ1, a marker for neurons. It is possible that Fgf2 is secreted and binds to Fgfr1 to promote the survival of cochlear neurons. Other studies have shown the ability of Fgf2 to bind to Fgfr1b and 1c (Ornitz and Itoh, 2015).

In addition to Fgfr2's role as the Fgf3 and Fgf10 receptor in the cochlea, it appears to also be involved in cochlear innervation in mice. When Fgfr2 isoform IIIb is deleted, substantial cell death as measured by TUNEL in the cochleovestibular ganglion at E13, compared to the control ear, which has much less cell death at that age (Pirvola et al., 2000). Moreover, some of the nerve fibers that do remain are found close to the otocyst, but are not found innervating the epithelium.

1.7 The Auditory Organ of the Bird

In birds, the hearing organ is sickle-shaped and called the basilar papilla. Both hair cells of both the mammalian cochlea and avian basilar papilla have hair cells that vary along their radial axes. The hair cells communicate with the nerve fibers and are essential for proper auditory

function. If the hair cells do not develop properly, hearing problems can occur. In humans, 50% or more of the cases of hearing loss found at birth or during childhood are a result of genetic factors (Yang et al., 2019b).

In order to study the genes involved in inner ear development, the chicken embryo was used as the model system. The avian inner ear has radial asymmetry similar to the mammalian inner ear, but with greater ease of access to the ear during embryonic development compared to the mouse ear. The radial axis in both mammalian and avian hearing organs is divided into two parts which are called the neural and abneural sides in the bird (Fettiplace and Kim, 2014). Mammalian lateral compartment containing outer hair cells is homologous to the abneural side of the basilar papilla containing short hair cells in birds (Figure 1.1). Mammalian medial compartment containing inner hair cells is homologous to the neural side of the basilar papilla containing tall hair cells in birds (Figure 1.1).

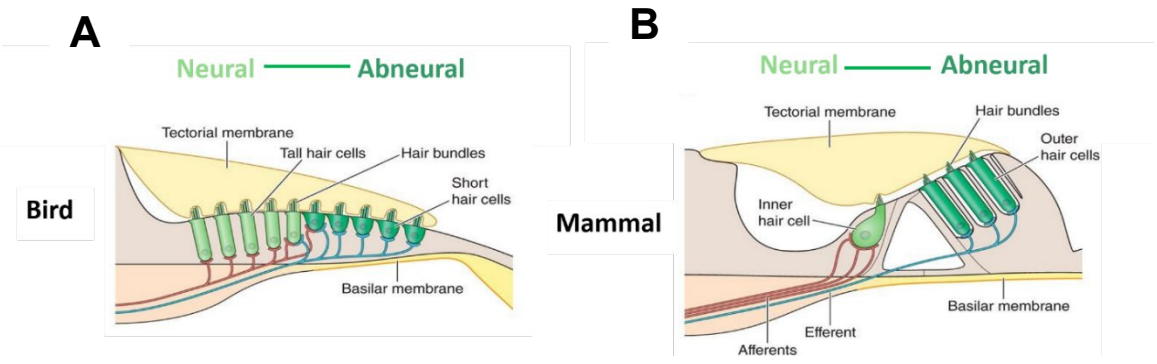

Figure 1.1: Bird and mammalian inner ears are homologous. A: Bird basilar papilla with hair cells labeled. The red neurons are the afferents and the blue neurons are the efferents. B: Mammalian cochlea with hair cells and innervation labeled. Adapted from (Fettiplace and Kim, 2014).

Within the mammalian cochlea, both Wnts and Fgfs are hypothesized to be involved in radial patterning due to their asymmetric expression across the radial axis reviewed by (Groves and Fekete, 2012). This project studies these two gene families for their involvement in the radial patterning of the avian basilar papilla during development.

1.8 Wnt9a Involvement in Radial Patterning of the Basilar Papilla

Wnt family members have been shown to be involved in patterning the organs of the chick inner ear. Early research into Wnt signaling in the chick developing ear showed that when truncated β-catenin, presumed to be a constitutively-active form, was overexpressed at stages 8-10 (E1.5-2) or stages 15-25 (E2.5-E4), ectopic sensory patches of vestibular hair cells and supporting cells were found in the chicken basilar papilla one to two weeks later (Stevens et al., 2003). This was demonstrated by hair cell morphology resembling vestibular hair cells with a kinocilum and the supporting cells between the hair cells having larger apical projections, and the presence of muscle segment homeobox 1 (Msx1), a molecular marker for vestibular sensory organs was found within the basilar papilla. Ectopic vestibular patches were also found when Wnt3a was overexpressed at stages 17-22.

Other research has been done to see which Wnt ligands effect the cochlear duct, including Wnt9a. cWnt9a transcripts have been found during otic development in the neural side of the basilar papilla at stage 25 (E4.5/E5) and then found in the future homogene cell region, located adjacent to the neural edge of the prosensory part of the basilar papilla, by stage 27 (E5/E5.5) (Sienknecht and Fekete, 2008) (Munnamalai et al., 2017). To determine its role, cWnt9a was overexpressed through the insertion of the gene into an RCAS virus. RCAS viruses (replication-competent ALV [avian leukosis virus] LTR with splice acceptor) are avian retroviruses (Hughes, 2004). These viruses are used to overexpress genes in birds and are capable of spreading to other dividing cells to increase the number of cells with the overexpression gene.

The RCAS(A)/Wnt9a virus was injected into the right otic vesicle at E3, with the left ear serving as a control (Munnamalai et al., 2017). The embryos were harvested at several timepoints, including E6 and E18. Overexpression was confirmed and shown through the presence of transcripts across the E6 basilar papilla within the prosensory domain. cWnt9a was shown to alter the radial patterning through the loss of the abneural side of the basilar papilla, leaving a mostly or completely neural-side fate. The hair cells present were primarily tall hair cells, and at E18, the innervation of the hair cells in the basilar papilla was significantly increased compared to the control. Furthermore, RNA-seq showed differential gene expression through comparison of E6 basilar papillas injected with either RCAS(A) parent virus (as a control) or RCAS(A)/Wnt9a. There were 24 ears pooled per experimental group, and three groups were obtained to give biological replicates. A sampling of the RNA-seq data is shown below in table 1.1; of note are

cFgf3 and cFgf19, whose mRNA transcripts were significantly increased following the overexpression of cWnt9a. Thus, the transcriptional regulation of both cFgf3 and cFgf19 is downstream of cWnt9a. This current study is a follow-up to the cWnt9a research focusing on some of the overexpressed genes, mainly cFgf19, to determine the role of cFgf19 in the radial patterning of the chick basilar papilla.

Table 1.1: Average normalized counts of transcripts for proteins linked to cWnt9a or the Fgf pathway following cWnt9a-overexpression (cWnt9a OE) RNA-seq data. n/s: no significant difference found between control and cWnt9a overexpression embryos. *: p-value < 0.05. Note the very low number of transcripts for a potential co-receptor for Fgfrs, □-Klotho, in both control and experimental samples. There is a high level of transcription for the four Fgfr genes. Data from (Munnamalai et al., 2017).

	cFgf3	cFgf19	cFzd4	cβKlotho	cFgfr1	cFgfr2	cFgfr3	cFgfr4
Control	476.7	899.9	4207.4	3.7	4139.4	9476.2	8412.5	456.7
cWnt9a OE	1527.2	2529.8	7254.4	2.9	4149.8	8096.8	5251.5	462.3
Significance	*	*	*	n/s	n/s	n/s	n/s	n/s

1.9 Fgf19 Overview

Fgf19 was first discovered in 1999 simultaneously in two different labs in several cell lines and tissue types, including a neuroepithelial cell line, Ntera-2, a colon adenocarcinoma cell line (SW480), human fetal brain, retina, skin, cartilage, kidney, and small intestine tissue, and adult gall bladder tissue (Nishimura et al., 1999) (Xie et al., 1999). As previously described, Fgf19 and Fgf15 are orthologs with the Fgf19 protein being 51% identical to the mouse Fgf15 protein (Nishimura et al., 1999), and found in the same chromosomal location after Fgf3 and Fgf4 (human 11q13.3 and mouse 7F5) (Wright et al., 2004). Thus, Fgf19 is, considered the human version of Fgf15. Comparing the chick and mouse precursor proteins using a blast search reveals that cFgf19 (NP_990005.2) is 41% identical to mFgf15 (NP_032029.1) (Altschul et al., 1997) (Altschul et al., 2005). Additionally, cFgf19 is 64% identical to precursor human Fgf19.

1.10 Fgf19 Secretion and Signaling

Human Fgf19 has a 22 amino acid secretion signal on its N-terminus (NP_005108.1) allowing secretion for movement to cells with the correct receptor. Initially, it was reported that

human Fgf19 bound exclusively to Fgfr4 with very high affinity. However, binding assays of Fgf19 with various Fgfrs in which the samples were run on a Western blot with reducing conditions showed weak bands of approximately 40 kilodaltons (kDa) in the lanes where Fgf19 was combined with Fgfr1, Fgfr3-IIIb, or Fgfr3-IIIc, compared to the strong ~33 kDa band in the Fgfr4 lane (Xie et al., 1999). These bands suggest that Fgf19 could bind to other Fgfrs. However, the reason for the larger size bands is unclear. Indeed, more recently, it has been reported that Fgf19 binds and acts through Fgfr1c, 2c, 3c, and 4 (Wu et al., 2009). Fgf19 and a receptor were added to L6 rat myoblasts and the activity of a known downstream pathway: RAS-RAF-ERK1/2-MAPK was measured through the phosphorylation of extracellular signal-regulated kinases (ERK) reviewed by: (Liu et al., 2020). Fgf19 binding to Fgfr1c, 2c, 3c, or 4 resulted in increased phosphorylated ERK (p-ERK).

Additionally, three different co-factors have been shown to be required or enhance downstream signaling. The co-factor used varies based on the receptor. Fgfr1c, 2c, and 3c require the single-pass transmembrane protein β-klotho for signaling to lead to phosphorylation of ERK (Wu et al., 2009). Only when Fgf19 binds to Fgfr4 can this signaling occur in the absence of β-klotho. The C-domain of Fgf19 (the last 39 amino acids) is likely responsible for this binding to β-klotho as deletion of this region prevents signaling to leads to the phosphorylation of ERK using any receptor other than Fgfr4. If the Fgf19-Fgfr4 ligand-receptor pair does not utilize β-klotho as a co-factor, it may instead use the polysaccharides, heparin or heparin sulfate. *In vitro* binding of Fgfr4 with Fgf19 was measured using a solid-phase binding assay in the presence of β-klotho or heparin. Arbitrary units were assigned to the interactions. The interaction of Fgf19 and Fgfr4 when in the presence of β-klotho was close to 1 compared to about 0.75 with heparin. Although Fgf19 binds better to Fgfr4 in the presence of β-klotho, the binding interaction with heparin was still quite high. When comparing the ability of Fgf19 to bind to Fgfrs 1-4 in the presence of heparin, a pull-assay showed substantial Fgf19 binding to Fgfr4 compared to Fgfr1c, 2c, and 3c (Wu et al., 2007). The amount of Fgf19 bound to Fgfr4 was even greater when heparin and β-klotho were added and the amount of p-ERK was higher when both β-klotho and heparin were added. Finally, Fgf19 plus heparin with β-klotho induced downstream signaling leading to increased phosphorylated ERK compared with no heparin added.

In addition to heparin and β-klotho, another klotho single-pass transmembrane protein, α-klotho may also serve as a co-factor for Fgf19. Pull-down assays show that Fgf19 binds better to

Fgfr4 when plasmids containing α-klotho were added to the cells, and when α-klotho and heparin were added, the interaction is even greater (Wu et al., 2007). When α-klotho plasmids were added human embryonic kidney 293 (HEK293) cells with Fgf19, there was increased p-ERK, although less than when β-klotho plasmids were added instead of the α-klotho plasmids. When none of these three potential co-factors were present, there was no significant amount of binding of Fgf19 to Fgfr4 suggesting that one or more is required for much if any binding to occur. All of this evidence suggests that Fgf19 uses β-klotho, heparin, and/or α-klotho as a co-factor(s) to start downstream pathways in cells.

The process of Fgf19 signaling generally occurs when Fgf19 binds to both Fgfr4 and β-klotho in a dimer form reviewed by (Liu et al., 2020). This binding results in the phosphorylation of the tyrosine kinase domains of the Fgfr4 receptor. Other than the RAS-RAF-ERK1/2-MAPK pathway other signaling cascades include the JAK/STAT and PI3K-AKT pathways and epithelial-mesenchymal transition (EMT).

1.11 The Roles of Fgf19 in Human Adult Tissue and Disease

Fgf19 plays roles in human adult tissue. One of these tissues is the liver where it regulates bile acid production by decreasing the amount of its rate-limiting enzyme: cholesterol 7 alpha-hydroxylase (CYP7A1) (Holt et al., 2003). Additionally, Fgf19 lowers the production of lipoprotein (a) (Lp(a)), a lipoprotein that is elevated in atherosclerosis (Chennamsetty et al., 2012). Fgf19 binds to Fgfr4, which turns on the MAP/ERK1/2 signaling pathway. This pathway results in phosphorylated ETS like 1 (Elk-1) binding to the negative control element of the Lp(a) promoter. Additionally, Fgf19 injections in mice leads to lower glucose levels in the blood (Fu et al., 2004).

Fgf19 overexpression has been found in various cancers including liver and lung cancer (Li et al., 2020) (Raja et al., 2019). Two lung squamous cell carcinoma lines, H520 and SK-MES-1, show increased levels of Fgf19 mRNA and protein when ER stress is induced using thapsigargin or tunicamycin (Li et al., 2020). Cell proliferation was also increased when Fgf19 was added to SK-MES-1, HCC15, and H1703 lung squamous cell lines. Moreover, Fgf19 overexpression increased markers associated with EMT, including N-cadherin, snail family transcriptional repressor 1 (Snail), twist family BHLH Transcription Factor (Twist), and Vimentin mRNA and N-cadherin and Vimentin protein.

1.12 Fgf19's Effect on Cell Proliferation

Initially, it was believed that unlike other Fgfs, Fgf19 did not have mitogenic activity as there was no increase in proliferation in fibroblasts, specifically 3T3 cells and primary human foreskin, or K562 cells, which are erythroleukemia cells (Xie et al., 1999). However, it is now known that Fgf19 is involved in proliferation in several different cell types. Keratinocytes are one of these cell types, which are studied due to their hyperproliferation in psoriasis. When HaCaT cells, a keratinocyte cell line, were given M5, a cytokine cocktail known to increase Fgf19 expression and proliferation, and an shRNA against Fgf19, there was a significant decrease in proliferating cells when there was less Fgf19 expression (Yu et al., 2019). Moreover, SK-MES-1 cells, a lung squamous cell carcinoma cell line when Fgf19 was added, had increased proliferation (Li et al., 2020). Furthermore, mice attached to a Fgf19 osmotic pump who were also given daily Fgf19 injections had increased proliferating hepatocytes compared to control mice (Wu et al., 2011).

Different molecular mechanisms have been proposed as to how Fgf19 induces proliferation within cells. In keratinocytes, when HaCaT cells are given M5 with or without Fgf19, there was an increase in phosphorylated glycogen synthase kinase 3β (p-GSK-3β), active β-catenin, and transcription factor 4 (TCF4) activity (Yu et al., 2019). The β-catenin activity was necessary for proliferation because if siRNA against it is used, there was less proliferation. As such, one proliferation mechanism is that Fgf19 binds to a receptor, which leads to pGSK-3β, to turn it off, so that β-catenin can be activated and go to the nucleus to turn on TCF4 transcriptional activity. This pathway could explain how psoriasis leads to hyperproliferation; however, it would indicate Fgf19 was upstream of canonical Wnt signaling, which is opposite of the experiments described here with Wnt signaling being upstream of changes in Fgf19 (and Fgf3) transcription.

Another mechanism proposed is that Fgf19 increases ERK/AKT signaling to induce proliferation (Li et al., 2020). When SK-MES-1 cells are given human Fgf19, there were increases phosphorylation of fibroblast growth factor receptor substrate 2 (p-FRS2), Fgfr4, AKT, and ERK. The authors proposed ERK/AKT signaling pathway for which proliferation occurred but only link AKT signaling with increased proliferation. When an m-Tor inhibitor, AZD2014, was given to SK-MES-1 cells with Fgf19 overexpression, there were significant decreases in p-AKT and tumor volumes sizes, indicating the AKT pathway is involved in proliferation. This model would have Fgf19 binding to Fgfr4, which gets phosphorylated. Frs2, membrane-anchored signal transducing

adaptor protein, would also bind to Fgfr4 and get phosphorylated, leading to downstream AKT and ERK signaling. It is possible that the phosphorylation of GSK-3β occurs via AKT, which would link the two listed possible mechanisms together; however, GSK-3β can be phosphorylated by multiple kinases, including PKA, so this is unclear (Hermida et al., 2017). However, this is a possible mechanism for the increased proliferation seen with cWnt9a overexpression.

More evidence for the Fgfr4 as the receptor used by Fgf19 to induce proliferation came from liver proliferation studies where mice were given daily Fgf19 injections and an osmotic Fgf19 pump (Wu et al., 2011). However, these mice were given a modified version of Fgf19 in which the first 24 amino acids are replaced with the first 20 amino acids of Fgf21, which was shown to have very little binding affinity to Fgfr4. These mice had significantly less proliferating hepatocytes, but interestingly, more proliferation than the phosphate buffered saline (PBS) control mice. This indicates that Fgf19 mediated proliferation in the liver is primarily done using Fgfr4.

Possible downstream genes turned on by Fgf19 to induce proliferation include Transforming Growth Factor Beta 1 (Tgfb1). When mice were fasted to induce low Fgf15 expression and were given one dose of human Fgf19 at 1mg/kg body weight, there were many differentially expressed proteins found within the liver 12 hours later (Massafra et al., 2017). Of the many genes found, Ingenuity upstream regulator analysis found several to be upstream regulators of proliferation. Tgfb1 was one of these proteins, which was upregulated with a fold change of 2.09. Additionally, other research has shown that when Tgfb1 was added to endometriotic cyst stromal cells, the number of proliferating cells significantly increased (Zhang et al., 2019). This shows that Tgfb1 is downstream of Fgf19 and thus Fgf19 could induce proliferation using this gene. Tgfb1 was also upregulated in the cWnt9a overexpression model (Munnamalai et al., 2017).

1.13 Fgf19's Role in Chick Eye Development

cFgf19 appears to play a role in both the development of the retina and the lens in the chick. Within the retina, Fgf19 is present as early as E2.5 and remains until P30 (Francisco-Morcillo et al., 2005). Between stage 16 and 22, Fgf19 mRNA transcripts were found in the retinal ganglion postmitotic neuroblasts. However, once these cells finished migrating to their final position in the mantle layer of the eye, Fgf19 was no longer is found in these fully differentiated cells.

Starting at stage 31, Fgf19 begins to appear within the outer region of the inner nuclear layer within *Pax6* positive horizontal cells; however, only a subset of the *Pax6* cells were Fgf19 positive P30 (Francisco-Morcillo et al., 2005). Further research investigated these horizontal cells. At stage 3, Fgf19 was found primarily within the horizontal cell layer, and some, but not all, of the Fgf19-positive horizontal cells were also labeled with a pan-horizontal cell marker, Prox1 (Okamoto et al., 2009). Specifically, the Fgf19 horizontal cells were the axon-bearing cells labeled with lim homobox 1 (Lim1); however, not all of the Lim1 cells were Fgf19-positive. The Islet1 axon-less cells were not Fgf19-positive. This nonoverlap between Islet1-positive cells and Fgf19-positive cells has also been shown at stages 25, 29, and 34 within the eye (Francisco-Morcillo et al., 2005).

Fgf19 has been studied also for its role in determining the dorsal versus ventral sides of the optic cup of the chick due to its location within the dorsal side of the optic cup (Okamoto et al., 2008). Interestingly, when Fgf19 was knocked down using shRNA, at stage 16 or 17, there was no change in the expression domains of genes that mark the dorsal and ventral sides, T-box transcription factor (Tbx5) and ventral anterior homeobox (Vax), respectively. The authors speculated that Fgf19 may be part of a parallel pathway within the eye and not involved in dorsal ventral patterning of the optic cup; however, the shRNA was electroporated into the eye and was likely mosaic, so cells that did not get the shRNA could have produced enough Fgf19 to compensate for those with the shRNA. Another possibility could be that Fgf19 is a redundant signaling molecule and if Fgf19 is knocked down, the other molecule is able to perform the same role as Fgf19.

Additionally, Fgf19 is involved in lens induction through its ability to bind to Fgfr4 (Kurose et al., 2005). Specifically, Fgf19 acts in opposition to Fgf8 by binding to Fgfr4 to stop the expression of the transcription factor L-Maf, which is upstream of prospero homeobox protein 1 (Prox1) and δ-crystallin. If Fgf8 bound to a different receptor, Fgfr3c, this allowed L-Maf expression. This pathway was discovered as a result of the misexpression of several genes. If Fgf19 was overexpressed, there was no change in L-Maf, Prox, or δ-crystallin at stage 12/13 or stage 15/16; however, if L-Maf was overexpressed, there was an increase in Prox1 and δ-crystallin in all embryos tested at stage 15/16 and in 17% of the stage 12/13 embryos there was an increase in Fgf19. This shows that Fgf19 is not upstream of L-Maf, Prox, or δ-crystallin, but that L-Maf is upstream of Prox and δ-crystallin. The authors also speculated that L-Maf turns on Fgf19 prior to

Prox and δ-crystallin. When a secreted form of Fgfr4 was added, in 30% of the embryos, there was an increase in L-Maf. This suggests that Fgf19 is able to turn off L-Maf because the secreted receptor would act as dominant negative and bind to Fgf19 to prevent it from signaling through the receptor. When Fgf8 was overexpressed, at stage 12/13, there was an increase in L-Maf in 30% of the embryos and an increase in Prox1 in 33% of the embryos. This shows that Fgf8 is upstream of L-Maf and Prox1. Overall, these data show that Fgf19 is involved in the regulation of transcription factor, L-Maf, and is regulated, at least partially by L-Maf.

CHAPTER 2. METHODS

2.1 Virus Injection and Tissue Sectioning

Pathogen-free *G. gallus* eggs were obtained from Charles River Laboratories. At embryonic day 2 (E2), about 2 ml of albumin was removed from the eggs. Injections of RCAS(A)/Wnt9a, RCAS(A)/EGFP-P2A-Fgf19 or RCAS(B)/Fgf19-P2A-EGFP were done into the otic vesicle at E3. Embryos were harvested at various timepoints before hatching occurred, including E6, E10, and E14. They were killed by decapitation, and the heads were fixed using 4% paraformaldehyde (PFA) in phosphate buffered saline (PBS) for about 24 hours. Over the next three days, 10, 20, and 30% sucrose solutions in PBS were added to dehydrate the tissue. Tissue freezing media (TFM) was used to create blocks for sectioning. The tissue blocks were frozen with liquid nitrogen and stored at -80°C until sectioning occurred. Cryostat sectioning created tissue slices of 15 or 20 μm added to Superfrost Plus Slides (Fisher Scientific) and then frozen at -20°C until needed. Tissue harvesting, fixation, dehydration, block creation, and cryostat sectioning were done in RNase-free conditions.

2.2 DAB (immunostaining)

Tissue slides were prepared as described above and warmed to room temperature. The tissue was then fixed at room temperature with 4% PFA diluted in PBS for 10 to 15 minutes. Three washes were done with PBS for five minutes each and dipped in PBST (PBS/0.5% Triton-X100). The slides were blocked with one of three different solutions based on the organism(s) used to create the secondary antibody. The solutions were 1) PBS with 5% goat serum (Vector S-1000), 0.05% Triton-X100, and 0.05% sodium azide, 2) PBS with 2% donkey serum (Jackson Immuno Research Labs #017-00-120), 0.05% Triton-X100, and 0.05% sodium azide, 3) PBS with 2% bovine serum albumin (BSA) (Sigma A9647), 0.05% Triton-X100, and 0.05% sodium azide, or 4) PBS with 5% horse serum (Vector S-2000), 0.05% Triton-X100, and 0.05% sodium azide. Blocking was done for one hour at room temperature.

Primary antibody staining was done with one or more of the following antibodies: 1) 3C2 monoclonal antibody prepared in the Fekete lab as culture supernatant from hybridoma cells (binds to gag-pro protein in RCAS viruses; mouse IgG_1) diluted between 1:1 and 1:40 depending on days

since thawing, 2) phospho-histone H3 (PH3) (detects proliferating cells; rabbit IgG) (MilliporeSigma 38215950UG) at 1:200, and 3) neurofilament associated antigen (3A10) (detects axons; mouse IgG1) between 1:1 and 1:20 depending on days since thawing. The primary antibodies diluted in the blocking solution were incubated either overnight at 4°C or 3 hours at room temperature. Afterward, the slides were washed three times in PBS for five minutes each. The endogenous peroxidases were blocked using 0.3% or 0.6% (if ~ one year old or more) hydrogen peroxide in ice-cold methanol at -20°C for an hour. The slides were washed three times in PBS for five minutes each and dipped in PBST before the secondary antibody was added.

The secondary antibodies used were one or both of the following: biotinylated goat α rabbit IgG (Vector Laboratories BA 1000) and biotinylated horse α mouse IgG (Vector Laboratories BA 2000). The secondary antibody or antibodies were diluted in the blocking solution and incubated for one hour at room temperature. Again, the slides were washed three times in PBS and dipped in PBST before the ABC reaction (Vectastain ABC kit; prepared 30 minutes prior with one drop A and one drop B/ 5 ml PBS and shaken) of one hour. The slides were washed twice for five minutes each in PBS and then for five minutes in 50 mM Tris, pH 7.5. Then the slides were dipped in 50 mM Tris, pH 7.5 with 0.05% triton.

The 3'-Diaminobenzidine (DAB) reaction, containing 5% DAB and 0.2% hydrogen peroxide (doubled if about one year old or more) in 50 mM tris, pH 7.5, was added to slides for 5 to 30 minutes until the color was clearly visible. The slides were washed for five minutes with 50mM tris, pH 7.5, and three times for five minutes each with PBS. Coverslips were adhered using Southern Biotech Fluoromount G slide mounting medium (Thermo Fisher Scientific OB100-01).

2.3 Transformation of DH5-α cells with cFgf3 or cFgf19 Plasmid

Plasmids containing chick Fgf3 and chick Fgf19 cDNA were sent from Dr. Matías Hidalgo-Sánchez's lab at the University of Extremadura in Spain. The plasmids were previously used to detect these genes' expression patterns within the developing chick inner ear (Olaya-Sanchez et al., 2017; Sanchez-Calderon et al., 2007). The plasmids were sent as dried spots on paper and were briefly placed into Tris-Ethylenediamine Tetraccetic Acid, Disodium Salt Dihydrate (EDTA) buffer (TE buffer) (10 mM Tris-Cl, 1 mM EDTA). After the paper circles were removed, the DNA concentration of the cDNA-TE solution was measured. cFgf3 was 90.6 ng/µl and cFgf19 was 9.3

ng/µl. Plasmid DNA in TE buffer was added to 10µl of freshly-thawed DH5-α cells and placed on ice for 30 minutes; 90.6 ng of cFgf3, 51.15 ng of cFgf19, or 1.25 ng of Puc19 (positive control). Then the cells were heat-shocked at 42°C for 30 seconds. After five more minutes on ice, 950 µl of Lysogeny broth (LB media) (1% bacto-tryptone, 0.5% bacto-yeast extract, 1% NaCl in MQ water) was added to the cells. The cells were shaken at 37°C for about one hour in a Thermo Forma Orbital Shaker and then mixed gently. The cells were incubated overnight on agar plates with carbenicillin. All of the plates formed colonies.

2.4 MaxiPrep of Transformed DH5-α cells with cFgf3, cFgf19 or cFzd4 Plasmid

A maxiprep was done using transformed colonies containing cFgf3 or cFgf19 plasmids or stored a glycerol stock of cells containing cFzd4 plasmids. These cells underwent overnight colony growth in LB media with carbenicillin, in preparation for a maxiprep using Qiagen Maxiprep reagents. The overnight colony growth was done at 37°C in a Thermo Forma Orbital Shaker. The following day, the cells were pelleted in a Beckman Coulter Avanti J-E Centrifuge at 6,000 x g for 15 minutes at 4°C. The supernatant was poured off the cell pellet, and the cells were resuspended in 10 ml Buffer P1 and mixed. The cells were lysed by mixing in 10 ml Buffer P2 for five minutes at room temperature. The solution was neutralized for 20 minutes on ice by mixing in 10 ml of pre-chilled Buffer P3. The solution underwent another centrifugation step at 20,000 x g for 30 minutes at 4°C in the same centrifuge as before. The DNA, now in the supernatant, was centrifuged again at the same speed and temperature but only for 15 minutes.

The DNA supernatant was then bound to a Qiagen-tip, previously equilibrated with 10 ml of Buffer QBT. The Qiagen-tip was twice washed with 30 ml of Buffer QC and the flow-through discarded. The DNA was eluted into an autoclaved tube using 15 ml of Buffer QF. The DNA was mixed with 10.5 ml of isopropanol to precipitate it. The DNA was centrifuged again in the same centrifuge for 40 minutes at 15,000 x g at 4°C. The DNA pellet was washed with 5 ml of 70% ethanol and centrifuged a final time at 15,000 x g for 10 minutes at 4°C. The solution was poured out, and the pellet air-dried for about 10 minutes. The cFgf3 and cFgf19 pellets were dissolved in 200 µl of sterile water overnight, whereas the cFzd4 pellet was dissolved in 200 µl of sterile water overnight. The next day, the DNA concentration was determined and the DNA diluted with more sterile water to reach the final concentrations. cFgf3 was 694.7 ng/µl with an A260/A180 ratio of 1.4. cFgf19 was 1019 ng/µl with an A260/A180 ratio of 1.42. cFzd4 was 9.2 ng/µl with an

A260/A180 ratio of 2.01. The DNA was not very pure, but was used in the preparation of the mRNA probes.

2.5 Linearization and Purification of cFgf3, cFgf19, and cFzd4 Plasmids

The DNA was confirmed to be the correct plasmids through linearization and visualization on an agarose gel. Approximately 0.5 µg of DNA was linearized using 10 or 20 units of the approximate enzyme (cFgf3: New England Biolabs Not-HF; cFgf19: New England Biolabs XhoI; cFzd4: New England Biolabs Nsil-HF), 10% Cutsmart Buffer, and sterile water. The solution was mixed and incubated for one to three hours at 37°C. Some of the DNA was visualized to confirm linearization on a 1.2% agarose gel comparing uncut and cut versions of the genes.

The remaining linearized DNA was purified. A solution of Phenol:Chloroform:Isolamyl Alcohol was added to create a 1:1 mixture with the DNA and vortexed. This and subsequent centrifugation spins were done at ~20,000 x g for 5 min unless otherwise stated. The aqueous layer contained the DNA and was moved to a new tube. To the phenol layer, an equal volume of TE buffer, pH 8 was added and vortexed before centrifugation. The aqueous layer containing the remaining DNA was added to the first aqueous layer tube. A 1:1 solution of the DNA and Phenol:Chloroform:Isolamyl Alcohol was created, vortexed and spun. Again, the aqueous layer was kept. An equal volume of chloroform was added to the aqueous layer of DNA, vortexed and spun. The aqueous layer was moved to a new tube, and a 0.1 volume of NaCl and 2.5X volume of ethanol were added. This solution was incubated at -20°C overnight to precipitate the DNA.

The following day, the DNA was pelleted by centrifugation for 30 minutes. If no pellet was visible, a second spin was performed. The ethanol was removed, and 200 µl of 70% ethanol were added to the 1.5 ml tube followed by a 15 minute spin. The ethanol was removed, and the pellet air-dried. The DNA was resuspended in 10-20 µl of sterile water. The purity and concentration of the DNA were then tested.

2.6 Creation of cFgf3, cFgf19, and cFzd4 In Situ Hybridization mRNA DIG Probes

The linearized, purified DNA was transcribed into anti-sense mRNA probes. The reaction was 25 µl total and contained 20% 5X transcription buffer (Promega 118B), 8% dithiothreitol (DTT) 100 mM (Promega P117B), 10% digoxigenin (DIG)-RNA labeling mix (nucleoside

triphosphates [NTP's]) (Roche 26591021), 2% Ribolock (RNase inhibitor) (Thermo Scientific EO0381), ~300 ng Template DNA , 8% polymerase (based on promoter prior to relevant gene within the plasmid, cFgf3: T7; cFgf19: SP6; cFzd4: SP6) (Promega P207B & New England BioLabs # M0207S, respectively), and sterile water to reach 25 µl. This reaction was incubated for 1 hour and 40 minutes at 37°C. Then the DNA was degraded using 3 µl sterile water, 3 µl RQ1 Dnase 10X Reaction Buffer (Promega M198A), and 1 µl RQ1 RNase- Free Dnase (Promega M610A) for 30 minutes at 37°C. The reaction was stopped using 1 µl RQ1 DNase Stop Solution (Promega M119A). 3µl of the reaction was saved for a gel, and to the remaining volume 1.25 µl of lithium chloride (Sigma L7026) and 75 µl of ethanol was added and incubated at -20°C overnight. The next day the RNA was centrifuged at ~20,159 x g for 40 minutes. The ethanol was removed, and 200 µl of 70% ethanol was added. This solution was centrifuged at ~20,159 x g for ten minutes. The ethanol was removed, and the pellet air-dried. The RNA was resuspended in TE buffer and stored at -80°C until needed. 1.2% agarose gels were used to compare the solutions containing the RNA with the DNA (so before the DNA was degraded), the RNA (without DNA as it was degraded), and the RNA probe after purification. These gels showed that the mRNA was made and the DNA was degraded.

2.7 DIG Probe In situ Hybridization

The mRNA probes created from the cDNA plasmids were used in these experiments. Cryostat sectioned slides were warmed for 20 minutes at 55°C in a FisherBiotech Hybridization Incubator to ensure the sections adhered to the slides. The sections were then fixed with 4% PFA in PBS for ten minutes and washed three times in PBS for ten minutes each. Sections underwent proteinase K (Roche 03115887001) digestion (1µg/ml) for ten minutes and were fixed again with 4% PFA in PBS for ten minutes. The slides were washed with PBS three times for ten minutes each and then acetylated with a solution containing 0.1M triethanolamine (Sigma T58300) and 0.25% acetic anhydride (Sigma-Aldrich 320102) in diethyl pyrocarbonate (DEPC)-treated water for ten minutes. Slides were permeabilizated with PBT for 30 minutes. Then the slides were immersed in a pre-hybridization buffer (50% formamide, 10% 10X ISH salt solution [1000mL: 17.5% NaCl, 1.404%Tris HCl, 0.78% Tris base, 0.78% $NaH_2PO_42H_2O$, 0.71% Na_2HPO_4, and 10% 0.5 EDTA, in DEPC-treated water], 5% 1mg/ml tRNA from brewer's yeast (Roche 10109525001), and 2% 50X Denhart's solution (VWR EM-3610) in DEPC-treated water) for 2 hours.

Hybridization using the complementary antisense mRNA to the mRNA of interest (cFgf3, cFgf19, or cFzd4) was done in a solution with the same ingredients as the pre-hybridization buffer plus 1 µg/ml of the probe overnight at 72°C in a Boekel Shake' N' Bake Hybridization Oven.

The following day the slides were moved to pre-warmed 2X Saline Sodium Citrate (SSC) (Promega V4261) for ten minutes and then into pre-warmed 0.2X SSC for one to two hours. Afterward, the slides were moved to new 0.2X SSC for five minutes and then washed twice for five minutes each in PBSw (PBS and 0.5% Tween-20). PAP pen was added to the edges of the slides, and then the slides were incubated in blocking solution (20% Roche blocking reagent [Roche 11096176001] and 10% Fetal bovine serum) in PBSw) for one hour. Next, 1:3500 anti-DIG AP Fab fragments antibody (Roche 11093274910) binding occurred overnight at room temperature.

On the third day, the slides were washed three times for ten minutes each with PBSw and then equilibrated in B2 buffer (100mM tris, pH 9.5, 100mM NaCl, and 50mM $MgCl_2$ in autoclaved water) twice for ten minutes each. The slides were dipped in B2 buffer plus 0.05% triton-X100 before the edges were lined with PAP pen. Then SigmaFast NBT/BCIP (Sigma B5655) was added to each slide. The color was developed at room temperature, at 37°C for faster development, or 4°C for slower overnight development, until color appeared to have reached maximum development with the minimum background color; incubation times ranged from 8 hours to overnight and varied for different probes. The slides were washed twice for ten minutes each with PBSw, and then the color development was stopped using AP stop solution (100mM tris, pH 7.5 and 1mM EDTA in autoclaved water) for 10 to 15 minutes. The slides were washed in PBS twice for ten minutes each. Coverslipping was either done using Fluoromount G slide mounting medium or SHUR/Mount (TBS LC). If SHUR/Mount was used, the slides were first dehydrated using a series of ethanol steps (70%, 95%, 95%, 100%) for one minute each and then placed in three Xylene Substitute d-Limonene (HemoDe) (Electron Microscopy Sciences 23412-01) incubations for two minutes each prior to coverslipping.

2.8 Viral Design

In order to understand the role of cFgf19 in the development of the radial axis in the chick basilar papilla, two different overexpression vectors were created: RCAS(A)/EGFP-P2A-Fgf19 and RCAS(B)/Fgf19-P2A-EGFP (see maps, Figure 2.1). RCAS(A)/EGFP-P2A-Fgf19 was

designed by a former post-doctoral student, Dr. M. Katie Scott. RCAS(B)/Fgf19-P2A-EGFP was designed by a current student, Vashi Negi. The overexpression plasmids were designed to express both GFP and cFgf19, but the order of transcription was reversed. In between the genes was P2A, a "self-cleaving" peptide.

Figure 2.1: Maps of plasmids for cFgf19 overexpression. A) Map of RCAS(A)/EGFP-P2A-Fgf19 plasmid. Designed by Dr. M. Katie Scott with cloning done by GenScript using ClaI to insert EGFP-P2A-Fgf19 into the RCAS(A) virus as the backbone. B) Map of RCAS(B)/Fgf19-P2A-EGFP plasmid. Designed by Vashi Negi using Dr. M. Katie Scott's design as basis. Cloning done by GenScript using ClaI to insert Fgf19-P2A-EGFP into the RCAS(B) virus as the backbone. Notes: ClaI* site is blocked by Dam methylation. Slax12 was part of the shuttle vector used that provided ClaI sites. The unlabeled orange and green arrows represent the directions of the open reading frames. Abbreviations: gag: group-specific antigen; pol: DNA polymerase; env: envelope protein; Slax12 5'UTR/Slax12 Fragment: part of shuttle vector; RSV promoter: Rous sarcoma virus enhancer/promoter; lac operator: operator that lac repressor binds to; lac UV5 promoter: promoter for lac operator; AmpR promoter: promoter for β-lactamase production; AmpR: β-lactamase: antibiotic against ampicillin and carbenicillin; ori: origin of bacterial replication; bom: basis of mobility region; rop: repressor of primer, keep plasmids at low-copy number

Figure 2.1 continued

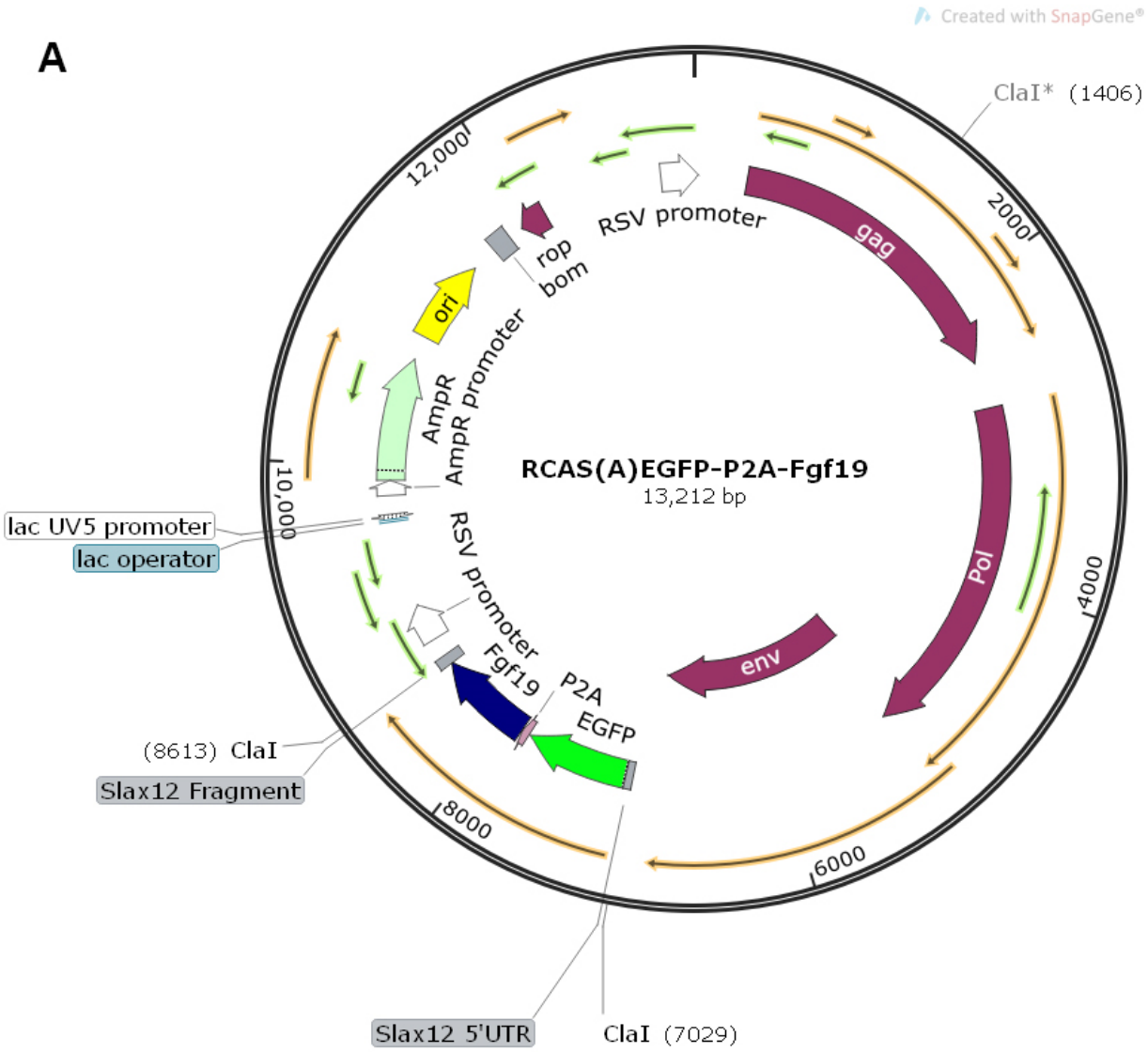

Figure 2.1 continued

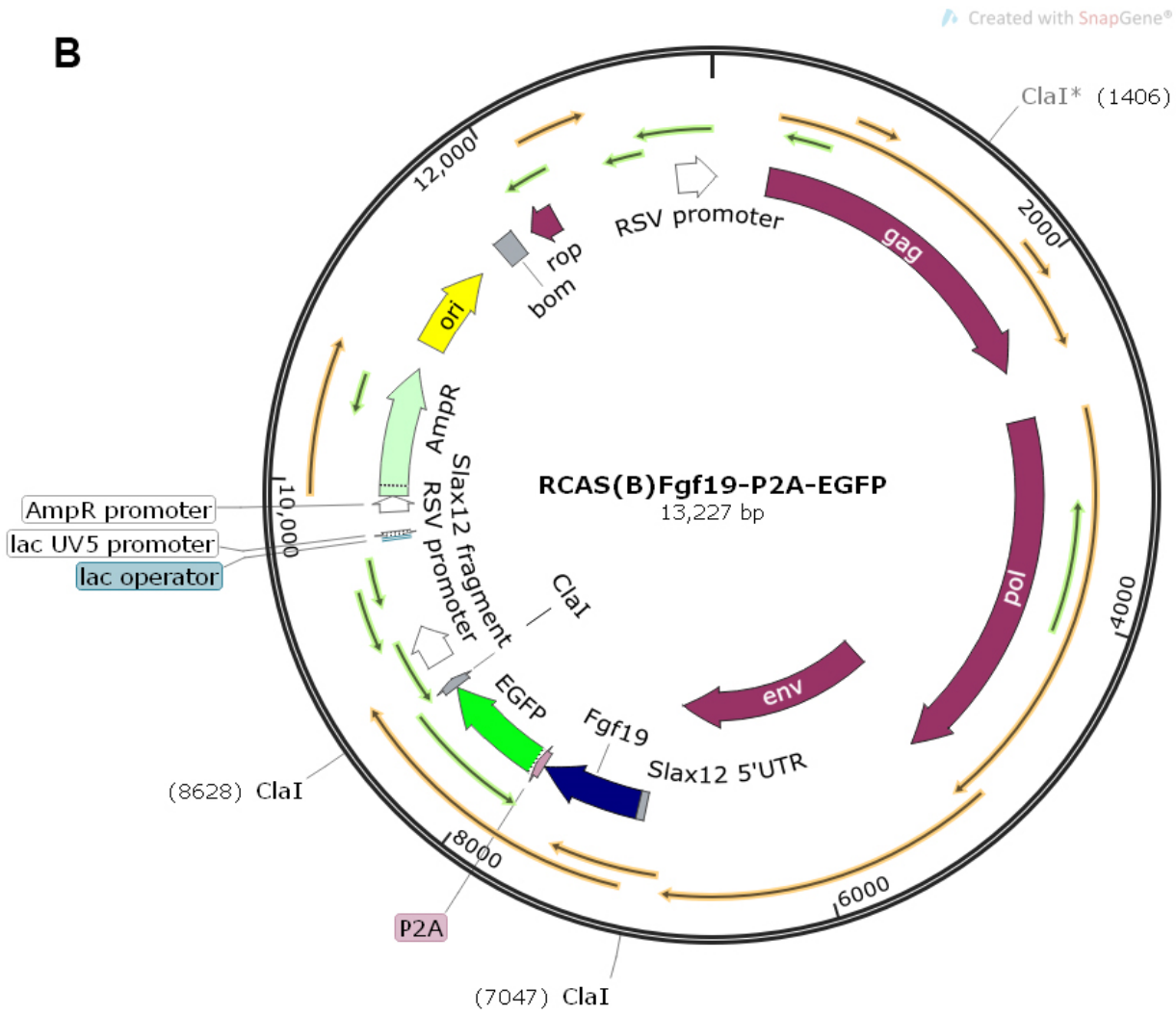

2A “self-cleaving” peptides are part of the viral genome but are employed to express two genes with one vector under the same promoter (Liu et al., 2017). They add very few amino acids to the sequence compared to other methods of dual expression as they range from 18 to 22 amino acids and interfere less with functionality. They contain a conserved GDVEXNPGP region. These peptides are called “self-cleaving” in quotes because although they were initially thought to self-cleave, they instead produce two proteins using ribosome skipping (Donnelly et al., 2001). This method of “cleavage” allows for three possible options to be produced (Donnelly et al., 2001; Liu et al., 2017). The three possible transcription options found through the usage of the P2A peptide include: 1) ribosome skipping, which produces the intended outcome of two independent proteins, whereby the first ends with the penultimate amino acid of the P2A peptide (glycine) and the second starts with the final P2A amino acid (proline) followed by serine and arginine at the N-terminus; 2) ribosome fall-off, which produces a transcript encoding only the first protein terminating with the penultimate amino acid of the P2A peptide (glycine); and 3) ribosome read-through, which encodes a fusion protein, linked by the P2A peptide.

Evidence to suggest that the proteins do not cleave as originally believed came from the difference in expression of the proteins found upstream versus downstream of the 2A peptide (Donnelly et al., 2001; Liu et al., 2017). For example, in both pGFP2AGUS and pGUS2AGFP plasmids, the upstream protein showed increased expression in immunoprecipitation compared to the downstream one, regardless of which protein it was (Donnelly et al., 2001). It was speculated that the increased expression could be from the upstream protein stalling in the ribosome and the sample preparation removing it from the ribosome; however, when puromycin (an antibiotic that causes premature termination of translation) was added to pGFPP2AGUS, only one band was visible at the size of GFP2A, which indicates a likely pause site. If the P2A peptide was not causing a pause, more bands would be expected due to multiple locations of termination from the antibiotic. This was further confirmed by the increased median intensity of GFP from cells transduced with a plasmid carrying the GFP gene placed before the 2A peptide compared to after the 2A peptide (Liu et al., 2017).

P2A, from the porcine techovirus-1, was chosen over the other 2A peptides because of its increased “cleavage” efficiency, compared to T2A, E2A, and F2A. P2A had the least amount of “uncleaved” whole product in multiple organisms and both *in vitro* and *in vivo,* including 1) several human cell lines, 24 hours after transfection, 2) one to two-stage zebrafish embryos, 24 hours after

fertilization, and 3) in adult mouse liver, three days after mouse tail vein injection (Kim et al., 2011). However, it should be noted that this finding is not universal. In multiple mouse cell lines, three days after transduction, and in HEK293T cells, two days after transfection, when GFP was downstream of T2A peptide, the median intensity was greater than if GFP was downstream of P2A (Liu et al., 2017). As the *in vivo* data showed that P2A has the greatest "cleavage" efficiency, it was used for our current chick embryo *in vivo* studies. Additionally, both overexpression plasmids contained a glycine, serine, glycine linker placed between the first protein and the P2A peptide in order to further increase "cleavage" efficiency, as this linker has been shown to result in almost 100% cleavage compared to the significant "uncleaved" band found without the linker (Szymczak-Workman et al., 2012)

The RCAS(A)/EGFP-P2A-Fgf19 plasmid was designed to yield separate localization of GFP and Fgf19. The GFP does not have a localization signal, so it was hypothesized that it should stay within the cells infected by the virus, serving as a marker. The Fgf19 has a secretion signal sequence so it would be secreted. cFgf19 was downstream of the P2A peptide to avoid secretion of the GFP by slipstreaming of both proteins through the translocon using cFgf19's secretion signal.

Due to concerns of cFgf19 not being secreted from the infected cells, a second overexpression vector was designed: RCAS(B)/Fgf19-P2A-EGFP. In this plasmid, the order of the genes in the insert was reversed so Fgf19 was upstream of the P2A peptide. GFP being downstream of cFgf19 could have reduced fusion proteins of both GFP and cFgf19 together. When a plasmid, containing EYFP upstream of a 2A peptide with ECFP downstream, was added to HeLa cells and the "cleavage" examined 24 hours later, a large band of "uncleaved" protein was found (de Felipe et al., 2010). When the C-terminal amino acids (220-240) of EYFP were removed, the "cleavage" efficiency was almost complete compared to without this deletion. A Blast search showed that the C-terminal region (220-240 amino acids) of EYFP is identical to this region of GFP from the overexpression plasmid other than the stop codon, which is not present in the plasmid (Altschul et al., 1997; Altschul et al., 2005). As such, if the GFP was upstream of the P2A, more of the "uncleaved" fusion protein would be produced and then would be able to move through the translocon and be secreted using Fgf19's secretion signal.

The insert was added to an RCAS(B) plasmid due to possible mismatch errors in the RCAS(A) plasmid previously used. Additionally, the stop codon at the end of the Fgf19 gene was removed due to recommendations from the RCAS website that RCAS plasmid inserts not have

stop codons (Hughes). In RCAS(A)/EGFP-P2A-Fgf19, the GFP has no stop codon, but the Fgf19 does have a stop codon. In RCAS(B)/Fgf19-P2A-EGFP, neither GFP nor Fgf19 has a stop codon.

2.9 Virus creation

Both overexpression vector maps described above, with complete sequence information and vials of RCAS(A) and RCAS(B) were sent to GenScript for DNA synthesis and virus assembly. GenScript sent completed plasmids in lyophilized form. Water was added to each lyophilized plasmid to create a 0.1µg/µl solution and vortexed. 20 µl of DH5α cells were transformed with 0.3µg of plasmid following a similar bacterial transformation protocol as described above for the cFgf3 and cFgf19 plasmids. The differences between the two protocols were 1) the amount of DH5α cells (20 µl versus 10 µl), 2) the removal of the five minutes on ice after the heat shock, 3) the amount of LB media added (400 µl versus 950 µl), 4) the use of a water bath at 37°C instead of a shaker, and 5) the lack of a positive control plate. Bacterial colonies were found on all of the antibiotic-infused agar plates, indicating successful transformation.

Transformed colonies were used to inoculate LB media containing carbenicillin for overnight growth at 37°C in a Thermo Forma Orbital Shaker. This overnight colony growth was used for a miniprep using Qiaprep Miniprep Spin reagents. The following day, the cells were centrifuged at 6,800 x g for three minutes at room temperature and the media removed. The cells were resuspended in 250 µl of Buffer P1 and vortexed. The cell lysis was done with 250 µl of Buffer P2 and gently mixed. The lysis was stopped after five minutes using 350 µl of Buffer N3 and mixed. The solution was centrifuged for ten minutes at 17,900 x g at room temperature. The supernatant was then added to a QIAprep 2.0 spin column and centrifuged for one minute at 17,900 x g at room temperature. The flow-through was discarded, and 750 µl of Buffer PE was added to the column. It was centrifuged for one minute at 17,900 x g at room temperature. The flow-through was removed again and the column centrifuged at the same speed. The DNA was eluted from the column using 50 µl of Buffer EB (10 mM Tris-Cl, pH 8.5) for one minute before centrifugation at the same speed. The concentration and purity of the DNA were tested using a Nanodrop. Each miniprep tested six colonies. RCAS(A)/EGFP-P2A-Fgf19 concentration ranged from 35.3 ng/µl to 73 ng/µl, and the purity ranged from A260/A280 of 1.7 to 1.95, indicating somewhat pure DNA as 1.8 is the generally accepted pure DNA value. RCAS(B)/Fgf19-P2A-

EGFP concentration ranged from 53.3 ng/µl to 67.5 ng/µl, and the A260/A280 ranged from 1.88 to 1.89, indicating generally pure DNA.

A diagnostic gel was performed to confirm the size of the plasmids. RCAS(A)/EGFP-P2A-Fgf19 DNA was digested for one hour at 37°C using 1 µg of DNA with 40 units of SalHF (New England BioLabs) and CutSmart Buffer (New England BioLabs) for 50 µl reactions. RCAS(B)/Fgf19-P2A-EGFP DNA was digested for 15 minutes at 37°C using 0.5 µg of DNA with 20 units of SalHF (New England BioLabs) and CutSmart Buffer (New England BioLabs) for 25 µl reactions. For both DNA vectors, the cut and uncut DNA was compared on 1.2% agarose gels using 0.5 µg of DNA. The cut DNA lanes showed two bands, one at about 2.5 kB and the other at about 11 kB, compared to only one band with uncut DNA. These bands indicated the plasmid was the correct size, as the plasmid is 13.2 kB.

New agar plates with carbenicillin were streaked with colonies from the original plates to create new colonies. Colonies from the new plates were used to inoculate LB media with carbenicillin for an overnight colony growth. The overnight colony growth was used in a maxiprep using Qiagen Maxiprep reagents. The maxiprep was done in the same manner as the one used for the cFgf3 and cFgf19 plasmids, with a few exceptions. For both overexpression vectors, the DNA was dissolved in TE (pH 8), not sterile water. For RCAS(A)/EGFP-P2A-Fgf19 DNA, the pellet was centrifuged a second time in the same manner while in 70% ethanol due to it not sticking to the side of the tube. Second, for RCAS(B)/Fgf19-P2A-EGFP DNA, there were a few changes, including 1) a table-top centrifuge used at ~ 4,500 x g for the first centrifugation due to the other centrifuge breaking down, 2) the pelleted cells being stored at -20°C for eight days after the first centrifugation step before the rest of the steps, and 3) the remaining centrifugation steps were done with an Optima L-100XP Ultracentrifuge using a SW28 swinging bucket rotor at either ~22,000 x g not 20,000 x g or ~14570 x g not 15,000 x g. For RCAS(A)/EGFP-P2A-Fgf19, there were two overnight colony growths that underwent maxiprep that included pure DNA. One of the colonies was 592.5 ng/µl and the other colony was 676 ng/µl. Both of the colonies had an A260/A280 of 1.85. For RCAS(B)/Fgf19-P2A-EGFP, only one of the overnight colony growths was pure enough to be used. The DNA was 963.4 ng/µl and pure with an A260/A280 of 1.87. Some of the RCAS(B)/Fgf19-P2A-EGFP DNA was run on a 1.2% agarose gel to confirm the DNA presence, and a strong band was found.

DNA from the maxipreps was used for transfection of DF-1 cells, embryonic chick fibroblasts. 0.5 ml of Hepes-buffered saline (HBS) (137 mM NaCl, 5 mM KCl, 0.7 mM Na_2HPO_4, 6 mM dextrose, 21 mM Hepes, pH 7.05) was combined with 10 µg of DNA (for RCAS(B)/Fgf19-P2A-EGFP, the more concentrated DNA was used). Then 32 µl of 2M $CaCl_2$ was added, and the tube tapped up and down for ~30 seconds. This solution was incubated for 45 minutes at room temperature. Media from a 10 cm plate of DF-1 cells at about 10-20% confluency was removed and the HBS-DNA-$CaCl_2$ solution was added to the center of the plate. The plate sat for 10 minutes before the solution was redistributed over the plate. The plate sat for 10 more minutes before 10 ml of DF-1 media (10% FBS [fetal bovine serum] [heat-inactivated] [Atlanta Biologics S11150], 2% chick serum [heat-inactivated] [Sigma C-5405], 1 % L-glutamine [200 mM from Gibco 25030-81], 1% Penicillin-Streptomycin [Sigma P4333], 86% Dulbecco's Modified Eagle's Medium [DMEM] with 4.5g/L glucose and sodium pyruvate [Sigma D6546]; filtered 0.22 µm) was added to the plate. The cells were incubated for 4 hours at 37°C, 5% $C0_2$. After four hours, the media was removed from the plate, and 2.5 ml HBS+15% glycerol (previously warmed to room temperature) was added to the center of the plate. This glycerol shock was done for 90 seconds at 37°C, 5% $C0_2$. Then the glycerol was removed, and the plate washed with DF-1 media. The media was removed, and a final 10 ml of DF-1 media was added for RCAS(A)/EGFP-P2A-Fgf19, or 6 ml for RCAS(B)/Fgf19-P2A-EGFP. 6 ml was the correct amount and so the 10 ml was an error in the experiment for RCAS(A)/EGFP-P2A-Fgf19. The cells were returned to the incubator at 37°C, 5% $C0_2$.

The cells were split two days later and then two days after that (4 days after transfection) to create a total of 24 plates for RCAS(A)/EGFP-P2A-Fgf19 and 12 plates for RCAS(B)/Fgf19-P2A-EGFP. Virus spread was visualized in fixed or live cells using GFP fluorescence to ensure most if not all cells contained the virus. Two days after the last split, the media on the cells was changed to 10% Nuserum (same as DF-1 media except that the chick serum and FBS were replaced with Nuserum [BD Biosciences 35-5505] and was 88% DMEM instead of 86%). The secreted virus was concentrated by adding only 5 ml of media per plate instead of 10 ml.

2.10 Virus Concentration

Virus concentration was done on each of the two days following the Nuserum media addition. The media from the cells was collected and filtered through a 0.45µm filter to remove

floating cells and debris. The supernatant was added to autoclaved tubes and centrifuged for 2 hours 15 minutes at 4°C at 72,100 x g in an Optima L-100XP with a SW28 swinging bucket rotor. The supernatant was then concentrated by pouring out all but a tiny volume of it (~100 µl) out. The remaining supernatant was triturated five total rounds of ten triturations each over the course of an hour. The supernatant was stored in liquid nitrogen as 18µl aliquots. The RCAS(A)/EGFP-P2A-Fgf19 supernatant was concentrated at ~150x volume and ~48x volume on days 1 and 2, respectively, and RCAS(B)/Fgf19-P2A-EGFP was concentrated at ~137x volume and ~111x volume on days 1 and 2, respectively. The protocol was the same for both days except 1) after media collection on the first day, 5 ml of 10% Nuserum was added back to each plate and the plates were returned to the incubator at 37°C, 5% CO_2 and 2) day 2 with RCAS(A)/EGFP-P2A-Fgf19 instead of filtering the supernatant, a low-speed spin in an Eppendorf Centrifuge 5804 R in a A-4-44 rotor at 1,000 x g was performed, and the supernatant was frozen for several days before the faster centrifugation step.

The virus concentration was determined using DAB immunostaining. DF-1 cells were split into 6 well plates, with one plate each for unconcentrated and concentrated virus and one for each day of virus concentration, making 4 total plates. The day after the cells were added to the 6 well plates, the media from the cells was removed and 1 ml of DF-1 media was added for RCAS(A)/EGFP-P2A-Fgf19 and 1 ml of DF-1 media containing 1 µg/ml polybrene for RCAS(B)/Fgf19-P2A-EGFP. Then the virus was added.

The RCAS(A)/EGFP-P2A-Fgf19 unconcentrated plates had one well with virus diluted 10^{-2}, two wells 10^{-5}, two wells 10^{-6}, and one well with no virus. The RCAS(B)/Fgf19-P2A-EGFP unconcentrated plates had one well with virus diluted 10^{-3}, two wells 10^{-5}, two wells 10^{-6}, and one well with no virus. The concentrated plates had one well with virus diluted 10^{-4}, one well 10^{-6}, two wells 10^{-7}, and two wells 10^{-8}. After four hours of incubation at 37°C, 5% CO_2 with the virus, an addition ml of media either with (RCAS(B)/Fgf19-P2A-EGFP) or without (RCAS(A)/EGFP-P2A-Fgf19) polybrene at 1 µg/ml, was added. The cells were then further incubated at 37°C, 5% CO_2, for about 42 hours without agitation.

After 42 hours, the media was removed, and the cells were washed for three minutes with PBS. Then the cells underwent DAB immunostaining. This staining was performed in the same manner as described earlier with the following modifications: 1) there were no dips into solutions with Triton-X100, and the first wash described in the DAB section earlier is with PBST not PBS,

2) incubations at room temperature were done on a rocker for even distribution of solution on the cells, 3) the blocking was with PBS with 2% bovine serum albumin (BSA), 0.05% Triton-X100, and 0.05% sodium azide, 4) the primary antibody used was 3C2 and the incubation was only one hour at room temperature, 5) endogenous peroxidase blocking used 3% hydrogen peroxide instead of 0.3 or 0.6% and was only 30 minutes long, 6) the secondary antibody used was the biotinylated horse α mouse IgG antibody, and 7) the cells were not coverslipped but left in PBS and wrapped in foil and placed at 4°C until the virus-infected colonies were counted.

DAB (brown) positive colonies (not individual cells) were counted. Either approximately half of the well was counted and doubled, or the whole well was counted. If possible, wells in which there was a duplicate well of the same virus concentration and contained between 10 and 100 colonies are used to determine the virus concentration. However, if more than 100 colonies were found within the least concentrated virus well with a duplicate, it was still counted. An example of how virus concentration is determined is as follows. In the day 1 unconcentrated virus, half of both 10^{-6} wells were counted (129 and 119 colonies, respectively) and each were doubled, under the assumption that the virus spread similarly on both sides of the well, (258 and 238). Then these colonies counts are averaged (248). Finally, average colonies per well (248) was divided by the virus concentration in these wells (10^{-6}) to give 2.48×10^{8} cfu/ml. The concentrations of the viruses are found in Table 2.1. The viruses were concentrated about 100-fold, which is roughly consistent with the concentration by volume described above.

Table 2.1: List of virus concentrations for RCAS(A)/EGFP-P2A-Fgf19 and RCAS(B)/Fgf19-P2A-EGFP for day 1 and day 2 unconcentrated and concentrated vials.

	Day 1 unconcentrated	Day 1 concentrated	Day 2 unconcentrated	Day 2 concentrated
RCAS(A)/EGFP-P2A-Fgf19	3.85×10^{6} cfu/ml	3.9×10^{8} cfu/ml	2.3×10^{6} cfu/ml	2.85×10^{8} cfu/ml
RCAS(B)/Fgf19-P2A-EGFP	2.48×10^{8} cfu/ml	3.79×10^{10} cfu/ml	N/A (not counted)	4.55×10^{10} cfu/ml

2.11 Immunocytochemistry (ICC)

DF-1 cells previously transfected with RCAS(B), RCAS(A)/EGFP-P2A-Fgf19 or RCAS(B)/Fgf19-P2A-EGFP until most if not all of the cells contained the virus were immunostained with one or more of the following antibodies: 3C2 (detects a viral core protein), anti-GFP (evidence of virally-transduced protein expression), or anti-phosphorylated Extracellular Signal-Regulated Kinases 1 and 2 (p-ERK1/2) (readout of downstream kinase of Fgf19 signaling). The cells were washed for three or five minutes with PBS. The cells were fixed using 4% PFA in PBS for ten minutes at room temperature. The cells were washed again, three times for five minutes each with PBS. In some experiments, the cells were also washed with PBST for five minutes. The cells were then blocked for one hour at room temperature on a rocker using either PBS with 2% donkey serum, 0.05% Tween-20, and 0.05% sodium azide or PBS with 5% donkey serum, 0.05% Tween-20, and 0.05% sodium azide. Afterward, primary antibody or antibodies (mouse IgG1 3C2: 1:1; rabbit IgG GFP [Invitrogen A11122]: 1:500; rabbit polyclonal p-ERK1/2 [Sigma E7028]: 1:100) were incubated with the cells for one hour at room temperature on a rocker. The same wash steps done after fixation and before blocking were repeated. After the wash steps, the secondary antibody or antibodies (Alexa Fluor 488 donkey α rabbit IgG [Invitrogen A21206]: 1:250; Alexa Fluor 568 donkey α mouse IgG [Invitrogen A10037]: 1:250; Alexa Fluor 568 donkey α rabbit IgG [Invitrogen A10042]: 1:250) were incubated on the cells for one hour at room temperature on a rocker. The cells were washed three times for five minutes each with PBS. The cells were then coverslipped using Fluoromount G slide mounting medium.

2.12 Western Blot Analysis

Western blot analysis was performed on samples of supernatant from DF-1 transfected cells. DF-1 cells were transfected with RCAS(B), RCAS(A)/EGFP-P2A-Fgf19, or RCAS(B)/Fgf19-P2A-EGFP until most if not all of the cells contained the virus as previously described. After about one week, the cell media was changed to 1% Nuserum (same reagents as 10% Nuserum but less Nuserum) at 5 ml per plate.

The following day, the samples were prepared for the Western Blot. The media from the plates was collected, and protease inhibitor (Pierce Protease and Phosphatase Inhibitor Mini Tablets, 50X, Fisher Scientific A32963) added to the media at ~2X concentration. The media was

allowed to sit for several minutes before being filtered through a 0.22 µm filter to remove floating cells, debris, and virus particles. Half of the resulting filtrate was concentrated using an Amicon Ultra-15 Centrifugal Filter Unit (10,000 Molecular weight cut-off [NMWCO] for proteins between 20 and 60 k DA) (Sigma-Aldrich UFC9011008). The media was centrifugated at 4,000 x g for 20 minutes at 4°C. The concentrate was ~500 µl from the starting volume of 8.8 ml (RCAS(A)/EGFP-P2A-Fgf19), 9.5 ml (RCAS(B)/Fgf19-P2A-EGF), or 10.25 ml (RCAS(B)) of media. The concentrated supernatant was combined with 6X SDS sample buffer (0.375 M Tris, pH 6.8, 12% SDS, 60% glycerol, 0.6 M DTT, 0.06% bromophenol blue) to achieve a 1X concentration of loading buffer. These samples and the positive control purified ~2000 ng human recombinant Fgf19 (rhFgf19) protein (R&D Systems 969-FG-025) were then boiled for 5 minutes at 95 to 100°C and aliquoted. Jennifer Lee from Dr. Ruben Aguilar's lab provided a plasmid containing GFP was a positive control for GFP. The samples were frozen at -20°C until use in the Western Blot.

Students from Dr. Ruben Aguilar's lab, Jennifer Lee and Sneha Subramanian, performed the Western Blot analysis of the samples and positive control. The samples were blocked using milk. The gels were cut to remove the proteins above 55 kDa to minimize antibody usage, before the proteins were transferred to nitrocellulose membranes. The anti-cFgf19 primary antibody was an affinity-purified rabbit IgG antibody produced against two synthesized peptides matching amino acids 196 to 208 of cFgf19 and amino acids 211 to 223 of cFgf19 (NP_990005.2), donated to the Fekete lab from Dr. Ohuchi Hideyo. The anti-cFgf antibody was made in 2004 by FUJIFILM Wako Shibayagi Corporation (1062-1, Ishihara, Shibukawa, Gumma Pref., 377-0007, Japan) through Promega Corporation. This antibody was used at 1:1000 for these experiments. The anti-GFP antibody was the same one used in the immunocytochemistry experiments, but was used at 1:3000. Each nitrocellulose membrane was incubated with a single primary antibody. The second antibody used for both primary antibodies was an anti-rabbit-HRP conjugate at 1:1200, incubated for one hour at room temperature. The substrate used for detection was SuperSignal West Femto (Pierce). An Alpha-Innotech imaging system (San Leandro, CA, USA) was used for imaging of the membranes using chemiluminescence ranging from ten seconds to 20 minutes.

2.13 Immunohistochemistry (IHC)

The IHC experiments were performed similarly to the ICC experiments, but there were a few differences based on using tissue sections, not cells. The tissue sections were prepared in the same fashion as described earlier, with minor changes. The slides were thawed and PAP pen applied to the edges of the slides and then post-fixed in 4% PFA in PBS. Immediately before the blocking solution and the antibodies were added, the slides were dipped in either PBT or PBSw. Blocking was done with one of the following: 1) PBS with 5% goat serum, 0.05% Triton-X100, and 0.05% sodium azide or 2) PBS with 2% donkey serum, 0.05% Triton-X100, and 0.05% sodium azide. Primary antibodies were incubated either overnight at 4°C or for one hour at room temperature. The primary antibodies diluted in the blocking serum included: GFP: concentrations ranging from 1:500 to 1:1500; 3C2: concentrations ranging from 1:1 to 1:40 depending on days since thawing the aliquot; 3A10 (mouse IgG) (tissue culture supernatant taken from mouse hybridoma cells; Developmental Studies Hybridoma Bank): concentrations ranging from 1:1 to 1:20 depending on days since thawing the aliquot; HCS-1 (antibody against hair cells) (mouse IgG_{2a}) (Developmental Studies Hybridoma Bank): 1:200; Ctbp2 (antibody against pre-synaptic ribbons) (mouse IgG_1) (BD Biosciences 612044): 1:300); PH3 (polyclonal rabbit) (MilliporeSigma 38215950UG): 1:200. The secondary antibodies diluted in the blocking serum included: Alexa Fluor 488 donkey α-rabbit IgG: 1:250 or 1:500; Alexa Fluor 568 donkey α-mouse IgG: 1:250 or 1:500; Alexa Fluor 568 donkey α-rabbit IgG: 1:250; Alexa Fluor 488 goat α-rabbit IgG [Invitrogen A11034]: 1:250; Alexa Fluor 568 goat α-mouse IgG_1 [Invitrogen A21124]: 1:250; Alexa Fluor 647 goat α-mouse IgG_2 [Invitrogen A21241]: 1:250; Alexa Fluor 633 Phalloidin [Invitrogen A22284]: 1:200.

2.14 Alcian Blue Staining

After the slides were stained with DAB and underwent the 50 mM tris, pH 7.5, and three PBS washes, the slides were immersed in alcian blue (0.2% alcian blue (Allied Chemical 74240), 30% acetic acid, and 70% ethanol) for 30 minutes at room temperature. The slides were then washed with water once for five minutes and PBS three times for five minutes each. Finally, the slides were coverslipped using Fluoromount G slide mounting medium.

If no DAB staining was done, slides were first brought to room temperature, and PAP pen was added around slide edges before the slides were fixed using 4% PFA in PBS. The slides were then washed twice with PBS for five minutes each before immersion in Alcian blue as before. The washes followed as above, but the next step was dehydration. The slides were moved through a series of graded ethanol solutions for three minutes each (70%, 95%, 95%, 100%) and then three HemoDe solutions for three minutes each, before being coverslipped using SHUR/Mount.

2.15 RNAscope In Situ Hybridization

RNAscope® 2.5 HD Assay-RED (ACD Biotechnology Ltd.) in situ hybridization experiments were based on the manufacturer's protocol with some modifications. The slides used contained the same cryostat sections described above, except that the sections were placed close together in the middle of the slides. The slides were baked in a FisherBiotech Hybridization Incubator at 60°C for 30 minutes and then washed in PBS for five minutes while moving the slide rack up and down several times. Fixation of the sections was done using 4% PFA in PBS for one hour at room temperature. The sections were dehydrated through a series of five-minute ethanol washes moving from 50% to 70% and then 100% twice. A second baking step was done at 60°C for 30 minutes in the same oven.

Next, the target retrieval buffer was prepared. 20 minutes into the second baking step above, the buffer and water were started boiling. 150 ml of RNAscope® target retrieval buffer in a high profile 200 ml beaker with a small stir bar was boiled. The beaker was covered with foil, and the Corning PC-4200 heated stir plate was set to 350°F with the stir speed at 85 RPM. Once the buffer reached 100°F, the temperature was reduced to 240°F and adjusted as needed to keep the temperature at 100°F and with only gentle bubbling in some parts of the bottom of the beaker. In addition to the retrieval buffer, water was boiled in a high profile 200 ml beaker and kept at a gentle boil with a slide rack in it.

After the second baking step, the slide edges were lined with a PAP pen and eight to ten drops of RNAscope® H_2O_2 was added to each slide. These slides were incubated for ten minutes at room temperature and then were rinsed with water. The heated slide rack from the boiling water was removed, and the slides were placed in it. The rack was slowly returned to the boiling water for 30 seconds. The rack was moved to the boiling RNAscope® target retrieval buffer for five minutes and then put in a staining dish with water. The rack with slides was washed twice in water

and once in 100% ethanol while moving the rack up and down a few times. The slides were baked a third time in the same oven at 60°C for 15 minutes. PAP pen was applied again before tissue digestion.

200µl of Protease Plus was added to each slide, and a hybrid-slip coverslip was applied. These slides were incubated in a Hybaid OmniSlide at 40°C for 15 minutes, while the probes for the cFgfr4 mRNA were equilibrated at room temperature. The coverslips were removed from the slides in a deep Petri dish with water, and the dish gently moved to allow the coverslip to come off. The slides were washed twice in water while moving the rack up and down a few times to stop the tissue digestion. The slides were removed from the water, and the extra water was drained off. Then 200µl of the cFgfr4 probe was added to the slides, and coverslipping was done as before. The slides were incubated for two hours in the Hybaid OmniSlide at 40°C. The coverslips were removed as before, and the slides washed twice in RNAscope® wash buffer for two minutes at room temperature. The slides were moved to 5X SSC in a mailer box and left at room temperature overnight.

The following day, the slides were washed twice with RNAscope® wash buffer for 2 minutes at room temperature while moving the rack up and down a few times. The signal was amplified with a series of amplifier solutions labeled AMP1 through AMP6. AMP1 was hybridized to the slides for 30 minutes at 40°C in the Hybaid OmniSlide. The solution and coverslips were added to the slides in the same manner as the probe step above and the coverslips removed as before. The slides were washed with RNAscope® wash buffer as before. The following AMP steps used different temperatures and times; however, the method of AMP and coverslip application, coverslip removal, and wash were the same. AMP2 was hybridized for 15 minutes at 40°C in the Hybaid OmniSlide. AMP3 was hybridized for 30 minutes at 40°C in the Hybaid OmniSlide. AMP4 was hybridized for 15 minutes at 40°C in the Hybaid OmniSlide. AMP5 was hybridized for 30 minutes at room temperature. AMP6 was hybridized for 15 minutes at room temperature.

During the second wash after the AMP6 hybridization step, the RNAscope® Fast RED solution was mixed with 1:60 Fast RED-B in Fast RED-A. 200µl was prepared per slide. The signal was developed for ten minutes after adding the RNAscope® Fast RED to each slide in a humified box covered in foil, and a coverslip added as previously described. Afterward, coverslip removal and RNAscope® wash were done as before. The slides were baked one final time for at

least 30 minutes at 60°C in the FisherBiotech Hybridization Incubator. Coverslips were added in the hood after the slides were dipped in Xylene, and Fluoromount G slide mounting medium were added.

2.16 Imaging

Imaging of the cells and tissue, other than those in which antibodies with three different fluorescent colors were used, was done using SPOT software with a SPOT Insight sCMOS camera attached to a Nikon Eclipse E800 microscope. The slides were imaged at either 100X or 200X. When slides were incubated with secondary antibodies with three different fluorescent colors, confocal imaging was done using (Nikon Eclipse 90i) using a Nikon D-Eclipse C1 camera and NIS Elements softeware. These slides were imaged at 100X or 600X.

CHAPTER 3. RESULTS

3.1 cWnt9a Overexpression Results in Increased and/or Ectopic cFgf3, cFgf19, and cFzd4 mRNA Expression

The previous RNAseq experiment showed that viral-induced cWnt9a overexpression stimulated cFgf3 and cFgf19 mRNA expression within the chick basilar papilla (Table 1.1); however, this experiment did not indicate if these mRNAs were found on the neural side, abneural side, or both. Additionally, this experiment yielded no data on cFgf3 and cFgf19 mRNA expression within the statoacoustic ganglion (SAG), whose neurons innervate the basilar papilla. As such, to determine where cFgf3 and cFgf19 mRNA was found when cWnt9a was overexpressed and confirm the RNAseq experiment, in situ hybridization was performed. The cWnt9a viral vector was not added to the left ears, so they were used as a control for the amount and location of wild-type expression of cFgf3 and cFgf19. Both cFgf3 and cFgf19 mRNA were examined in E6 harvested embryos. As a positive control, cFgf19 mRNA expression was also observed in the developing chick eye, which has known expression at this age (Francisco-Morcillo et al., 2005). The tissue was sliced in cross-section from dorsal to ventral. Adjacent sections stained for different proteins or mRNA were compared to one another.

The cWnt9a overexpression was visualized using 3C2, an antibody against a core protein in the viral vector. This antibody has been shown to be a good proxy for cWnt9a transcripts produced by this vector (Munnamalai et al., 2017). 3C2 was found throughout the cochlear duct in both the sensory and nonsensory sides, with none in the control ear (Figure 3.1A & B). However, cWnt9a induced cFgf3 and cFgf19 mRNA were found only in the sensory region. The expression patterns overlap in their general location, but differ in the base of the basilar papilla. cFgf3 mRNA expression was found on the abneural side of the basilar papilla, whereas cFgf19 mRNA expression was located in the middle part of the basilar papilla. Further ventral, both mRNAs cover > ~75% of the basilar papilla (cFgf3: Figure 3.1D; cFgf19: Figure 3.1F) before ending in the abneural side as the organ transitions into the lagena.

These Wnt9a-induced expression patterns in the right ears contrasted with the left control ears, which showed significantly less total mRNA expression with faint expression of cFgf3 and cFgf19 in the abneural edge of the basilar papilla close to the future hyaline cell region or even in this region (cFgf3: Figure 3.1C; cFgf19: Figure 3.1E). Additionally, cFgf19 mRNA was found in

the left control and right overexpression SAGs and appeared increased in the right SAG of some embryos (Figure 3.1F). Overall, these experiments indicated that cWnt9a overexpression induced ectopic cFgf3 and cFgf19 mRNA expression throughout the basilar papilla and significantly increased the number of transcripts produced.

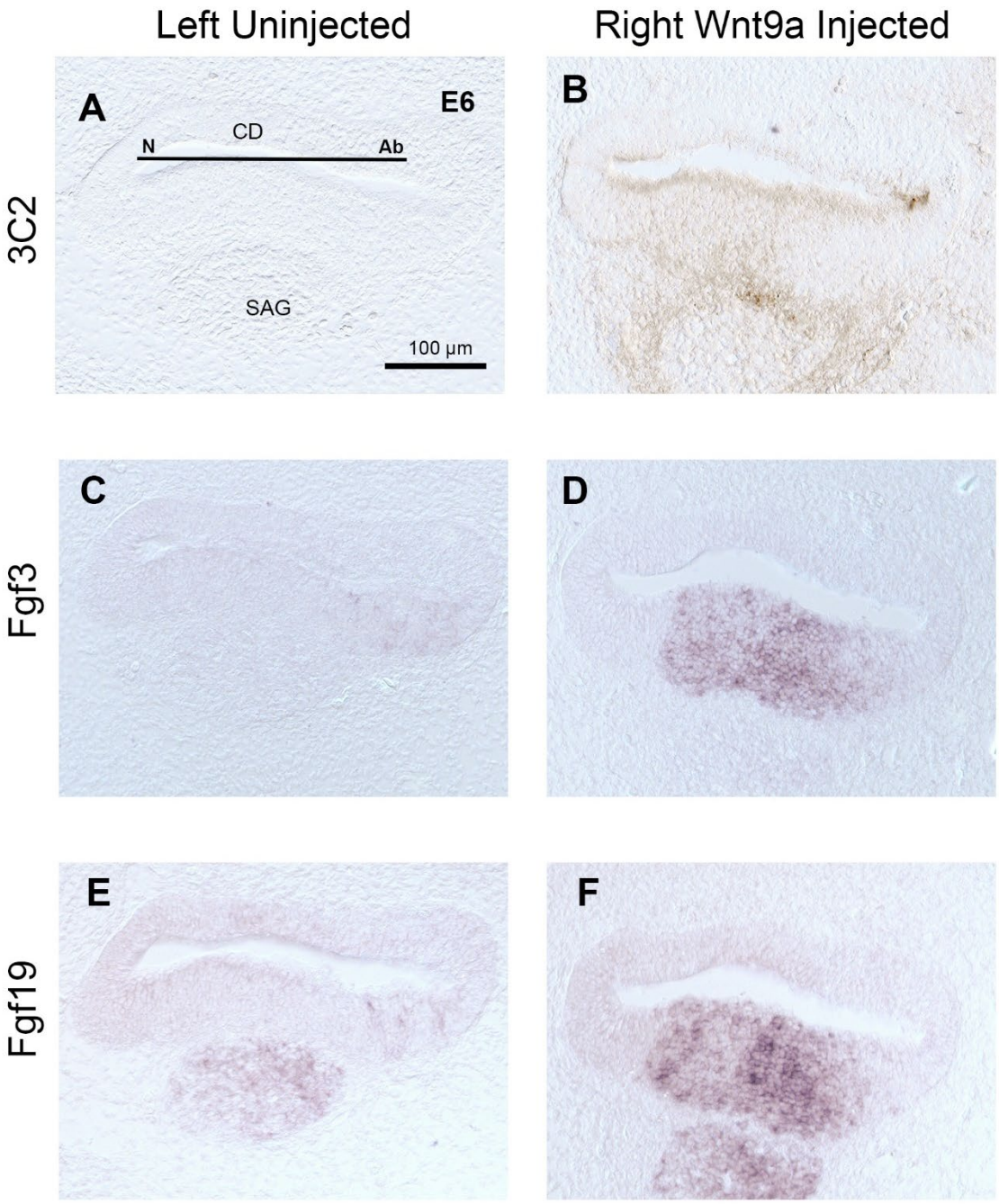

Figure 3.1: Wnt9a overexpression induced cFgf3 and cFgf19 expression. A & B: 3C2 (brown) expression indicated viral infection and the comparison shows cWnt9a expression only in the right ear. C & D: cFgf3 expression was robust throughout the basilar papilla with cWnt9a overexpression compared to a weak signal on the abneural side in the control left ear; n=5. E & F: Strong cFgf19 expression was found throughout the basilar papilla with cWnt9a overexpression, while it was confined to an abneural domain in the control left ear. In the SAG, the intensity of cFgf19 expression increased with cWnt9a overexpression; n=6. CD: cochlear duct; Ab: abneural side of basilar papilla; N: neural side of basilar papilla; SAG: statoacoustic ganglion

Additionally, to better understand the relationship between cFgf expression and cWnt9a expression, the expression of two Wnt receptors were tested in control and experimental ears. Both cFzd4 and cFzd10 mRNA were significantly altered due to cWnt9a overexpression. cFzd10 expression was found on the abneural side of the basilar papilla in wild-type ears, but was decreased with cWnt9a overexpression and was not found in the basilar papilla tissue through in situ hybridization (Munnamalai et al., 2017). cFzd4 expression was increased with cWnt9a overexpression, but was not previously tested with in situ hybridization. Moreover, other experiments have shown that both Fzd4 and Fzd10 these genes induce greater the Wnt9a activity compared to the other Fzds (Voloshanenko et al., 2017). CRISPR was used to knock out the expression of various Fzds in HEK293T cells, and then rescue experiments were done. Wnt activity was measured and showed that Wnt9a activity was greatest when Fzd4 was present and second greatest with Fzd10. The activity was much lower with the other Fzds. We therefore tested for the cFzd4 mRNA location in E6 embryos. Samples were selected that showed 3C2 viral expression throughout the basilar papilla in the right injected ears and none in the control ears (Figure 3.2A & B). In situ hybridization of nearby sections showed that cFzd4 was found in the future homogene cell region, the neural side of the basilar papilla and in part of the abneural region in both wild-type and cWnt9a overexpression ears; however, the expression domain extended further into the basilar papilla and the expression was stronger with cWnt9a overexpression (Figure 3.2C & D).

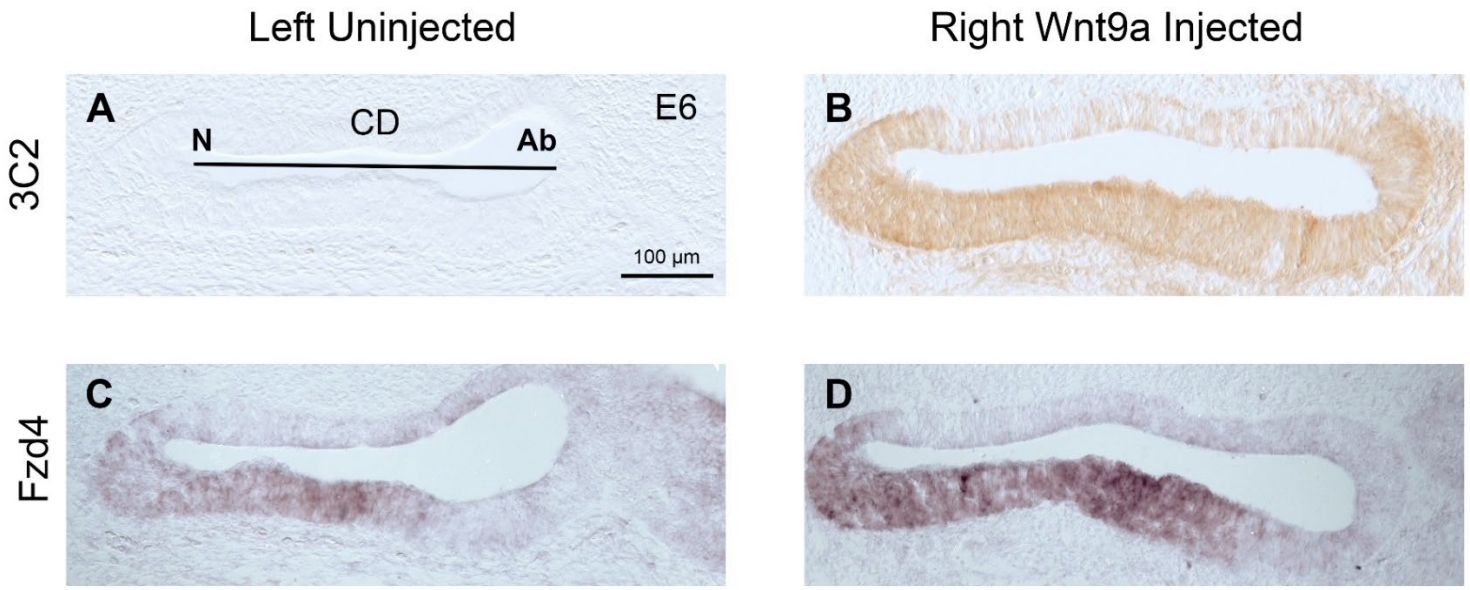

Figure 3.2: Wnt9a overexpression induced cFzd4 expression. A & B: 3C2 (brown) expression indicated viral infection and cWnt9a expression in the right ear. C & D: cFzd4 expression was found in the future homogene cell region and neural side of the basilar papilla in the wild-type embryos, but expression was extended in the basilar papilla of the right ears; n=1; E7 embryos n=2 but not shown. CD: cochlear duct; Ab: abneural side of basilar papilla; N: neural side of basilar papilla

3.2 RCAS(A)/EGFP-P2A-Fgf19 and RCAS(B)/Fgf19-P2A-EGFP Virus Proof of Concept

As we were using the viruses to drive overexpression of cFgf19 within the chick inner ear, they were tested to see if they produced the expected gene products. The viruses were designed to express both GFP and cFgf19, but only GFP and its endogenous fluorescence could be visualized in cells. There was no anti-cFGF19 antibody available that was usable in immunocytochemistry experiments.

Both overexpression vectors were used to create viruses through transfection of DF-1 cells and during this process, the GFP production was confirmed through its visualization in fixed or live cells. The approximate percentage of GFP+ cells in reference to all of the cells present within the field of view was determined. For RCAS(A)/EGFP-P2A-Fgf19, by six days after transfection, >75% of the cells were GFP+. For RCAS(B)/Fgf19-P2A-EGFP, by six days after transfection, ~75% of the cells were GFP+. This confirmed the viral spread and that the cells both contained and transcribed the GFP gene; however, this did not indicate if cFgf19 was transcribed within the cells. These data were sufficient to allow progression of the *in ovo* experiments designed to determine the role of cFgf19 in radial patterning of the basilar papilla.

3.3 Comparison of 3C2 and GFP within DF-1 Cells Transfected with RCAS(B), RCAS(A)/EGFP-P2A-FGF19 or RCAS(B)/Fgf19-P2A-EGFP

After confirmation of GFP production from both RCAS(A)/EGFP-P2A-FGF19 and RCAS(B)/Fgf19-P2A-EGFP, experiments were done to ask which produced more GFP using a more direct comparison. The previous experiments were done at different times so the imaging settings varied. The cells in this comparison experiment were imaged at the same time with the same settings. Cells previously transfected with RCAS(B), RCAS(A)/EGFP-P2A-FGF19 or RCAS(B)/Fgf19-P2A-EGFP were fixed and stained for 3C2 (virus backbone) and GFP (Figure 3.3). All three of the transfected cell lines had strong 3C2 expression in nearly 100% of the cells, indicating that the cells were efficiently producing virus (Figure 3.3A, C, E); however, the GFP expression differed. Cells transfected with RCAS(B) vector showed no GFP expression as expected since this virus had no insert containing GFP (Figure 3.3B). Cells transfected with RCAS(A)/EGFP-P2A-FGF19 or RCAS(B)/Fgf19-P2A-EGFP produced GFP as previously found; however, this direct comparison helped to distinguish the difference in production. RCAS(A)/EGFP-P2A-FGF19 transfected cells showed stronger GFP production compared to

RCAS(B)/Fgf19-P2A-EGFP transfected cells (Figure 3.3D and F). Most of the RCAS(A)/EGFP-P2A-FGF19 transfected cells had GFP production with a handful of brighter cells likely indicating higher levels of GFP. The RCAS(B)/Fgf19-P2A-EGFP transfected cells had little GFP with only about 25% or less of the transfected cells being GFP+. This experiment confirmed that both RCAS(B)/Fgf19-P2A-EGFP and RCAS(A)/EGFP-P2A-FGF19 transfected DF-1 cells produce EGFP, but that the expression of GFP in the RCAS(B)/Fgf19-P2A-EGFP transfected cells was reduced.

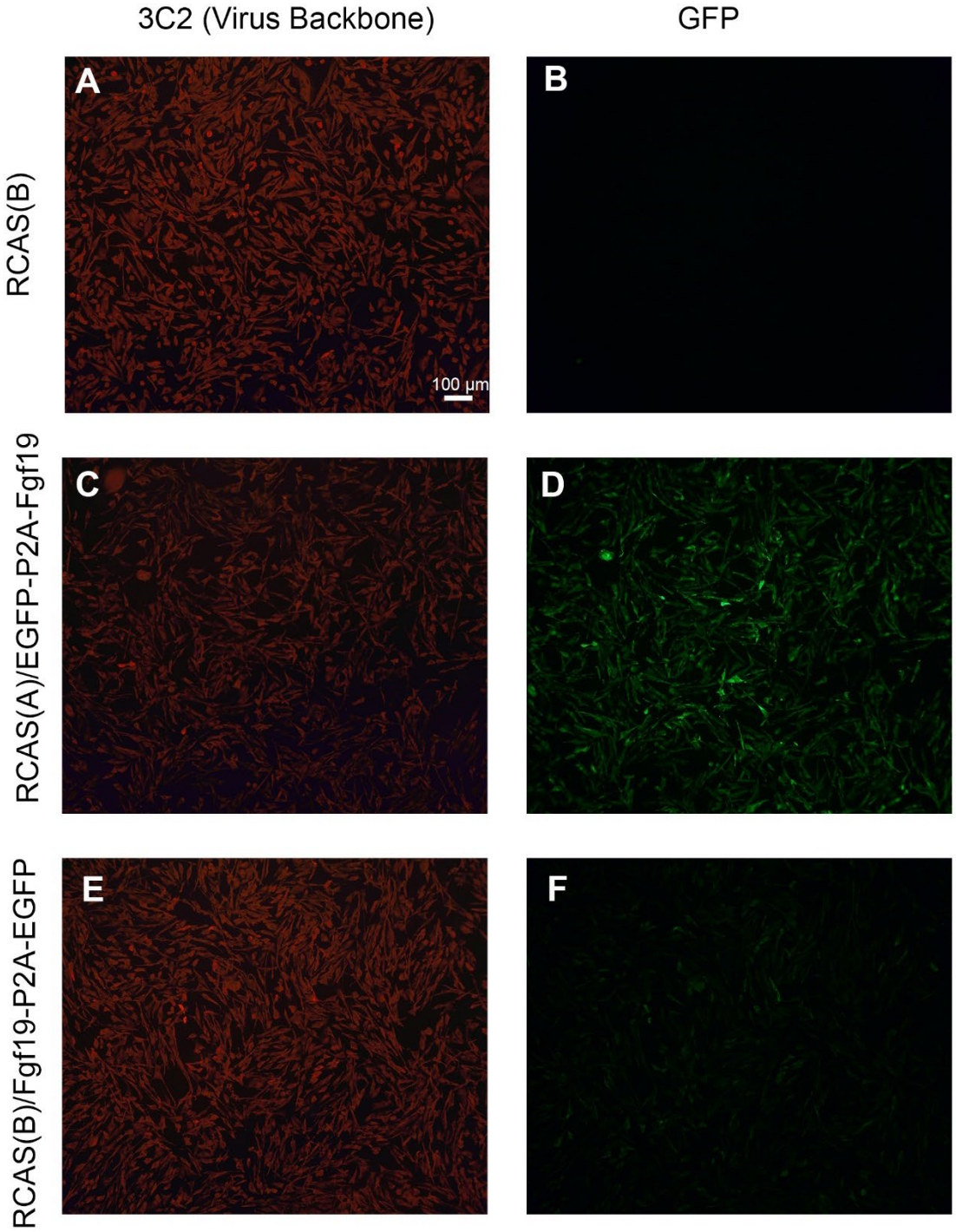

Figure 3.3: RCAS(A)/EGFP-P2A-Fgf19 and RCAS(B)/Fgf19-P2A-EGFP both produce GFP, but in different quantities. DF-1 cells were transfected with RCAS(B) (A & B), RCAS(A)/EGFP-P2A-Fgf19 (C & D), or RCAS(B)/Fgf19-P2A-EGFP (E & F). The cells were imaged with the same settings. All of three transfections showed similar expression of RCAS core protein (3C2+), but RCAS(B), without an insert, produced no GFP and RCAS(A)/EGFP-P2A-Fgf19 produced more GFP than RCAS(B)/Fgf19-P2A-EGFP. A-F n=1.

3.4 Western Blot Analysis of cFgf19 and GFP Secretion

In addition to visualizing GFP within the cells to see transcription of the insert, experiments were needed to see if cFgf19 was being transcribed. Since there was not a cFgf19 antibody usable in immunocytochemistry experiments, there was no way to confirm ectopic, virus-mediated production and secretion of cFgf19 protein within or around the chick inner ear. Instead, the Fekete lab obtained an antibody against cFgf19 that works in Western blots. The antibody was generously donated by Dr. Hideyo Ohuchi of Okayama University. This antibody was created in 2004 and stored at 4°C for many years. In 2020, Dr. Ohuchi's lab tested that antibody on Western Blots of supernatant from HEK293T cells transfected with a plasmid containing cFgf19 and determined a dilution for which it could detect Fgf19 protein.

With the antibody specificity confirmed, Western blot analysis was done on supernatant from DF-1 cells transfected with one of three constructs: RCAS(B), RCAS(A)/EGFP-P2A-FGF19 or RCAS(B)/Fgf19-P2A-EGFP. These cells were transfected in the same manner as previously done and the supernatant concentrated down on average ~94.5%. Graduate students Jennifer Lee and Sneha Subramanian of Dr. Ruben Aguilar lab's at Purdue University performed several Western Blots of the samples. The samples were separated with a sample buffer lane in order to prevent protein slipover between lanes. The brightness and contrast of the chemiluminescence detection were adjusted to better visualize the different bands.

Human Fgf19 was used as a positive control for these experiments as this antibody has been shown to bind human Fgf19 (Kurose et al., 2005). There were two synthesized peptides used as antigens for affinity purification of the cFgf19 primary antibody. Blast analysis showed that one of these antigens corresponding to amino acids 196 to 208 of cFgf19 is identical to the last nine amino acids in the recombinant human Fgf19 (rhFgf19) protein but not the first four, whereas the second antigen only matches with six of the 13 amino acids in rhFgf19 (Altschul et al., 1997) (Altschul et al., 2005). As such it is most likely that the nine amino acid sequence that is identical in both rhFgf19 and cFgf19 is what allows for binding of the cFgf19 antibody with both human and chick Fgf19 protein. The rhFgf19 protein was detected on the membrane; however, 20 minutes of exposure was needed for a band to be visible by chemiluminescence, longer than what was needed for bands to be visible in the experimental lanes (Figure 3.4B). As such, there was more than 2000 ng of cFgf19 in the experimental lanes since that was the approximate amount in the positive control lane. The band was ~20 kDa, which was as expected since the rhFgf19 protein

was supposed to be 21 kDa according to the manufactory's website. The negative control lane of RCAS(B) transfected concentrated supernatant showed no cFgf19, indicating there is little if any cFgf19 secretion from DF-1 cells.

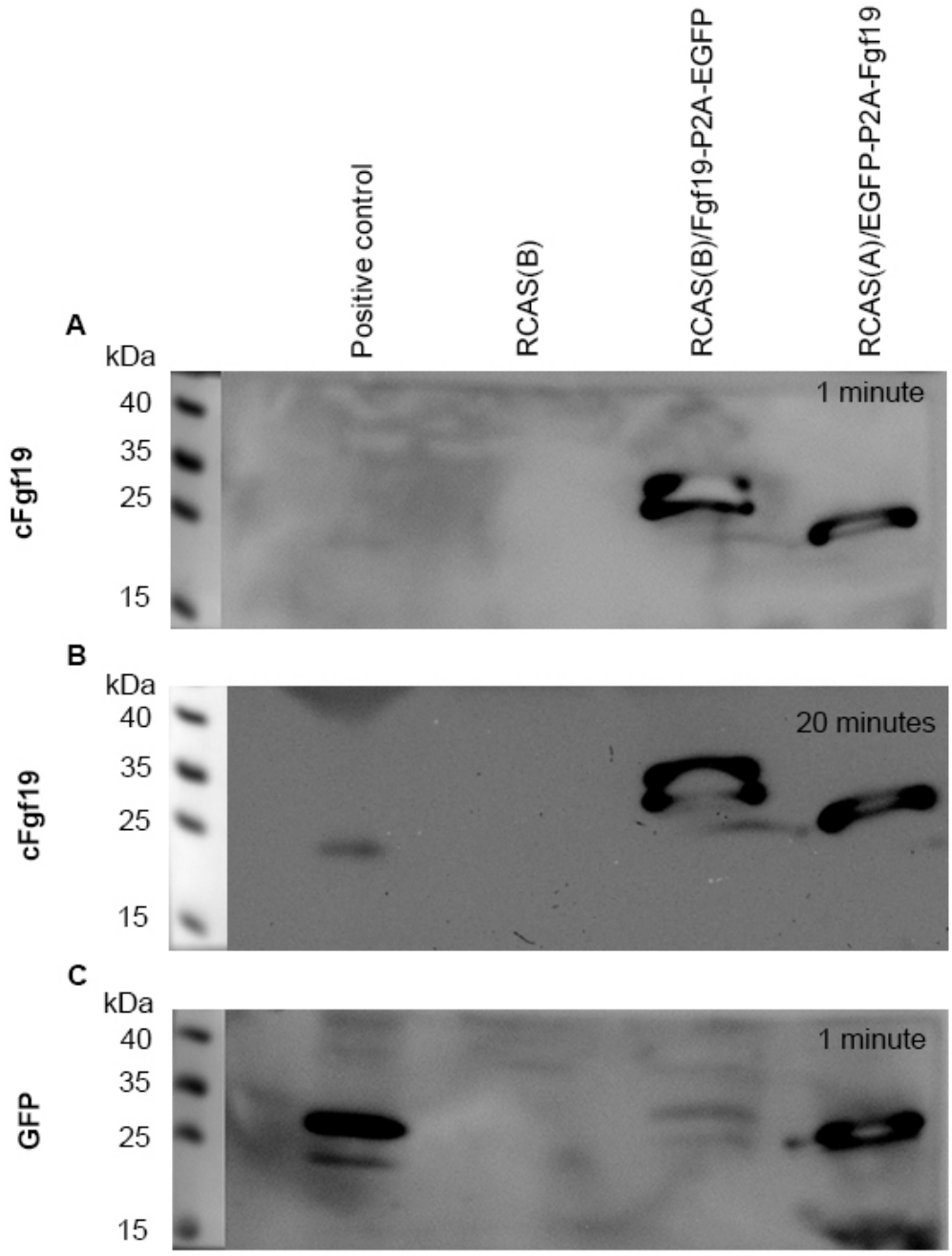

Figure 3.4: RCAS(A)/EGFP-P2A-Fgf19 and RCAS(B)/Fgf19-P2A-EGFP both produce Fgf19 and GFP, but the protein sizes differ. DF-1 cells were transfected with RCAS(B), RCAS(A)/EGFP-P2A-Fgf19, or RCAS(B)/Fgf19-P2A-EGFP. Western blot analysis was done on membranes incubated with α-cFgf19 antibody and exposed to 1 or 20 minutes of chemiluminescence (A & B) (n=2) or GFP but the GFP membrane was incubated with α-GFP antibody and exposed to 1 minute of chemiluminescence (C) (n=1). RCAS(B)/Fgf19-P2A-EGFP transfected cells secreted cFgf19 at ~30 and ~35 kDa and GFP at ~25 and ~30 kDa. RCAS(A)/EGFP-P2A-Fgf19 transfected cells secreted cFgf19 at ~25 kDa and GFP at ~25 kDa. The positive control for cFgf19 antibody was rhFgf19 and for GFP was free GFP.

Concentrated supernatant from RCAS(A)/EGFP-P2A-FGF19 and RCAS(B)/Fgf19-P2A-EGFP transfected cells both showed cFgf19 secretion; however, the cFgf19 band size and number differed. With one and twenty minutes of chemiluminescence, membranes containing RCAS(B)/Fgf19-P2A-EGFP supernatant had two similar sized cFgf19 proteins (Figure 3.4A and B). One protein was ~30 kDa and the other was ~35 kDa. These doublets were found in multiple independent runs of the Western blot. The expected size of cFgf19 was ~25 kDa, smaller than the bands found. RCAS(A)/EGFP-P2A-FGF19 supernatant membranes had only one cFgf19 protein ~25 kDa, meaning this band was the expected size (Figure 3.4A and B).

In addition to cFgf19 secretion, GFP secretion was also tested on a second membrane that was run concurrently. Interestingly, the supernatant from the RCAS(B)/Fgf19-P2A-EGFP transfected cells also showed a doublet for GFP (Figure 3.4C). These bands were slightly smaller than the cFgf19 bands at ~25 and ~30 kDa. The supernatant from the RCAS(A)/EGFP-P2A-FGF19 transfected cells showed one band at ~25 kDa, which is the expected size. These experiments showed that both overexpression viruses induced cFgf19 and GFP production and secretion.

3.5 Comparison of 3C2 and GFP within RCAS(A)/EGFP-P2A-FGF19 Infected Chick Embryos

In addition to comparing 3C2 virus core protein and GFP expression within DF-1 transfected cells, 3C2 and GFP expression were compared with RCAS(A)/EGFP-P2A-FGF19 infected chick basilar papillas. RCAS(A)/EGFP-P2A-FGF19 was injected into E3 otocysts and harvested at E6. Similar to the DF-1 cells, not all of the 3C2 positive cells were also GFP positive (Figure 3.5A & B). There are several possible reasons for finding higher 3C2-positive (i.e., virus-infected) cells in RCAS(A)/EGFP-P2A-Fgf19 injected embryos without a corresponding GFP signal in these same cells. One possibility is the virus was not producing similar amounts of the two splice variants needed to translate these two distinct proteins, and this might vary for different cell-types. For example, periotic mesenchymal cells often showed wide discrepancies between these two proteins. Another possibility is that the genomic RNA carried in different viruses may vary, with some having jettisoned the non-viral elements in favor of faster replication and spread; that is, some of the viral particles would not contain the full-length insert. We considered the possibility that this may have occurred during the period of creating the first virus stock, generating a mixed

pool of two distinct virus populations, one with at least the GFP part of the insert and one without. To address this, a second independent virus stock of RCAS(A)/EGFP-P2A-FGF19 was generated and concentrated; however, the period of time in which the virus was allowed to spread was reduced by 24 hours (from 6 days to 5 days before adding Nuserum on the day before supernatant was first collected). We reasoned that there would be less replication time for any subpopulation carrying a smaller genome to dominate the viral stock, hoping that all cells still had time to become infected. Indeed, at five days after transfection, ~100% of the cells were GFP+. This was a higher percentage of GFP+ than the ~75% found with the first stock. This second virus stock was also used for injections into chick otocysts at E3 to see if there were any differences in phenotype of the inner ear, including the basilar papilla, compared to the first batch of the virus. However, this virus stock showed similar results of 3C2 positive cells that were not GFP positive.

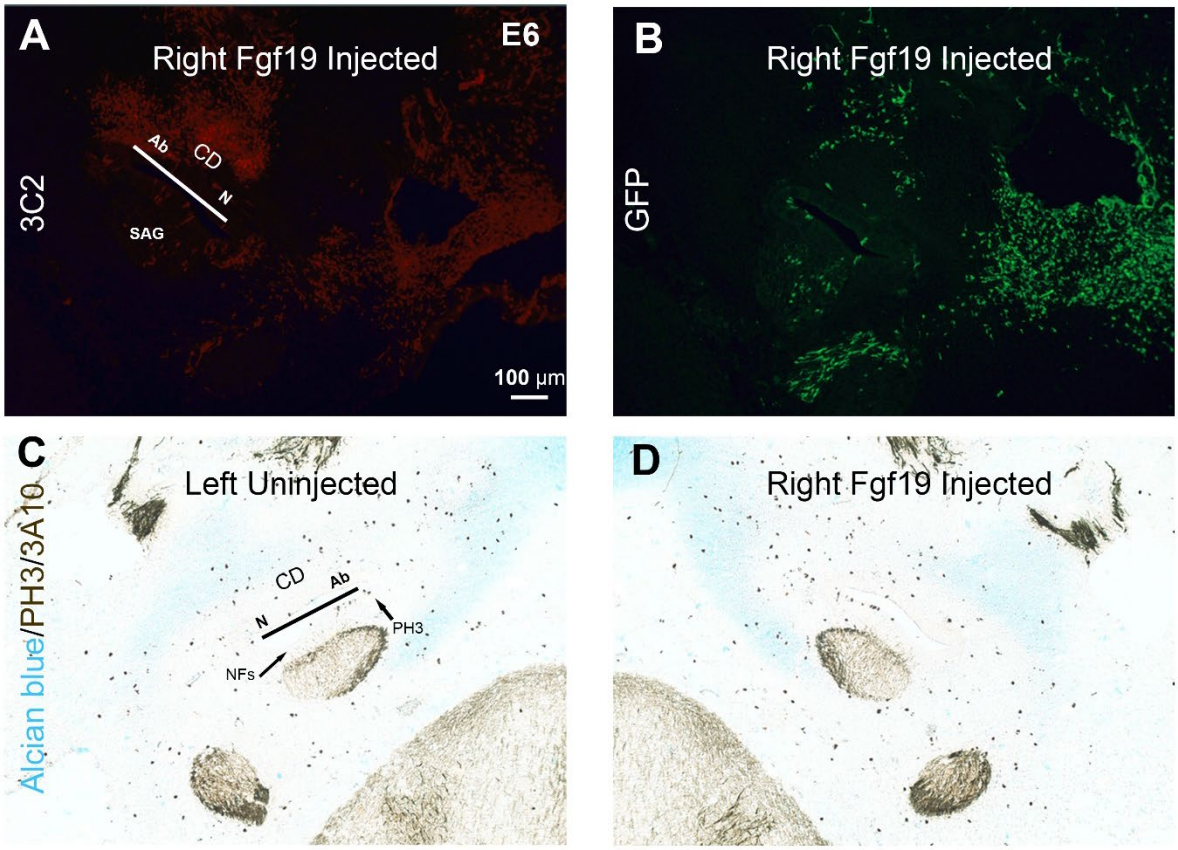

Figure 3.5: RCAS(A)/EGFP-P2A-FGF19 injected tissue showed no changes in mesenchyme, number of proliferating cells in the basilar papilla, or innervation at E6. A & B: 3C2 and GFP expression from one section which is adjacent to the section in D; n=11. C & D: No change in mesenchyme labeled by Alcian blue around the cochlear duct or in innervation, neurofilaments labeled by 3A10 (linear axonal profiles), or in proliferation, labeled with PH3 (isolated brown punctae), within the abneural side of the basilar papilla; n=4. CD: cochlear duct; Ab: abneural side of basilar papilla; N: neural side of basilar papilla; SAG: statoacoustic ganglion; PH3: antibody against proliferating cells; 3A10: antibody against afferent innervation; NFs: neurofilaments labeled with 3A10; Alcian blue: stain for developing cartilage

3.6 Effect of cFgf19 Overexpression on Innervation and Hair Cells

The innervation of basilar papilla by the statoacoustic ganglion was tested in the inner ears injected with RCAS(A)/EGFP-P2A-Fgf19 as E3 otocysts and harvested at E6, E10, and E14 when the cochlear duct has elongated ventrally. For both E6 and E10 embryos, immunostaining for virus infection (with GFP and/or 3C2) and 3A10 was done to compare the location of the virus with neurofilaments of the statoacoustic ganglion on the injected side. The hypothesis was that there would be an increase in the overall innervation, especially on the abneural side, as a result of

otocyst injection with RCAS(A)/EGFP-P2A-Fgf19. The reasoning behind this hypothesis was that when cWnt9a was overexpressed in the previous experiments, there was a large increase in the innervation of the basilar papilla at E18 (Munnamalai et al., 2017). The left ear was used as a control for normal innervation and was compared to the right ear to see if there was a change in innervation. The region of the basilar papilla innervated by the statoacoustic ganglion on the right side appeared similar in size and location to the innervation in the left control ear despite the viral infected cells within the basilar papilla, statoacoustic ganglion, and mesenchyme (Figure 3.5C & D). E10 innervation was also unchanged between the left control ear and the right injected RCAS(A)/EGFP-P2A-Fgf19 ear despite the viral infected cells within the basilar papilla, statoacoustic ganglion, and cartilage (Figure 3.6). The hair cells of the basilar papilla were also stained, using HCS-1 antibody at E10 to look for changes between the left control ear and right injected ear. There were no differences found in the size or relative amount of hair cells within the basilar papilla (Figure 3.6A & B).

E14 cochlear ducts were also tested to see if the RCAS(A)/EGFP-P2A-Fgf19 injection altered the innervation or hair cells. By this stage, differences in the length of tall and short hair cells are emerging. These embryos were stained with GFP to test for virus infection, HCS-1 for hair cells, and Ctbp2 for pre-synaptic ribbons of afferent innervation (Figure 3.7A). The neural side of the basilar papilla contains more pre-synaptic ribbons due to more afferent innervation so if cFgf19 overexpression induced a larger neural fate region of the basilar papilla, than this phenotype would be present across the length of the organ. However, there was not a shift in phenotype. Figure 8B & C shows an example where despite the many GFP positive cells found in the abneural region there were still many fewer pre-synaptic ribbons in this region compared to the neural region which happened to have only sparse GFP expression in this section.

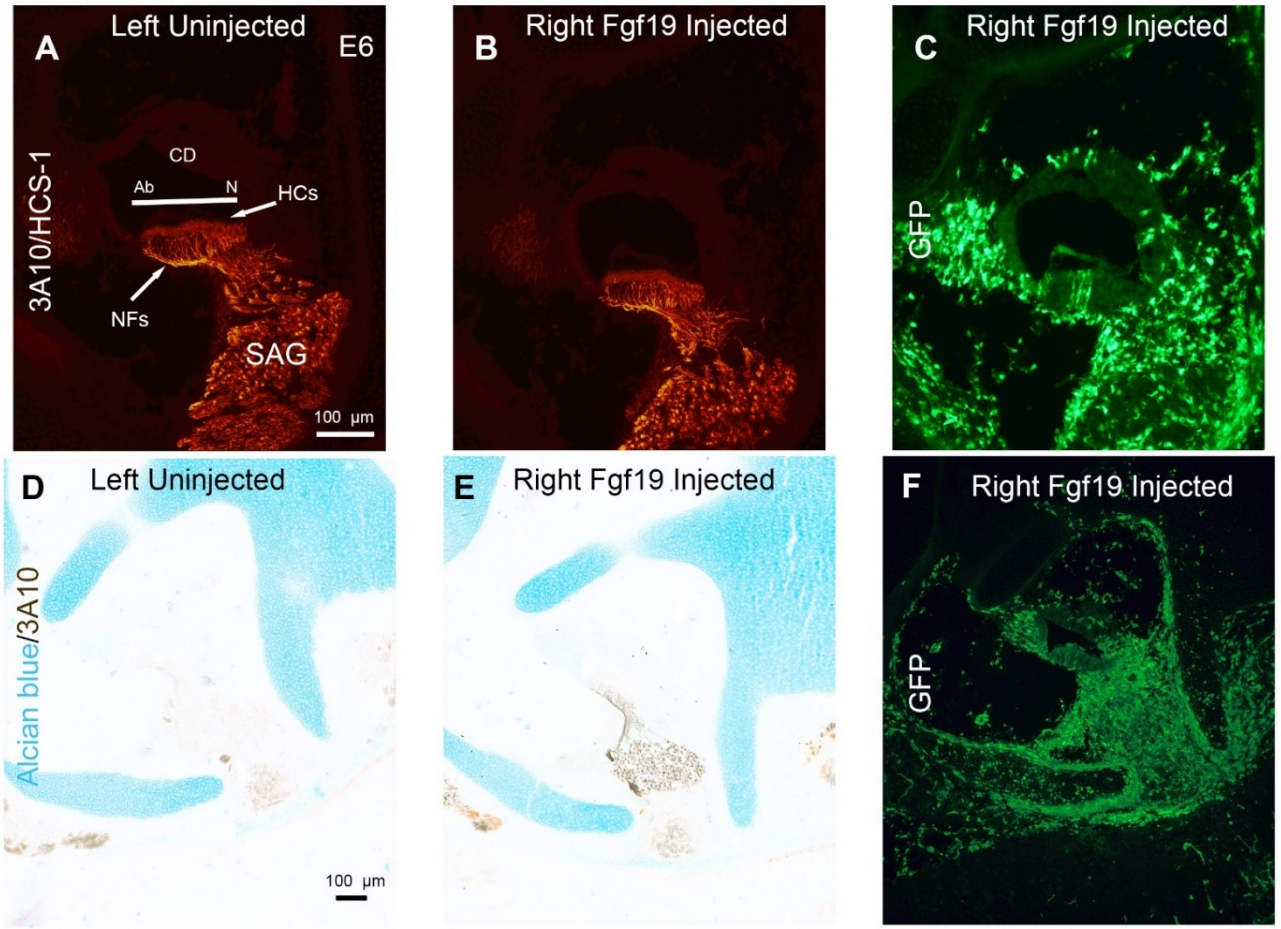

Figure 3.6: RCAS(A)/EGFP-P2A-FGF19 injected tissue showed no changes in cartilage or innervation at E10. A & B: No alterations in hair cells and innervation, neurofilaments labeled by 3A10, were found in the right side compared to the left. C: GFP expression in same tissue section as B; n=4. D & E: No alterations in cartilage labeled with Alcian blue; n=4. Note: Differences in 3A10 staining between E and F was not representative of embryos imaged. F: GFP expression in same tissue section as E. CD: cochlear duct; Ab: abneural side of basilar papilla; N: neural side of basilar papilla; SAG: statoacoustic ganglion; 3A10: antibody against afferent innervation; NFs: neurofilaments labeled with 3A10; HCs: hair cells labeled with HCS-1; HCS-1: antibody against hair cells

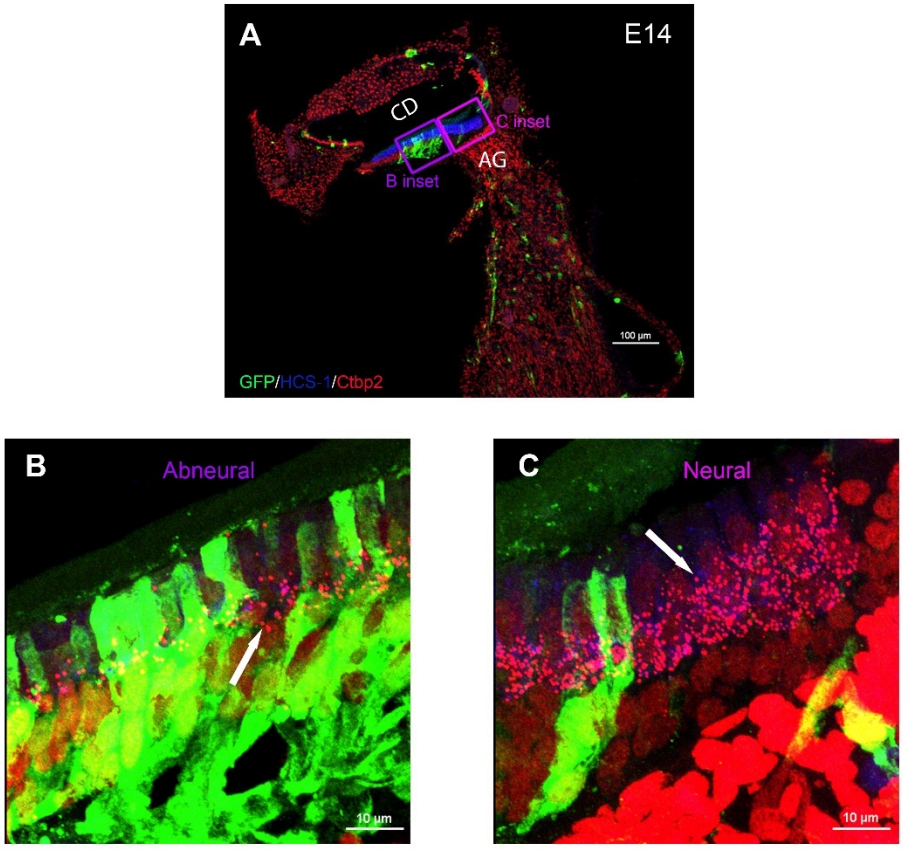

Figure 3.7: RCAS(A)/EGFP-P2A-FGF19 injected tissue showed no changes in hair cell differentiation or innervation at E14. A: Cochlear duct with GFP expression on the abneural side (B inset). B: Abneural side of the basilar papilla with GFP expression and smaller number of pre-synaptic ribbons of afferent innervation labeled in red (white arrow indicates one example). C: Neural side of the basilar papilla with less GFP expression and larger number of pre-synaptic ribbons of afferent innervation labeled in red (white arrow indicates one example). A-C n=1. CD: cochlear duct; AG: auditory ganglion; HCS-1: antibody against hair cells (blue); Ctbp2: antibody against pre-synaptic ribbons (red)

3.7 Effect of cFgf19 Overexpression on Cartilage Development around the Cochlear Duct

Another way the bioactivity of the RCAS(A)/EGFP-P2A-Fgf19 virus was tested was by seeing if the cartilage formation surrounding the cochlear duct was altered. The hypothesis generated was that the virus would reduce or eliminate the mesenchyme or cartilage around the duct. This hypothesis is partially based on unpublished data from our lab that β-catenin, a downstream target of Wnts, stops chondroblast differentiation into chondrocytes. It appears that

Wnts may keep the cells in a proliferative state and stale cartilage formation. As Fgf19 is likely a downstream effector of Wnt9a, Wnt9a may direct Fgf19 to stop this differentiation. If this is the case, then it would be predicted there would be less or no cartilage formation around the cochlear duct and more proliferation of the pre-cartilage cells.

Otocysts were injected at E3 with RCAS(A)/EGFP-P2A-Fgf19 and the ears were examined at E6 and E10 to evaluate cartilage formation using Alcian blue staining. This was compared to the location of the virus, specifically the location of GFP. There was no apparent difference in Alcian blue staining between the left uninjected and right injected ears around the cochlear duct at the two ages (Figure 3.5C & D, 3.6D & E). Additionally, the region of GFP did overlap with the part of the location of Alcian blue suggesting that cFgf19, if secreted ectopically, was not affecting the cartilage differentiation process.

3.8 Effect of cFgf19 Overexpression on Proliferation within the Cochlear Duct

Another phenotype found with cWnt9a overexpression was an increase in proliferating cells in the abneural side of the basilar papilla at E6 (Munnamalai et al., 2017). This phenotype was tested in embryos in which the otocyst was injected with RCAS(A)/EGFP-P2A-Fgf19 at E3 and the ears were evaluated at E6. The tissue was stained with the PH3 antibody which binds to proliferating cells. This antibody is directed against histone H3 phosphorylated at serine 10, a modification found in cells undergoing mitosis (Wei et al., 1998). Qualitatively, there was no apparent increase in PH3 positive cells within the abneural side of the basilar papilla with cFgf19 overexpression compared to the left control ear (Figure 3.5C & D). This would indicate the cFgf19 is not at all or is not solely responsible for the increase in proliferation in the abneural side of the basilar papilla with cWnt9a overexpression.

3.9 Test of cFgf19 Downstream Signaling

The downstream signaling of cFgf19 was tested by seeking evidence for increased phosphorylated ERK. The antibody used binds to human p-ERK1 $pThr^{202}$, $pTyr^{204}$ and human p-ERK2 $pThr^{185}$, $pTyr^{187}$, which both correspond to the single chicken p-ERK1/2 protein's amino acids 193 and 195. Previous literature showed that Fgf19 addition induces more ERK phosphorylation both in primary human hepatocytes and rat myoblast L6 cells transfected with

Fgfr1c, Fgfr2c, Fgfr3c, or Fgfr4c and β-klotho or transfected with only Fgfr4 (Song et al., 2009) (Wu et al., 2009). Additionally, this antibody has been shown to work with immunocytochemistry in B65, rat neuronal cells at 1:500 (Zhu et al., 2002). As such, it was chosen to see if either RCAS(A)/EGFP-P2A-Fgf19 or RCAS(B)/Fgf19-P2A-EGFP induced more phosphorylated ERK when the plasmids were transfected into DF-1 cells. The assumption with this approach was that autocrine signaling would take place, whereby the DF-1 cells would secrete virus-transduced Fgf19 and then respond to it using one or more endogenously-expressed receptors (or coreceptors) for the cFgf19 ligand. RCAS(B) transfected DF-1 cells were used as a control for endogenous levels of phosphorylated ERK. Images were taken of the GFP signal not enhanced with an antibody and the p-ERK immunofluorescence signal. The imaging settings were the same within each fluorescent color so that the images could be directly compared. As expected, the RCAS(B) transfected cells had no GFP expression since no GFP gene was added (Figure 3.8A). The GFP expression in the RCAS(A)/EGFP-P2A-Fgf19 and RCAS(B)/Fgf19-P2A-EGFP transfected cells appeared similar (Figure 3.8C & E). Additionally, the p-ERK signal was very comparable inall three of the transfected cell lines (Figure 3.8B, D, & F). These experiments showed no increase in phosphorylation of ERK with either virus containing Fgf19.

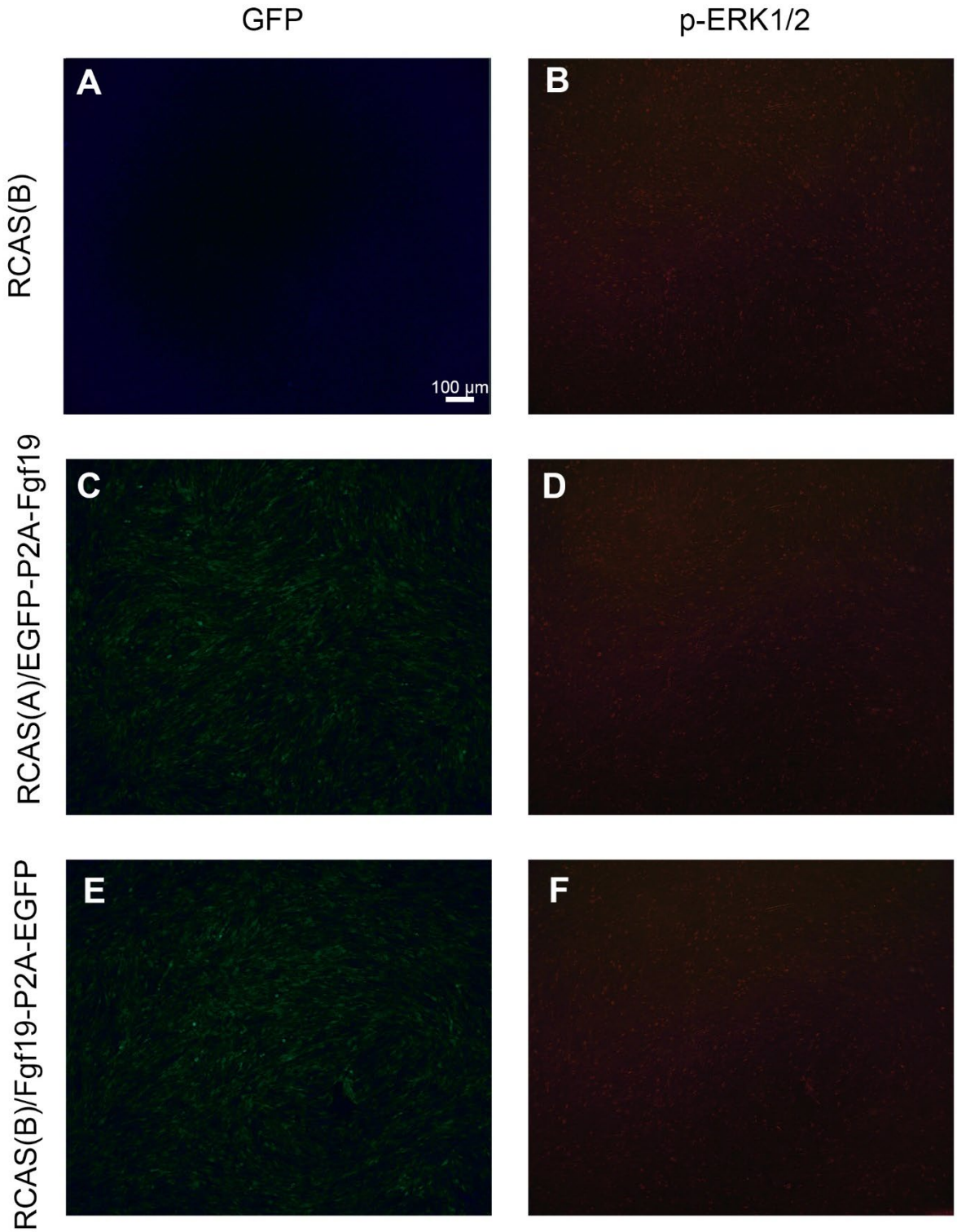

Figure 3.8: RCAS(B), RCAS(A)/EGFP-P2A-Fgf19, and RCAS(B)/Fgf19-P2A-EGFP all produce similar amounts of p-ERK1/2. DF-1 cells were transfected with RCAS(B) and showed no GFP (A & B), RCAS(A)/EGFP-P2A-Fgf19 (C & D), or RCAS(B)/Fgf19-P2A-EGFP (E & F), both of which had similar GFP expression. Each fluorescent color was imaged with the same settings. GFP was not enhanced with an antibody. A-F n=1.

3.10 Effect of Fgf19 Overexpression on Fgf3 mRNA production

RCAS(A)/EGFP-P2A-Fgf19 injected embryos were tested for Fgf3 mRNA expression. It was hypothesized that cFgf19 might be partially responsible for inducing expression of cFgf3 in the basilar papilla, considering how the transcript levels were changed in the cWnt9a overexpression model. Additionally, it has been shown that cFgf19 can induce cFgf3 expression in very early chick ear development (Ladher et al., 2000). Figure 3.9 compares the increase in cFgf3 mRNA expression in the context of virus-mediated cWnt9a overexpression (Figure 3.9A & B) with the absence of a change in cFgf3 mRNA expression using the cFgf19 viral vector (Figure 3.9C & D). Adjacent sections showed good virus infection using GFP and 3C2 (data not shown). These embryos underwent in situ hybridization at the same time. Infection with a virus encoding cFgf19 did not appear to alter cFgf3 expression.

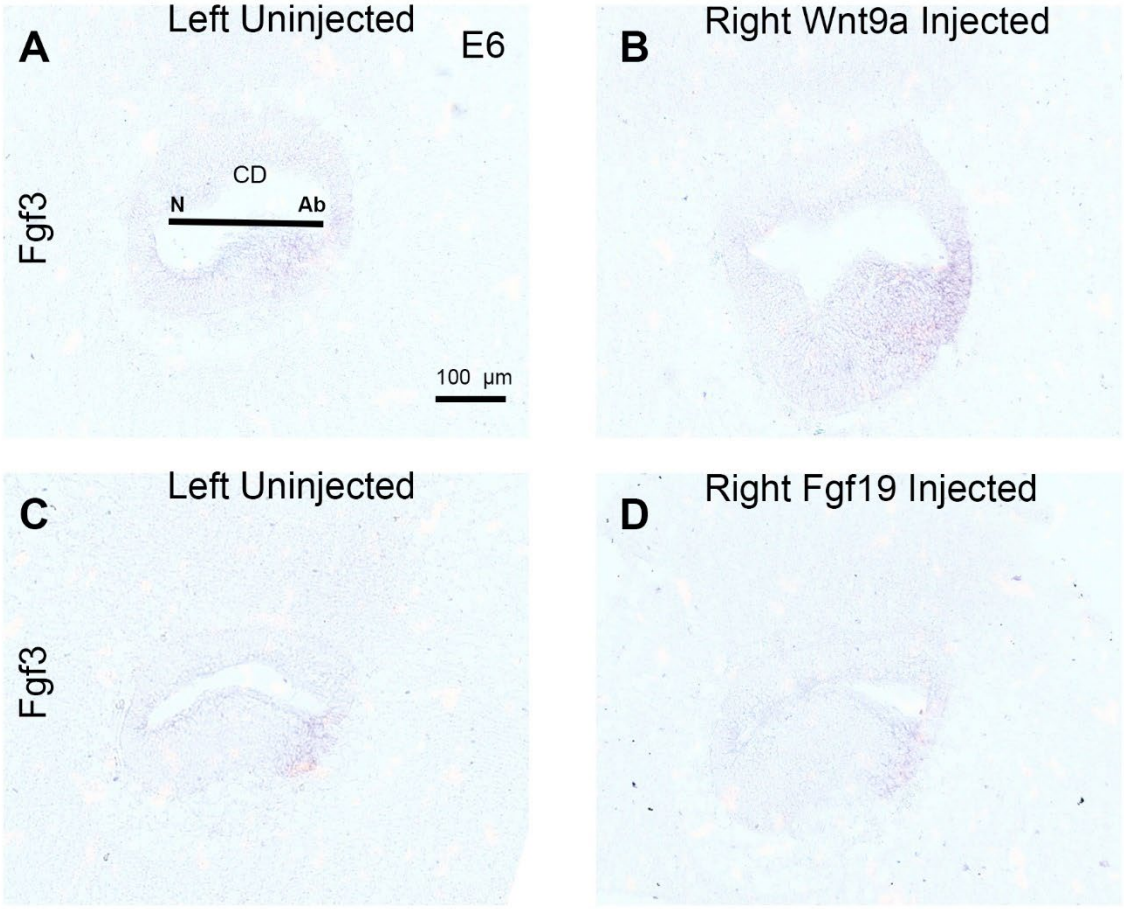

Figure 3.9: Virus encoding Fgf19 does not alter Fgf3 expression. RCAS(A)/Wnt9a injected embryos were compared to RCAS(A)/EGFP-P2A-Fgf19 injected embryos to see the difference in cFgf3 expression. cWnt9a overexpression increased cFgf3 expression (A & B; n=4) but cFgf19 overexpression did not alter cFgf3 expression (C & D; n=3). These embryos underwent in situ hybridization at the same time. CD: cochlear duct; Ab: abneural side of basilar papilla; N: neural side of basilar papilla

3.11 cFgfr4 Expression within and around the Developing Inner Ear

Since no phenotypic changes were seen following infection with cFgf19 virus, the question arises as to whether the appropriate receptors are available to respond to excess or ectopic ligand. As previously discussed, Fgf19 binds to receptors Fgfr1c, Fgfr2c, Fgfr3c, and Fgfr4. Fgfr4 expression was picked for two reasons. One, it is a prominently studied receptor for Fgf19. Second, the cWnt9a overexpression mRNA data supported its use. Again, as mentioned earlier, Fgf19 can bind to Fgfr4 without needing β-klotho to induce downstream signaling (Wu et al., 2009); this was significant due to the extremely low levels of β-klotho in both control and cWnt9a overexpression

basilar papillas (Table 1.1). The hypothesis was that if cFg19 was acting within the basilar papilla to cause any of the phenotypic changes seen with cWnt9a overexpression, then it was acting through cFgfr4. Normal expression patterns of cFgfr4 were determined using RNAscope in situ hybridization. E6 and E8 embryos both showed weak expression of cFgfr4 within the basilar papilla; however, the expression was much stronger in the precartilage and cartilage of the periotic capsule surrounding the cochlear duct (Figure 3.10).

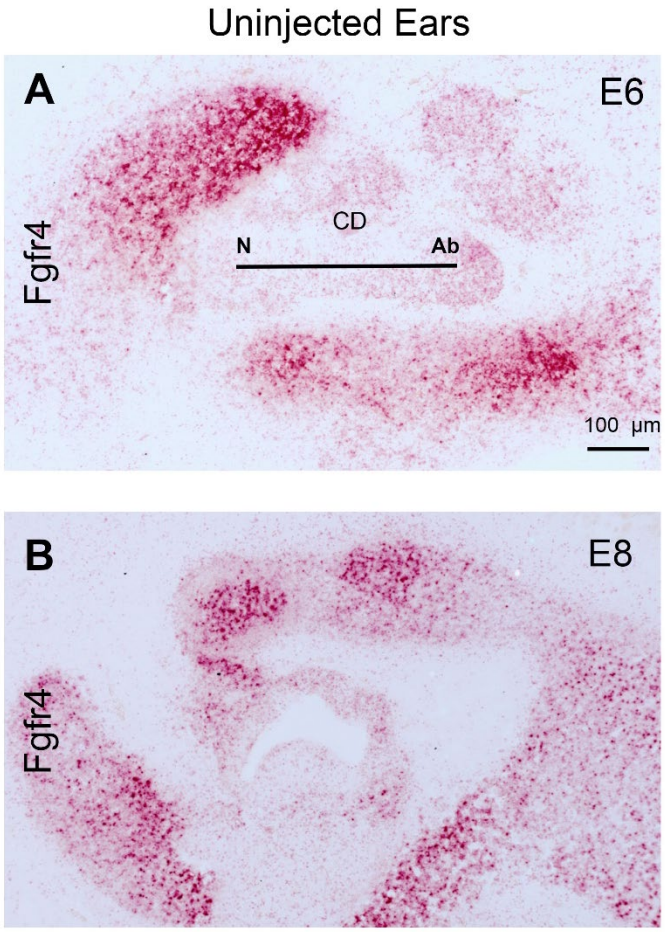

Figure 3.10: cFgfr4 is found within the basilar papilla and around the cochlear duct. RNAscope in situ hybridization for Fgfr4 was done on wild-type E6 (A; n=2) and E8 embryos (B; n=1) and showed the greatest expression in the epithelium of the cochlear duct, but in the surrounding precartilage and cartilage of the developing otic capsule. CD: cochlear duct; Ab: abneural side of basilar papilla; N: neural side of basilar papilla

CHAPTER 4. DISCUSSION

4.1 Differences in cFg3 and cFgf19 Expression Within the Chick Basilar Papilla Compared to Published Data

First, it is essential to note that although cWnt9a overexpression increased cFgf3 and cFgf19 mRNA expression, the wild-type mRNA expression detected in the left control ear was far less than reported in earlier papers that used the same plasmids to make the in situ hybridization anti-sense RNA probes. Both cFgf3 and cFgf19 mRNA were previously reported in high levels at both E5 and E8 (Olaya-Sanchez et al., 2017) (Sanchez-Calderon et al., 2007). These papers and the results described above used White Leghorn chickens, meaning this should not have contributed to the difference in mRNA expression. The protocol used in these experiments was adapted from the previously published papers; however, one possible reason for the reduced mRNA expression could have been the protocol was not fully optimized for our reagents and supplies. Proteinase K was tested using a new vial, and a different concentration was used to see if an increase in mRNA was found. Unfortunately, this did not produce a noticeable change in signal intensity.

4.2 Mechanisms of Action of cWnt9a, cFgf3, and cFgf19 to Induce Neural Side Fate in the Basilar Papilla

One possible mechanism by which cWnt9a secretion can induce neural-side fate versus abneural-side fate is that cWnt9a is secreted from the future homogene cell region as previously proposed and then travels to the nearby cells in the region fated to be the neural side. Then, binding of cWnt9a to these cells turns on one or more downstream pathways to induce production and secretion of cFgf19 and cFgf3. However, for this mechanism to work, there would need to be an appropriate receptor for cWnt9a in the same region as the wild-type cFgf19 expression in the left control ears.

To test this hypothesis and understand how cWnt9a is turning on the Fgfs, the expression patterns of different Wnt receptors, Fzds, were studied. The Fzds chosen were based on the CRISPR study described earlier, showing which Wnt-Fzd binding pairs induce the most Wnt activity and based on the RNAseq data for cWnt9a overexpression (Munnamalai et al., 2017;

Voloshanenko et al., 2017). Both of these methods indicated the same two Fzds as being potential receptors for Wnt9a: Fzd4 and Fzd10.

The RNAseq data showed that two Fzd receptors were differentially expressed in the E6 basilar papilla in response to cWnt9a overexpression: cFzd4 expression increased and cFzd10 expression decreased. Previously published data showed wild-type cFzd10 was found in a gradient with greatest expression in the abneural side of the basilar papilla and fading away close to the middle of the basilar papilla; however, with cWnt9a overexpression, there was no visible cFzd10 expression. This result is consistent with cFzd10 serving as a marker of abneural fate. However, it is also consistent with a mechanism in which cFzd10 is a receptor for a Wnt that induces abneural fate; no Wnt ligand with this inductive capacity has yet been identified for the chicken basilar papilla. cFzd4 expression was found in the opposite expression pattern as cFzd10. It was found in the future homogene cell region, in the neural side of the basilar papilla and fading into the abneural side. With cWnt9a overexpression, the expression extended further into the abneural side of the basilar papilla but not through the entire basilar papilla. This expression pattern would make it a suitable candidate for the cWnt9a receptor responsible for the neural side fate of the basilar papilla. However, the cells with the cFzd4 receptors are not likely the ones producing cFgf3 and cFgf19 based on the expression locations of cFgf3 and cFgf19 mRNA in the control wild-type ears. This would indicate one or more intermediate steps between cWnt9a binding to cFzd4 and the production of cFgf3 and cFgf3. Also of note is that although 3C2 was present all around the basilar papilla, cFgf3 and cFgf19 were only found on the sensory half of the cochlear duct. This would mean that only a subset of the cells in the cochlear duct responded to the cWnt9a overexpression which is why it was important to get information on the location of potential cWnt9a receptors.

It is still possible though that cWnt9a uses a different receptor or multiple receptors, but that those other receptors are not upregulated when cWnt9a is upregulated. This would likely result from the cWnt9a binding and then being released from the receptor so that one receptor could induce multiple downstream signaling cascades using multiple ligands. cWnt9a could also have various effects using different receptors.

The next mechanism of interest is what occurs after cWnt9a induces cFgf3 and cFgf19 expression, as in the developmental roles of cFgf3 and cFgf19. The expression patterns of cFgf3 and cFgf19 mRNA although similar were not identical. This indicates that the roles of these Fgfs

are not likely redundant. The second half of this project focused on the role of cFgf19 to see if its overexpression phenocopied cWnt9a overexpression.

4.3 Reduction in GFP Production from RCAS(B)/Fgf19-P2A-EGFP DF-1 Transfected Cells

The reduction in GFP production in RCAS(B)/Fgf19-P2A-EGFP DF-1 transfected cells could have been because of the location of the GFP gene relative to the P2A cassette. Literature has shown that when plasmids with GFP downstream of P2A are transfected in various embryonic fibroblast cell lines and HEK-293T cells, the median intensity difference of GFP is significantly less than if GFP is placed upstream of P2A and T2A together (Liu et al., 2017). However, these embryonic fibroblast cell lines were mouse as opposed to chick embryonic fibroblast cells which could react differently. It is also of note these experiments showed a varied percentage of GFP-positive cells based on the cell type transfected, with some cell lines as low as about 37% positive. It is possible that these DF-1 cells had decreased GFP-positive cells due to the location of the gene in the construct and that using a different type of cell line or a cell line from a different organism for transfection could result in a greater percentage of GFP-positive cells.

4.4 Fgf19 and EGFP Secretion by RCAS(A)/EGFP-P2A-FGF19 or RCAS(B)/Fgf19-P2A-EGFP Transfected DF-1 Cells

Western Blot analyses showed that DF-1 cells transfected with RCAS(B)/Fgf19-P2A-EGFP do produce and secrete at least part of the cFgf19 that binds to the primary antibody used. However, it is unclear why two bands (~30kD and ~35kD) were present, both larger than expected for just cFgf19 (~25 kD). It is possible that these bands are a particularly degraded form of a higher molecular weight protein, which could be the entire insert into the virus: Fgf19-P2A-EGFP or a fusion protein with part of cFgf19 and part of something else or a dimer of cFgf19. If the entire insert was being produced from the virus, this would be as a result of ribosome readthrough in which the ribosome does not leave the mRNA after translating Fgf19 and most of P2A, but continues to translates some or all of the GFP gene that follows.

If a fusion protein was made and secreted, this could affect the ability of Fgf19 to bind to either a receptor, co-receptor, or both. Ultimately this would depend on the final tertiary structure of the fusion protein. However, some predictions can be made in regards to the primary structure

of the protein, based on what is known about the Fgf19 human protein (NP_005108.1) which contains 216 amino acids, 22 of which are the signal sequence. The literature would suggest that Fgf19-P2A-EGFP may be able to bind normally to an Fgf receptor but could have issues binding to a co-receptor. The following studies all use human Fgfs to study the role of the N and C-terminal amino acids. The amino acids at the N-terminal of Fgf19 appear important to binding to Fgfr4 and inducing downstream activity, specifically amino acids 38-42. When amino acids 38-42 of Fgf19 were replaced with amino acids 41-43 of Fgf21, the ability of Fgf19 to phosphorylate ERK in the presence of cells with Fgfr4, with and without β-klotho was diminished, especially so without β-klotho (Wu et al., 2010). The n-terminal amino acids are also important for binding to Fgfr2c and Fgfr3c and causing downstream activity. When amino acids 23 to 42 and 50 to 57 of Fgf19 were replaced with amino acids from Fgf21, the phosphorylation percentage of ERK1/2 decreased in cells transfected with Fgfr2c, 3c, or 4c and β-klotho, but there was no change with cells transfected with Fgfr1c (Ge et al., 2012). There was some phosphorylation with Fgfr2c but none with Fgfr3c and Fgfr4c. In summary, amino acids close to the N-terminal are required for normal binding and downstream activity with Fgfr2c, Fgfr3c, and Fgfr4. This side may not be affected in a fusion protein situation as the extra amino acids are on the C-terminal side of cFgf19.

The C-terminal end of Fgf19 is needed for binding to α and β-klotho. If amino acids 156-195 (using the numbers based on the mature protein not including the signal sequence), are replaced with amino acids 149 to 182 (also based on mature protein) of Fgf21, the percentage of maximum binding to α-klotho is decreased compared to normal Fgf19; however, normal binding percentage is not very high (Wu et al., 2008). If amino acids 156-195 of Fgf19 are replaced with amino acids 147 to 228 (also based on mature protein) of Fgf23, the percentage of maximum binding to β-klotho is essentially eliminated. As such, due to possible additional amino acids at the end of the Fgf19 fusion protein, the ability of Fgf19 to bind to α or β-klotho may be severely reduced.

Finally, as previously discussed, Fgf19 can also use heparin to aid in binding to Fgfr4. The N-terminal of Fgf19 is also required for heparin binding. If the amino acids, based on mature proteins, 50-57 of Fgf19 are replaced with amino acids 51-57 of Fgf21, the ability of Fgf19 to bind to Fgfr4 in the presence of heparin is essentially zero (Wu et al., 2010).

Combining all of this evidence, it is possible that a Fgf19-GFP fusion protein could have reduced ability to bind to α or β-klotho because of the extra amino acids found on the C-terminal

end but could use heparin instead, as one of these three co-factors are needed for much binding to occur, and the N-terminal side should not be obstructed. Nonetheless, it is unknown what the tertiary structure of this fusion protein would look like and how the N and C-terminal sides of cFgf19 would be affected in terms of their ability to bind to receptors or co-receptors. Additionally, as cFgf19 protein (NP_990005.2) is only 64% identical to human Fgf19 (NP_005108.1), it is possible that these regions of human Fgf19 may not have the same roles in cFgf19 (Altschul et al., 1997) (Altschul et al., 2005).

4.5 3C2 and GFP Expression Differences in RCAS(A)/EGFP-P2A-FGF19 Infected Chick Embryos

It is possible that the reason that some of the cells contained 3C2 core protein and not GFP is that the EGFP-P2A-FGF19 insert was detrimental to virus replication. If the viruses containing the insert were not able to produce as many new viral particles, virus without the insert would have an advantage and could infect more cells than those with the insert. This explanation has not been directly evaluated.

4.6 cFgf19 Overexpression Effect on Cartilage Formation

RCAS(A)/EGFP-P2A-Fgf19 injection did not alter the cartilage formation around the cochlear duct. It is possible that instead of stopping cartilage formation, Fgf19 instead promotes its formation. Literature results provided do not provide a clear role for Fgf19 in cartilage formation. For example, Fgf19 mRNA was found in human fetal cartilage of a lower limb between 12 and 16 weeks of age and Fgf19 protein has been found in the resting, proliferating, and hypertrophic cartilage of the human fetal growth plate cartilage between 23 and 26 weeks of age; however, the protein was unable to affect the proliferation of chondrocytes with or without heparin (Xie et al., 1999) (Krejci et al., 2007). Additionally, if zebrafish are given estrogen, the cartilage was reduced, and Fgf19 levels are increased (He et al., 2018). Although Fgf19 plays a role in cartilage, it is not clear what the role is or if the role varies based on species.

4.7 Fgf19 Overexpression Effect on p-ERK

RCAS(A)/EGFP-P2A-Fgf19 or RCAS(B)/Fgf19-P2A-EGFP transfected DF-1 cells did not have increased phosphorylation of ERK. One possible reason the phosphorylation of ERK was not be altered is that Fgf19 in these cells did not turn on the RAS-RAF-ERK1/2-MAPK pathway at all and instead turned on other pathways or not much signaling occurred using this pathway so the amount of phosphorylated ERK produced was not substantial. Additionally, it is possible there was very little or no Fgfrs and/or co-factors present on the DF-1 cells. Without the receptors and co-factors, the Fgf19 would not be able to induce downstream signaling.

4.8 Fgf19 Overexpression Effect on Fgf3 Expression

One possible reason that the Fgf19 virus did not alter Fgf3 expression was that in the cWnt9a overexpression model Fgf3 induces Fgf19 expression instead. Alternatively, it is possible that neither cFgf3 or cFgf19 induces the expression of the other. If this was the case, it would point to the possibility that Fgf3 and Fgf19 have independent roles in the cWnt9a overexpression model.

4.9 Fgfr4 Expression Around the Cochlear Duct

To better understand how cFgf19 operated, experiments were done to see where cFgf19 might have an effect based on the location of its receptor. As cFgf19 is a secreted ligand and one that is capable of moving further distances than some other Fgfs, it was important to have an idea how far the ligands might be traveling to find their targets. This was done by looking for cFgfr4 mRNA. cFgfr4 was found around the cochlear duct in greater abundance than within the cochlear duct. As such it is possible that cFgf19 leaves the basilar papilla and binds to cFgfr4 on cells around the cochlear duct and its effect on the basilar papilla is mediated via these cells. This could be tested by seeing if cWnt9a or cFgf19 overexpression alters the cFgfr4 location or amount outside of the cochlear duct.

4.10 Fgf19 Overexpression Failure to Induce Phenotypic Changes in the Basilar Papilla or the Region Surrounding the Cochlear Duct

There are multiple reasons that the Fgf19 overexpression vectors did not induce phenotypic changes within the ear or surrounding region. First, it is possible that the overexpression vectors

did not work as expected. For example, the RCAS(B)/Fgf19-P2A-EGFP virus appeared to produce a fusion protein with GFP which may or may not have been able to bind to receptors and/or co-factors. If binding could not occur, then downstream signaling and phenotypic changes could not occur. Additionally, RCAS(A)/EGFP-P2A-Fgf19 could have produced Fgf19 with a small extra tail not distinguishable on the Western Blot but that affected binding to receptors and/or co-factors. Second, the amount of Fgf19 protein produced and secreted by the overexpression vectors may not have been sufficient to see phenotypic changes but if significantly more Fgf19 was added, a phenotype would be visible. Third, it is possible that cFgf19 is responsible for an unknown aspect of the cWnt9a overexpression phenotype that was not evaluated. Finally, it is possible that cFgf19 needs to work in conjunction with misregulation of other proteins to produce its effect within the basilar papilla and those other genes were not altered, preventing the phenotypic changes from being produced.

CHAPTER 5. FUTURE EXPERIMENTS

5.1 Examine Downstream Proliferation Genes in Response to cFgf19

As referenced earlier, Tgfb1 is a downstream gene of Fgf19, which is upregulated with the addition of Fgf19 (Massafra et al., 2017). Two Tgfb1 targets vascular cell adhesion molecule 1 (Vcam1) and vinculin (Vcl) were also upregulated with a 1.76-fold and 1.6-fold changes, respectively. Additionally, all three of these genes were also upregulated when cWnt9a was injected into the chick otic cup at E3 (Munnamalai et al., 2017). If these genes are found to be upregulated when cFgf19 was virally delivered to the otic cup at E3, it would show cFgf19 overexpression resulted in differential gene expression.

Moreover, this proposed experiment could show whether and how Fgf19 has a proliferative effect in the chick basilar papilla. The reasoning for this is that when Tgfb1 was added to endometriotic cyst stromal cells with siRNA-Nc (negative control) or siRNA-Vcam1, there was a significant decrease in proliferating cells when Vcam1 was silenced (Zhang et al., 2019).

5.2 Block Fgf Signaling to Determine the Role of cFgf19 with cWnt9a Overexpression

Due to the lack of a radial phenotype in the basilar papilla when overexpression of cFgf19 was attempted, another way to test the effect of cFgf19 would be through blocking the signal. One way to do this would be to block Fgf signaling using the drug, SU5402. SU5402 was previously used to inhibit outgrowth of chicken statoacoustic ganglion neurite explants (Fantetti and Fekete, 2012). When SU5402 was added along with Fgf19 protein, there was significantly less outgrowth compared to adding Fgf19 alone. This shows that SU5402 blocks the effect seen with Fgf19, but it is unclear if this is direct. SU5402 is a pan-Fgfr inhibitor that inhibits the Fgfrs with different efficiencies (Gudernova et al., 2016). Cell-free kinase assays were used to test the activity of SU5402 using phosphorylated signal transducer and activator of transcription 1 (STAT1) as the read-out. The percentage of phosphorylation relative to when no inhibitor was added determined how well SU5402 inhibited the different Fgfrs. SU5402 was found to inhibit Fgfr1 more than Fgfr2, Fgfr3, and Fgfr4. By adding 10μM of SU5402, there is only 5.5 ± 0.9% of the Fgfr1 kinase activity when compared to no inhibitor. Fgfr4 was the least inhibited Fgfr with 20.1 ± 2.8% of kinase activity left when SU5402 was added compared to no inhibitor. It is also important to note

that these experiments also showed that SU5402 also substantially inhibits kinases other than those activated downstream of the Fgfrs such as fibromelanosis (Fm) related receptor tyrosine kinase 3 (FLT3) whose activity was nonexistent compared to when no inhibitor is added. As such, SU5402 is not a specific Fgfr inhibitor, so if a change is seen while using it, what downstream kinase(s) was inhibited would not be clear.

In addition to inhibiting neural outgrowth, SU5402 is known to alter both the chick vestibular organs and the basilar papilla (Chang et al., 2004) (Jacques et al., 2012). In regards to the vestibular organs, when 10mM SU5402 was added to the otocyst between E2.5 and E3, there were no visible canals present and a deformed canal pouch when paint-filled inner ears were examined at E6 and E9 (Chang et al., 2004). In addition, E9 embryos had enlarged and shorter basilar papillas.

Another study showed that when SU5402 was added to basilar papilla explants at E6 and then cultured for five days, the density of hair cells in the basilar papilla was greatly increased across the whole organ (Jacques et al., 2012). However, there was no increase in proliferating cells with SU5402, indicating that there was no increase in cell proliferation causing the increase in hair cell density. To account for the increased number of hair cells, there appeared to be fewer progenitor and supporting cells. These supporting cells appeared to transdifferentiate into hair cells. This research shows that another role of Fgf signaling in chick basilar papillas is to prevent progenitors or supporting cells from becoming hair cells.

In order to examine the effect of Fgf signaling with cWnt9a overexpression, one method would be to inject into the otic vesicle of E3 chick embryos RCAS(A)/Wnt9a and SU5402-soaked beads. The *in vivo* experiments with SU5402 above used a large dose of SU5402 (Chang et al., 2004). When a smaller dose of SU5402 was used, the posterior canal pouch of the vestibular system was lost, but the basilar papilla appeared similar to wild-type ones of this age (Chang et al., 2004) (Brigande et al., 2000). As such, this future experiment would also use a smaller dose of SU5402 in order not to affect the basilar papilla. If Fgf signaling (via cFgf3 and/or cFgf19) is an essential downstream pathway used by cWnt9a to induce a neural-side basilar papilla fate, then these embryos would not show the mostly neural-side phenotype as the SU5402 would block the Fgf signaling. Instead, these embryos may show a mostly abneural-side phenotype. If the mostly neural-side phenotype was found, it would indicate that Fgf signaling plays a different role within or around the inner ear. To confirm this, SU5402 would need to be shown as active through the

loss of the posterior canal pouch as described above. In either scenario, more information on the downstream pathway of cWnt9a would be known, either that SU5402-blocked signaling is used or it is not used. It would not be possible to know for sure that the SU5402-blocked signaling was Fgf signaling, as described above, since SU5402 blocks other tyrosine receptor kinases as well.

To determine if the SU5402-blocked phenotype was only or primarily because of Fgf signaling, one method would be adding plasmids containing secreted forms of all four of the receptors to create dominant negative forms of the Fgfrs. Based on the size of the receptors, it would likely be necessary to add two different RCAS plasmids each containing two of the receptors so all four would be added. It would not be necessary for all cells to contain both plasmids as the goal would simply be production and secretion of the receptors into the extracellular space around the cells. As such one plasmid could be RCAS(A) and the other RCAS(B), mixed together before addition to the otic vesicle. This would allow for secreted Fgfs to bind to the secreted forms of the Fgfrs, so there would be less Fgfs binding to the endogenous Fgf receptors on the cells. Less Fgf binding and signaling would mimic a loss or reduction of the ligands. The phenotype expected would be the same as the one found by adding RCAS(A)/Wnt9a virus and SU5402-soaked beads, in which there was a mostly neural-side basilar papilla. If this phenotype was not found but the plasmids were shown to secrete the receptors, then it would show the SU5402 was blocking different kinases to stop the cWnt9a mostly neural-side phenotype.

5.3 Determine the Role of cFgfr3 in the Chick Basilar Papilla Regarding Radial Asymmetry

Another gene of interest found in the RNAseq data for cWnt9a overexpression was cFgfr3. Although this gene was not significantly decreased with cWnt9a overexpression, there was a drop in mRNA expression from an average of 8412 copies in the control basilar papilla compared to an average of 5251 copies in the cWnt9a overexpression basilar papilla. It is possible then, in at least some of the embryos, that cWnt9a overexpression resulted in the downregulation of cFgfr3. The mechanism for this change in expression is not known.

Previous research has shown that cFgfr3 mRNA is present within the chick basilar papilla at E5.5 in both the hair cells and the supporting cells (Bermingham-McDonogh et al., 2001). However, as the ear developed, the Fgfr3 became restricted to the supporting cells and was not found within the hair cells at E11 and E14. Based on this specificity of Fgfr3 and gentamicin

treatment experiments, Fgfr3 has been shown to play a part in hair cell regeneration within the chick. The hair cells were destroyed by gentamicin treatment, causing Fgfr3 levels to drop, while proliferating cells increased, indicating that there was an increase in proliferation. Once the hair cells were replaced, the Fgfr3 returned to the pre-treatment levels. The hypothesis presented was that the hair cells secreted an Fgf that bound to Fgfr3 on the supporting cells and stopped proliferation of the supporting cells; however, if the hair cells were not present and not making the Fgf, the supporting cells downregulated Fgfr3 and proliferation occurred. When the hair cells were replaced, they produced the Fgf and stopped the proliferation.

In mice, the role of Fgfs in hair cells and Fgfr3 in supporting cells has been further explored. Fgf8 was found in inner hair cells at P0, while Fgfr3 was found only in the pillar cells and Deiter's cells, which are subtypes of supporting cells (Jacques et al., 2007). To determine the role of Fgf8, a Cre-lox system developed to inactivate Fgf8, was used. This system uses Foxg1 to inactivate Fgf8 by E9, which is earlier than Fgf8 is turned on. $p75^{NTR}$ was used as marker for pillar cells and was co-expressed with Fgfr3 in cochlear development. By inactivating Fgf8, there was a decrease in the number of pillar cells. Conversely, through overexpression of Fgf8, there was an increase in pillar cells. A similar outcome occurred when Fgfr3 was knocked out in mice (Hayashi et al., 2007). Using cross sections of P0 mouse cochleas in which Fgfr3 was knocked out, there was a loss of $p75^{NTR}$ positive pillar cells between the inner and outer hair cells. These two papers indicate that Fgf8 in the inner hair cells likely binds to Fgfr3 to specify pillar cells and the amount of Fgf8 determines how many such cells are specified based on how far it diffuses across the radial axis.

Another Fgfr3 ligand, Fgf17 also appears to be necessary for normal pillar cell and Hensen's cell fates, and to repress outer hair cell specification (Jacques et al., 2007). Fgf17 was added to mouse cochlear cultures (equivalent to E14.5) to activate Fgfr3. Through this, there was an increase in $p75^{NTR}$ positive cells and β-catenin+ cells. However, only two regions were positive for both: along the edge of the inner hair cells and in the region that typically becomes the Hensen's cells (beyond the outer hair cells). As only pillar cells are strongly positive for β-catenin at P0, these double-positive cells should have differentiated into pillar cells. The pillar cells along the edge of the inner hair cells were expected, and became larger than in control cultures. The other pillar cells were ectopic. The region in between the double-positive cells consisted of undifferentiated cells. In addition, the Fgf17 resulted in fewer outer hair cells. When the reverse

was done by knocking out Fgfr3, in the apical 2/3rds of the cochlea there appeared to be a fourth row of Deiters' cells and an additional fourth row of outer hair cells (Hayashi et al., 2007). These two papers suggest that Fgfr3 activation in mice can regulate medial-lateral (equivalent to neural-abneural) fate determination of cells to direct them to be pillar cells as opposed to outer hair cells and Hensen's cells whereas Fgfr3 inactivation allows cells to become outer hair cells and Deiter's cells as opposed to pillar cells.

It appears that within the mouse that Fgfr3 is responsible at least partially for the medial fate of the inner ear as activating it (presumably ectopically) results in fewer outer hair cells (a lateral-side fate). It is not clear what side of the basilar papilla cFgfr3 in the chick is responsible for patterning. Since with cWnt9a overexpression there is a decrease in cFgfr3, it is possible that cFgfr3 is responsible for induction of the abneural side of the basilar papilla (the fate which is mostly gone in this experiment). While this might be considered opposite to its role in the mouse, its main effect in the mouse is on the fate of pillar cells that reside at the boundary between medial and lateral sides.

The avian inner ear does not contain pillar cells; however, it is possible that it specifies one or more other types of cells. One way to determine its role in the chick basilar papilla would be use a translation-blocking morpholino against cFgfr3 (Mende et al., 2008) (Norris and Streit, 2014). Morpholinos have been shown to work to downregulate mRNA translation in chick embryos (Mende et al., 2008). To downregulate cFgfr3 through translation blocking, the morpholino would need to be directed against the 5' untranslated region (UTR) through the first 25 bases (Norris and Streit, 2014). It would need to be electroporated *in ovo* into the otic vesicle and in order to confirm that cFgfr3 was downregulated, a tagged full-length version of cFgfr3 with the same 5'UTR would also need to be electroporated. If an antibody against the tag showed significant cFgfr3 present, then the morpholino would not have worked well to decrease cFgfr3.

By downregulating cFgfr3 in one ear and comparing it to the other ear, it would be possible to know what the role of cFgfr3 is within the basilar papilla. The hypothesis would be that by downregulating cFgfr3, the experiment should phenocopy the cWnt9a overexpression phenotype. This should lead to a decrease in short hair cells. The reasoning of this hypothesis is that cWnt9a appears to decrease cFgfr3 and cWnt9a overexpression decreases short hair cells. However, based on the mouse Fgfr3 data described above, another hypothesis would be that downregulating cFgfr3 would result in an increase in the abneural-side fate with an increase in short hair cells.

REFERENCES

Altschul, S.F., Madden, T.L., Schaffer, A.A., Zhang, J., Zhang, Z., Miller, W., Lipman, D.J., 1997. Gapped BLAST and PSI-BLAST: a new generation of protein database search programs. Nucleic acids research 25, 3389-3402.

Altschul, S.F., Wootton, J.C., Gertz, E.M., Agarwala, R., Morgulis, A., Schaffer, A.A., Yu, Y.K., 2005. Protein database searches using compositionally adjusted substitution matrices. The FEBS journal 272, 5101-5109.

Bermingham-McDonogh, O., Stone, J.S., Reh, T.A., Rubel, E.W., 2001. FGFR3 expression during development and regeneration of the chick inner ear sensory epithelia. Developmental biology 238, 247-259.

Brigande, J.V., Kiernan, A.E., Gao, X., Iten, L.E., Fekete, D.M., 2000. Molecular genetics of pattern formation in the inner ear: Do compartment boundaries play a role? Proceedings of the National Academy of Sciences 97, 11700-11706.

Carnicero, E., Garrido, J.J., Alonso, M.T., Schimmang, T., 2001. Roles of fibroblast growth factor 2 during innervation of the avian inner ear. Journal of neurochemistry 77, 786-795.

Chang, W., Brigande, J.V., Fekete, D.M., Wu, D.K., 2004. The development of semicircular canals in the inner ear: role of FGFs in sensory cristae. Development 131, 4201-4211.

Chennamsetty, I., Claudel, T., Kostner, K.M., Trauner, M., Kostner, G.M., 2012. FGF19 signaling cascade suppresses APOA gene expression. Arteriosclerosis, thrombosis, and vascular biology 32, 1220-1227.

de Felipe, P., Luke, G.A., Brown, J.D., Ryan, M.D., 2010. Inhibition of 2A-mediated 'cleavage' of certain artificial polyproteins bearing N-terminal signal sequences. Biotechnol J 5, 213-223.

Donnelly, M.L.L., Luke, G., Mehrotra, A., Li, X., Hughes, L.E., Gani, D., Ryan, M.D., 2001. Analysis of the aphthovirus 2A/2B polyprotein ‘cleavage’ mechanism indicates not a proteolytic reaction, but a novel translational effect: a putative ribosomal ‘skip’. Journal of General Virology 82, 1013-1025.

Fantetti, K.N., Fekete, D.M., 2012. Members of the BMP, Shh, and FGF morphogen families promote chicken statoacoustic ganglion neurite outgrowth and neuron survival in vitro. Developmental neurobiology 72, 1213-1228.

Fettiplace, R., Kim, K.X., 2014. The physiology of mechanoelectrical transduction channels in hearing. Physiological reviews 94, 951-986.

Fokina, V.M., Frolova, E.I., 2006. Expression patterns of Wnt genes during development of an anterior part of the chicken eye. Developmental dynamics : an official publication of the American Association of Anatomists 235, 496-505.

Francisco-Morcillo, J., Sanchez-Calderon, H., Kawakami, Y., Izpisua Belmonte, J.C., Hidalgo-Sanchez, M., Martin-Partido, G., 2005. Expression of Fgf19 in the developing chick eye. Brain research. Developmental brain research 156, 104-109.

Fu, L., John, L.M., Adams, S.H., Yu, X.X., Tomlinson, E., Renz, M., Williams, P.M., Soriano, R., Corpuz, R., Moffat, B., Vandlen, R., Simmons, L., Foster, J., Stephan, J.-P., Tsai, S.P., Stewart, T.A., 2004. Fibroblast Growth Factor 19 Increases Metabolic Rate and Reverses Dietary and Leptin-Deficient Diabetes. Endocrinology 145, 2594-2603.

Ge, H., Baribault, H., Vonderfecht, S., Lemon, B., Weiszmann, J., Gardner, J., Lee, K.J., Gupte, J., Mookherjee, P., Wang, M., Sheng, J., Wu, X., Li, Y., 2012. Characterization of a FGF19 variant with altered receptor specificity revealed a central role for FGFR1c in the regulation of glucose metabolism. PloS one 7, e33603-e33603.

Gospodarowicz, D., 1974. Localisation of a fibroblast growth factor and its effect alone and with hydrocortisone on 3T3 cell growth. Nature 249, 123-127.

Groves, A.K., Fekete, D.M., 2012. Shaping sound in space: the regulation of inner ear patterning. Development 139, 245-257.

Gudernova, I., Vesela, I., Balek, L., Buchtova, M., Dosedelova, H., Kunova, M., Pivnicka, J., Jelinkova, I., Roubalova, L., Kozubik, A., Krejci, P., 2016. Multikinase activity of fibroblast growth factor receptor (FGFR) inhibitors SU5402, PD173074, AZD1480, AZD4547 and BGJ398 compromises the use of small chemicals targeting FGFR catalytic activity for therapy of short-stature syndromes. Human molecular genetics 25, 9-23.

Hayashi, T., Cunningham, D., Bermingham-McDonogh, O., 2007. Loss of Fgfr3 leads to excess hair cell development in the mouse organ of Corti. Developmental dynamics : an official publication of the American Association of Anatomists 236, 525-533.

He, H., Wang, C., Tang, Q., Yang, F., Xu, Y., 2018. Elucidation of possible molecular mechanisms underlying the estrogen-induced disruption of cartilage development in zebrafish larvae. Toxicology letters 289, 22-27.

Hermida, M.A., Dinesh Kumar, J., Leslie, N.R., 2017. GSK3 and its interactions with the PI3K/AKT/mTOR signalling network. Advances in biological regulation 65, 5-15.

Holt, J.A., Luo, G., Billin, A.N., Bisi, J., McNeill, Y.Y., Kozarsky, K.F., Donahee, M., Wang, D.Y., Mansfield, T.A., Kliewer, S.A., Goodwin, B., Jones, S.A., 2003. Definition of a novel growth factor-dependent signal cascade for the suppression of bile acid biosynthesis. Genes Dev 17, 1581-1591.

Hughes, S.H., The RCAS System.

Hughes, S.H., 2004. The RCAS vector system. Folia biologica 50, 107-119.

Huh, S.H., Jones, J., Warchol, M.E., Ornitz, D.M., 2012. Differentiation of the lateral compartment of the cochlea requires a temporally restricted FGF20 signal. PLoS biology 10, e1001231.

Huh, S.H., Warchol, M.E., Ornitz, D.M., 2015. Cochlear progenitor number is controlled through mesenchymal FGF receptor signaling. eLife 4.

Itoh, N., Ornitz, D.M., 2011. Fibroblast growth factors: from molecular evolution to roles in development, metabolism and disease. Journal of biochemistry 149, 121-130.

Jacques, B.E., Dabdoub, A., Kelley, M.W., 2012. Fgf signaling regulates development and transdifferentiation of hair cells and supporting cells in the basilar papilla. Hear Res 289, 27-39.

Jacques, B.E., Montcouquiol, M.E., Layman, E.M., Lewandoski, M., Kelley, M.W., 2007. Fgf8 induces pillar cell fate and regulates cellular patterning in the mammalian cochlea. Development 134, 3021-3029.

Kim, J.H., Lee, S.-R., Li, L.-H., Park, H.-J., Park, J.-H., Lee, K.Y., Kim, M.-K., Shin, B.A., Choi, S.-Y., 2011. High Cleavage Efficiency of a 2A Peptide Derived from Porcine Teschovirus-1 in Human Cell Lines, Zebrafish and Mice. PloS one 6, e18556.

Krejci, P., Krakow, D., Mekikian, P.B., Wilcox, W.R., 2007. Fibroblast growth factors 1, 2, 17, and 19 are the predominant FGF ligands expressed in human fetal growth plate cartilage. Pediatric research 61, 267-272.

Kurose, H., Okamoto, M., Shimizu, M., Bito, T., Marcelle, C., Noji, S., Ohuchi, H., 2005. FGF19-FGFR4 signaling elaborates lens induction with the FGF8-L-Maf cascade in the chick embryo. Development, growth & differentiation 47, 213-223.

Ladher, R.K., Anakwe, K.U., Gurney, A.L., Schoenwolf, G.C., Francis-West, P.H., 2000. Identification of synergistic signals initiating inner ear development. Science 290, 1965-1967.

Ladher, R.K., Wright, T.J., Moon, A.M., Mansour, S.L., Schoenwolf, G.C., 2005. FGF8 initiates inner ear induction in chick and mouse. Genes Dev 19, 603-613.

Li, F., Li, Z., Han, Q., Cheng, Y., Ji, W., Yang, Y., Lu, S., Xia, W., 2020. Enhanced autocrine FGF19/FGFR4 signaling drives the progression of lung squamous cell carcinoma, which responds to mTOR inhibitor AZD2104. Oncogene 39, 3507-3521.

Liu, Y., Cao, M., Cai, Y., Li, X., Zhao, C., Cui, R., 2020. Dissecting the Role of the FGF19-FGFR4 Signaling Pathway in Cancer Development and Progression. Frontiers in Cell and Developmental Biology 8.

Liu, Z., Chen, O., Wall, J.B.J., Zheng, M., Zhou, Y., Wang, L., Ruth Vaseghi, H., Qian, L., Liu, J., 2017. Systematic comparison of 2A peptides for cloning multi-genes in a polycistronic vector. Scientific Reports 7, 2193.

Massafra, V., Milona, A., Vos, H.R., Burgering, B.M., van Mil, S.W., 2017. Quantitative liver proteomics identifies FGF19 targets that couple metabolism and proliferation. PloS one 12, e0171185.

Mende, M., Christophorou, N.A.D., Streit, A., 2008. Specific and effective gene knock-down in early chick embryos using morpholinos but not pRFPRNAi vectors. Mechanisms of Development 125, 947-962.

Munnamalai, V., Sienknecht, U.J., Duncan, R.K., Scott, M.K., Thawani, A., Fantetti, K.N., Atallah, N.M., Biesemeier, D.J., Song, K.H., Luethy, K., Traub, E., Fekete, D.M., 2017. Wnt9a Can Influence Cell Fates and Neural Connectivity across the Radial Axis of the Developing Cochlea. J Neurosci 37, 8975-8988.

Niehrs, C., 2012. The complex world of WNT receptor signalling. Nature reviews. Molecular cell biology 13, 767-779.

Nishimura, T., Utsunomiya, Y., Hoshikawa, M., Ohuchi, H., Itoh, N., 1999. Structure and expression of a novel human FGF, FGF-19, expressed in the fetal brain. Biochimica et biophysica acta 1444, 148-151.

Norris, A., Streit, A., 2014. Morpholinos: studying gene function in the chick. Methods 66, 454-465.

Okamoto, M., Bito, T., Noji, S., Ohuchi, H., 2009. Subtype-specific expression of Fgf19 during horizontal cell development of the chicken retina. Gene expression patterns : GEP 9, 306-313.

Okamoto, M., Tomonari, S., Naito, Y., Saigo, K., Noji, S., Ui-Tei, K., Ohuchi, H., 2008. Introduction of silencing-inducing transgene against Fgf19 does not affect expression of Tbx5 and beta3-tubulin in the developing chicken retina. Development, growth & differentiation 50, 159-168.

Olaya-Sanchez, D., Sanchez-Guardado, L.O., Ohta, S., Chapman, S.C., Schoenwolf, G.C., Puelles, L., Hidalgo-Sanchez, M., 2017. Fgf3 and Fgf16 expression patterns define spatial and temporal domains in the developing chick inner ear. Brain structure & function 222, 131-149.

Ornitz, D.M., Itoh, N., 2015. The Fibroblast Growth Factor signaling pathway. Wiley interdisciplinary reviews. Developmental biology 4, 215-266.

Pirvola, U., Spencer-Dene, B., Xing-Qun, L., Kettunen, P., Thesleff, I., Fritzsch, B., Dickson, C., Ylikoski, J., 2000. FGF/FGFR-2(IIIb) Signaling Is Essential for Inner Ear Morphogenesis. The Journal of Neuroscience 20, 6125-6134.

Raja, A., Park, I., Haq, F., Ahn, S.-M., 2019. FGF19-FGFR4 Signaling in Hepatocellular Carcinoma. Cells 8, 536.

Sanchez-Calderon, H., Francisco-Morcillo, J., Martin-Partido, G., Hidalgo-Sanchez, M., 2007. Fgf19 expression patterns in the developing chick inner ear. Gene expression patterns : GEP 7, 30-38.

Sienknecht, U.J., Fekete, D.M., 2008. Comprehensive Wnt-related gene expression during cochlear duct development in chicken. The Journal of comparative neurology 510, 378-395.

Song, K.-H., Li, T., Owsley, E., Strom, S., Chiang, J.Y.L., 2009. Bile acids activate fibroblast growth factor 19 signaling in human hepatocytes to inhibit cholesterol 7alpha-hydroxylase gene expression. Hepatology 49, 297-305.

Stevens, C.B., Davies, A.L., Battista, S., Lewis, J.H., Fekete, D.M., 2003. Forced activation of Wnt signaling alters morphogenesis and sensory organ identity in the chicken inner ear. Developmental biology 261, 149-164.

Szymczak-Workman, A.L., Vignali, K.M., Vignali, D.A., 2012. Design and construction of 2A peptide-linked multicistronic vectors. Cold Spring Harbor protocols 2012, 199-204.

Urness, L.D., Wang, X., Doan, H., Shumway, N., Noyes, C.A., Gutierrez-Magana, E., Lu, R., Mansour, S.L., 2018. Spatial and temporal inhibition of FGFR2b ligands reveals continuous requirements and novel targets in mouse inner ear morphogenesis. Development 145.

Voloshanenko, O., Gmach, P., Winter, J., Kranz, D., Boutros, M., 2017. Mapping of Wnt-Frizzled interactions by multiplex CRISPR targeting of receptor gene families. FASEB journal : official publication of the Federation of American Societies for Experimental Biology 31, 4832-4844.

Wan, G., Corfas, G., Stone, J.S., 2013. Inner ear supporting cells: rethinking the silent majority. Semin Cell Dev Biol 24, 448-459.

Wei, Y., Mizzen, C.A., Cook, R.G., Gorovsky, M.A., Allis, C.D., 1998. Phosphorylation of histone H3 at serine 10 is correlated with chromosome condensation during mitosis and meiosis in Tetrahymena. Proceedings of the National Academy of Sciences 95, 7480-7484.

Wright, T.J., Ladher, R., McWhirter, J., Murre, C., Schoenwolf, G.C., Mansour, S.L., 2004. Mouse FGF15 is the ortholog of human and chick FGF19, but is not uniquely required for otic induction. Developmental biology 269, 264-275.

Wright, T.J., Mansour, S.L., 2003. Fgf3 and Fgf10 are required for mouse otic placode induction. Development 130, 3379-3390.

Wu, A.-L., Coulter, S., Liddle, C., Wong, A., Eastham-Anderson, J., French, D.M., Peterson, A.S., Sonoda, J., 2011. FGF19 Regulates Cell Proliferation, Glucose and Bile Acid Metabolism via FGFR4-Dependent and Independent Pathways. PloS one 6, e17868.

Wu, X., Ge, H., Gupte, J., Weiszmann, J., Shimamoto, G., Stevens, J., Hawkins, N., Lemon, B., Shen, W., Xu, J., Veniant, M.M., Li, Y.-S., Lindberg, R., Chen, J.-L., Tian, H., Li, Y., 2007. Co-receptor Requirements for Fibroblast Growth Factor-19 Signaling. Journal of Biological Chemistry 282, 29069-29072.

Wu, X., Ge, H., Lemon, B., Vonderfecht, S., Baribault, H., Weiszmann, J., Gupte, J., Gardner, J., Lindberg, R., Wang, Z., Li, Y., 2010. Separating mitogenic and metabolic activities of fibroblast growth factor 19 (FGF19). Proceedings of the National Academy of Sciences of the United States of America 107, 14158-14163.

Wu, X., Ge, H., Lemon, B., Weiszmann, J., Gupte, J., Hawkins, N., Li, X., Tang, J., Lindberg, R., Li, Y., 2009. Selective activation of FGFR4 by an FGF19 variant does not improve glucose metabolism in ob/ob mice. Proceedings of the National Academy of Sciences of the United States of America 106, 14379-14384.

Wu, X., Lemon, B., Li, X., Gupte, J., Weiszmann, J., Stevens, J., Hawkins, N., Shen, W., Lindberg, R., Chen, J.-L., Tian, H., Li, Y., 2008. C-terminal tail of FGF19 determines its specificity toward Klotho co-receptors. J Biol Chem 283, 33304-33309.

Xie, M.H., Holcomb, I., Deuel, B., Dowd, P., Huang, A., Vagts, A., Foster, J., Liang, J., Brush, J., Gu, Q., Hillan, K., Goddard, A., Gurney, A.L., 1999. FGF-19, a novel fibroblast growth factor with unique specificity for FGFR4. Cytokine 11, 729-735.

Yang, L.M., Cheah, K.S.E., Huh, S.H., Ornitz, D.M., 2019a. Sox2 and FGF20 interact to regulate organ of Corti hair cell and supporting cell development in a spatially-graded manner. PLoS genetics 15, e1008254.

Yang, T., Guo, L., Wang, L., Yu, X., 2019b. Diagnosis, Intervention, and Prevention of Genetic Hearing Loss. Springer Singapore, pp. 73-92.

Yu, X., Yan, N., Li, Z., Hua, Y., Chen, W., 2019. FGF19 sustains the high proliferative ability of keratinocytes in psoriasis through the regulation of Wnt/GSK-3beta/beta-catenin signalling via FGFR4. Clinical and experimental pharmacology & physiology 46, 761-769.

Zhang, J., Li, H., Yi, D., Lai, C., Wang, H., Zou, W., Cao, B., 2019. Knockdown of vascular cell adhesion molecule 1 impedes transforming growth factor beta 1-mediated proliferation, migration, and invasion of endometriotic cyst stromal cells. Reproductive biology and endocrinology : RB&E 17, 69.

Zhu, J.H., Kulich, S.M., Oury, T.D., Chu, C.T., 2002. Cytoplasmic aggregates of phosphorylated extracellular signal-regulated protein kinases in Lewy body diseases. The American journal of pathology 161, 2087-2098.